NANYANG TECHNOLOGICAL UNIVERSITY

Chemiluminescent Fibre Optic Immuno- and Genosensors for Pathogens Detection in Water

YE KEHAN

SCHOOL OF MATERIALS SCIENCE AND ENGINEERING

[2017]

Chemiluminescent Fibre Optic Immuno- and Genosensors for Pathogens Detection in Water

YE KEHAN

SCHOOL OF MATERIALS SCIENCE AND ENGINEERING

A thesis submitted to the Nanyang Technological University in partial fulfilment of the requirement for the degree of Doctor of Philosophy

2017

Statement of Originality

I hereby certify that the work embodied in this thesis is the result of original research and has not been submitted for a higher degree to any other University or Institution.

13 Aug 2017

. . . . . .
Date

. . . . . .
YE KEHAN

Abstract

Waterborne pathogens related diseases are the major threats to public health worldwide. They not only cause high levels of enormous morbidity and mortality losses but also inflict great economic harm on human society. More challenges can be expected in the future, as due to the increasing water scarcity, reuse or recovery of water is becoming an important strategy. Proper assessment of pathogens on water and water quality monitoring are the key procedures for waterborne pathogen infections prevention. Chemiluminescent fibre optic biosensors emerge as the powerful tools for this purpose attributed to their specificity, sensitivity, rapidity, cost-effectiveness, the possibility for in-field operation and being user-friendly. This work focuses on the development of a chemiluminescent fibre optic immunosensor (for detection of *E. coli*, as a fecal indicator bacteria) and a genosensor (for detection of hepatitis A virus, as a common RNA virus) which are fitted in a portable black box. The immunosensor is based on a micro-ELISA procedure implemented on the end face of a fibre optic. A critical factor that defines the sensing performance is the antibody immobilization on the fibre optic. Silane-diazirine, as an effective photoinducible crosslinker, has been studied and applied in this system. After optimization, it has shown superior adaptability over the traditional chemiluminescent ELISA and a commonly used glutaraldehyde chemical immobilization method in terms of lower detection limit and dynamic range. For the genosensor, a set of ssDNA probes were designed and a sandwich-type hybridization process was constructed. After optimization of the probes and the working conditions, it has demonstrated the ability to work on both cDNA and RNA of HAV with a relatively large signal/noise ratio and a good sensitivity. An excellent specificity was also confirmed by screening with a broad range of other pathogen samples. The nucleic acid probes method was also validated by optimized PCR and qPCR techniques. The relatively affordable and dispatchable biosensor can be used in the early warning monitoring for the putative presence of target pathogens either in an individual sample screening or in continuous monitoring of the environment to indicate the need for further investigation.

Acknowledgements

The student has been under the joint Ph.D. programme between Nanyang Technological University (NTU, Singapore) and Ben-Gurion University of the Negev (BGU, Israel). She is grateful to all of those with whom she has had the pleasure to work during her study in Singapore and Israel for making the study experience a life-transforming one.

The author would like to express her sincere gratitude to her graduate study supervisors, Associate Professor Alfred Tok (NTU) and Professor Robert Marks (BGU) for offering the study opportunity and sharing their valuable knowledge and experience. Their continuous guidance and support have helped the author overcome the difficulties. The author is immensely grateful for Prof. Marisa Manzano for the generous help on the genosensor project and the confidence that she has given to her during the work.

The author would like to thank the thesis committee members, Prof Timothy John White and Associate Professor Dong Zhili for giving advice for the improvement to this dissertation. The author also appreciate examiners' time spent in reading, commenting and improving the dissertation.

The author is also thankful for meeting all the group members and friends from NTU and BGU for a great deal of support and the friendship: Dr. Cheng Ting, Ms. Firoz Algaar, Dr. Wei Chao, Dr. Wu Yuanyuan, Dr. Ma Bing, Dr. Evgeni Eltzov, Prof. Levi Gheber, Prof. Ariel Kushmaro, Dr. Karine Goldberg, Dr. Hilla Ben-Hamo, Ms Prima Dewi Sinawang, Ms. Sarah Gurevich, Dr. Oleksandr Pokholenko and Dr. Qi Huan.

It is my pleasure to thank all the staff from MSE, the department of biotechnology engineering and the Kreitman school for their support and help.

The author is also grateful for the research funding provided by CREATE programme, NTU and BGU.

Last but definitely not the least, the author wants to thank her family for their love through the past years.

Table of Contents

Table Captions

Figure Captions

Figure 4.7 Results of the set-up optimization, left: the point where the UV light was placed at. The far-end means the non-functionalized end of the fibre strand, the light comes in from this end and propagates to the near-end surface to induce the photo-reaction; while the near-end means the functionalized end, the UV shined directly at this end from outside of the tubes containing antibody solution. Right: the roughness of the far-end where the light comes from.

Figure 5.1 RLU report of the two routes of diazirine functionalization. Silane or silane-diazirine was dissolved in toluene in 1%, 10%, 50% and 100% (v/v) concentrations. Each bio-structure for the signal generation was visualized accordingly at the upright corner of the signal column chart.

Figure 5.2 Selection of bacteria strains. -2, -3, -4, -5 stands for the cells are diluted in 1/100, 1/1000, 1/10000 and 1/100000. The control experiments are performed in the 1/1000 dilution.

Figure 5.3 Selection of detection antibody. -2, -3, -4, -5 stands for the cells are diluted in 1/100, 1/1000, 1/10000 and 1/100000. The control experiments are performed in the 1/1000 dilution.

Figure 5.4 The effect of addition of IPTG.

Figure 5.5 Calibration Curve of DPD2794 strain CFU counts against OD600 reading.

Figure 6.1 the florescence signal of the fibre optic pieces exposed under different incubation temperatures: 1, 90 ºC;2, 60 ºC; 3, 30 ºC; 4, 120 ºC; and 5, no silane as control.

Figure 6.2 The optimization of blocking conditions. The skim milk and BSA were dissolved in PBST (0.1% v/v) solution in concentrations of 1%, 3%, 5% and 10% (w/v).

Figure 6.3 RLU immunoassay responses using two different UV light sources, illuminating from 5 to 60 minutes. MAX 303 stands for a Xenon UV lamp emitting light from 340 nm to 370 nm with a final power of 200 mW/cm^2 measured at 365 nm.

UV 365 represents an ENF-280C (8 W) hand-held UV lamp emitting light at 365 nm with a power of 1090 μW/cm^2.

Figure 6.4 RLU responses from the immunoassay and S/N values reported for each silane and diazirine species combination illustrated on the right. The silane species employed are 4-atom and 7-atom arm-length amine tailed silanes. A typical aliphatic and aromatic diazirine were adopted for comparison.

Figure 6.5 Calibration curves for A: chemiluminescent ELISA (CL-ELISA); B: optical fibre immunosensors using either glutaraldehyde as a crosslinker (FOBS-AmGlu); C: diazirine as crosslinker (FOBS-AmDia). The calibrations were obtained using target E. coli dilutions ranging from 6.44 CFU/ml to 6.44*108 CFU/ml. In each calibration, the linear range are visualized on the top left corner with the r2 values.

Figure 6.6 Specificity test covering several *E. coli* strains: K-12, DPD 2794, B and ATCC 25922; and antigens from other sources: *Salmonella* (*salmonella* bacteria culture), *V. cholerae* (LPS from *Vibrio cholerae*), *Brucella* (suspension of inactivated *Brucella*), *S. aureus* (suspension of inactivated *Staphylococcus aureus*), *M. luteus* (*Micrococcus luteus* bacteria culture), Hep. A (Hepatitis A virus VP3 antigen), Hep. B (Hepatitis B virus e antigen), dengue (dengue virus nonstructural protein 1), skim milk (1% w/v skim milk in PBST), commercial milk (1% w/v commercial milk in PBST), LDL (lower detection limit as determined by the calibration curve the of AmDia FOBS using polyclonal antibody).

Figure 6.7 SEM images of optical fiber surfaces after each treatment in photoimmobilization procedures utilizing APTES as silane and SDA as diazirine source following Route B. (A) plain surface after piranha activation. (B) after silanization by APTES. (C) after reaction with SDA. (D) after antibody immobilization. (E). *E. coli* bacteria attached on the surface. (F) Zoom-in image of an immobilized bacteria.

Figure 7.1 DNA agarose gel from the conventional end-point PCR using Set 1 primers. (A) are the PCR products from the outer primers using cDNA samples and templates

and (B) are the products from the inner primers using PCR products from (A) as templates. Water instead of cDNA was used as the negative control (N).

Figure 7.2 PCR and qPCR results from Set 2 primers. (A) Results of external PCR; (B) Results of the internal PCR. In both pictures: Lane 1~ 10: DNA Ladder 100 bp; HAV5 1.0 ng/µL; 0.1 ng/µL; 0.01 ng/µL; 0.001 ng/µL; $1.0 * 10^{-4}$ ng/µL; $1.0 * 10^{-5}$ ng/µL; $1.0 * 10^{-6}$ ng/µL; $1.0 * 10^{-7}$ ng/µL; blank. (C) Standard curve from qPCR using 10-fold serial dilutions.

Figure 7.3 Optimized dot blot results showing: P (positive controls) the sensitivity of the capture probe to its complementary sequence as the positive control. The concentrations of the complementary sequence are labeled on the top; S & N (samples and negative control), the responses to the reverse transcribed cDNA and RNA of HAV as samples and the cDNA of Norovirus as negative control.

Figure 7.4 Optimization of the capture probe concentration during overnight incubation at 4 °C. The concentrations for testing are 6 ng/µl, 12 ng/µl, 24 ng/µl and 48 ng/µl. The effect of BSA in the incubation mixture was also included in this test.

Figure 7.5 Optimization of the immobilization buffer during overnight incubation at 4 °C: TBS solution (25 mM Tris, 150 mM NaCl, 2 mM KCl, pH7.4); PBS (10 mM phosphate buffer, 2.7 mM potassium chloride and 137 mM sodium chloride, pH 7.4), HEPES (20 mM, pH 7.4), PBS + $NaBCNH_3$ (0.3 M), NaOAc (30 mM, pH 5.2) + $NaBCNH_3$ (0.3M), Borax (100 mM boric acid, 25 mM sodium tetraborate, 75 mM NaCl, pH 8.1).

Figure 7.6 Selection of the blocking conditions after the immobilization of the 1st probe. The blocking agents were dissolved in TBST (0.1% v/v) buffer and the incubation was at 40 °C for 1.5 hours.

Figure 7.7 Effect of the avidin-HRP concentration on the light response. The labeled concentrations represent the ratio of the volume of the avidin-HRP to the volume of the incubation buffer. The light response from the group without cDNA targets was used as the reference.

Figure 7.8 Optimization of the hybridization buffer: Church (0.5 M Na_2HPO_4, 0.5 M NaH_2PO_4, 1% (w/v) SDS and 10 mM EDTA, pH 7.5), Church + 1% (w/v) BSA, TBS pH 7.4, PBS pH 7.4, 0.1% (v/v) PBST pH 7.4, TBS pH 7.4 + 1% (w/v) SDS + 10 mM EDTA, Borax as in immobilization step + 1% (w/v) SDS + 10 mM EDTA.

Figure 7.9 Light responses to nucleic acid dilutions and controls. The linear range can be visualized on the top right corner, by plotting the RLU values against the lg values of nucleic acid concentrations in pg/µl. The linear range was found to be 5 pg/µl to 10 ng/µl for cDNA ($r^2 = 0.93$) and 50 pg/µl to 10 ng/µl for RNA ($r^2 = 0.87$). The sensitivity of the biosensor was determined by the slope of the linear range as it describes the power to discriminate the difference between the two signals with the change of the analyte concentrations, as represented by its form $\frac{y_A - y_B}{x_A - x_B}$. It was found to be 43948 for cDNA and 23819 for RNA.

Figure 7.10 Specificity test covering a series of other pathogens' cDNA or proteins. The column chart shows the results from fibre optic genosensor, where the dashed line represents the LDL (lower detection limit). The picture on the top right corner shows the results from the dot blotting experiment. The aberrations are corresponding to the names of the pathogens shown in the x-axis labels of the chart.

Figure 8.1 Chemiluminescence (CL) enhancement by: left, indirect detection ELISA; and right, metal nanoparticles enhanced chemiluminescence (MECL).

Figure 8.2 Orientated antibody immobilization strategies: proteins A/G facilitated immobilization; reaction of -NH2 functionalized surface and the –CHO bonds through oxidation of carbohydrates; and UV induced immobilization between C=C bonds and thiol bonds from IgG cleavage.

Abbreviations

APTES	(3-AminoPropyl)TriEthoxySilane
APTMS:	(3-AminoPropyl)TriMethoxySilane
CAC	Carbene-Alkene Complex
CAGR	Compound Annual Growth Rate
cDNA	copied DeoxyriboNucleic Acid
CFOB	Chemiluminescent Fibre Optic Biosensor
Immuno-CFOS	Immuno-Chemiluminescent Fibre Optic Biosensor
Geno-CFOS	Geno-Chemiluminescent Fibre Optic Biosensor
DEPT	Distortionless Enhancement by Polarization Transfer
DI	Deionized
EDC	1-Ethyl-3-(3-Dimethylaminopropyl)Carbodiimide
EDS	Energy-Dispersive X-ray Spectroscopy
ELISA	Enzyme-Linked Immunosorbent Assay
FO	Fibre Optic
FOIS	Fibre Optic Immunosensor
HAV	Hepatitis A Virus
HOMO	Highest Occupied Molecular Orbital
HRP	HorseRadish Peroxidase
LDL	Lower Detection Limit
LPS	LipoPolySaccharides
LUMO	Lowest Unoccupied Molecular Orbital
NA	Nucleic Acid
NHS	N-HydroxySuccinimide
NMR	Nuclear Magnetic Resonance
PBS	Phosphate-Buffered Saline
PBST	Phosphate-Buffered Saline with Tween 20
PCR	Polymerase Chain Reaction
PIC	PhotoInducible Crosslinker
PMT	Photomultiplier Tube
qPCR	quantitative Polymerase Chain Reaction
RIES	Rearrangement In the Excited State

RNA	RiboNucleic Acid
RT-PCR	Reverse Transcription Polymerase Chain Reaction
SD	Standard Deviation
SDA	Succinimidyl-DiAzirin
ssDNA	single stranded DeoxyriboNucleic Acid
S/N	Signal/Noise
SEM	Scanning Electron Microscope
TBS	Tris-Buffered Saline
TEM	Transmission Electron Microscopy
TIR	Total Internal Reflection
TLC	Thin Layer Chromatography
UV	Ultraviolet

Chapter 1

Introduction

This chapter provides a rationale for the research, determines the goals and scope and briefly outlines the structure of the dissertation. Waterborne pathogen infections have placed tremendous health burden on human society. The development of the portable detection tools makes it possible for the in-field detection, providing faster and specific information, which is fundamental for researchers, decision-makers, and the community, to take necessary actions to prevent waterborne pathogens infections and outbreaks. A portable black box device, filled with a modified fibre optic and a PMT, had been constructed as the concept of a chemiluminescent fibre optic biosensor for several pathogens detections for the above purpose. The thesis further addressed a few points to enhance the sensing performance and expand the applications: would a new silane-diazirine crosslinker be applicable for antibody immobilization and improve the performance of the immunosensor? Would it be possible to integrate the DNA hybridization system for HAV and how is the performance in the RNA detection? The thesis utilized E. coli as a model target for the evaluation of the immunosensor constructed by silane diazirine. The results showed its ability in immobilizing the antibody and maintaining its immunoactivity and the resulted immunosensor showed superior sensitivity in a comparative study. On the other hand, the genosensor targeted at both the cDNA and RNA of HAV. The results proved that the designed ssDNA probes had been integrated onto the CFOB platform and performed the sensing function to both cDNA and RNA of HAV after condition optimization with good sensitivity and specificity.

1.1 Background

Waterborne pathogens and related diseases are associated with 1.8 million human deaths annually and frequent illness cases everyday including diarrhea, gastrointestinal diseases and systematic illnesses [1]. An economic loss of nearly 12 billion USD per year worldwide has been estimated [2]. 88% of that health burden is due to unsafe water supply, sanitation and hygiene [3]. Until 2015, there are still about 663 million people lacking access to an improved source of drinking-water and nearly 2.4 billion people living without access to adequate sanitation [4]. It foresees more challenges for water supply systems in the future brought by urbanization, climate change and population growth. It is estimated that by 2025, half of the world's population will be living in water-stressed areas [5], where reuse of waste water is becoming an important strategy.

On the side of continued efforts in improving water sanitation condition, the development of proper waterborne pathogens detection techniques and tools is of crucial importance in preventing waterborne pathogens infections and outbreaks. There are 1407 species have been identified as waterborne pathogens including bacteria (538 species), viruses (208 types), parasitic protozoa (57 species), and several fungi and helminths species [6]. Using non-pathogenic strains of *E. coli* as indicator bacteria is a common water quality evaluation strategy which has been employed by many countries and districts in the drinking and recreation water safety regulations [7]. On the other hand, there is still need of the identification of virus pathogens in relatively higher occurrence, such as hepatitis A virus in the suspicious contaminated water. Most of the current detection methods are performed in the laboratory, which involve heavy lab equipment, well-trained personnel and usually a large time-commitment. Thus, this work aims at the development of the chemiluminescent fibre optic immuno- and genosensors, to serve as a portable, cheaper and user-friendly detection tool while maintaining the reliability for the early warning purpose. In spite of the rapid expanding of the biosensor field, there are still a few barriers that prevent the use of lab-developed biosensors in the real-world: (i) difficulties in achieving specific and sensitive detection in complex real environmental samples; (ii) difficulties in reducing the size and cost of certain systems; and (iii) difficulties in improving the reliability of the system with novel crosslinking methods [8].

Based on the review of the related work in recent decades (Chapter 2), the author has selected the chemiluminescent fibre optic biosensor (CFOB) as the basic model (in **Figure 1.1)** for the thesis, which is a portable black box with dimensions of 350/250/200 mm. A fibre optic is fitted in the black box and the biosensing activities happen at its modified end face (also called the near-end), including a micro sandwich ELISA assay and a sandwich type nucleic acids hybridization procedure. Once the completed structure is formed, the chemiluminescent light is generated through the oxidization of luminol by HRP catalysis, then transmitted immediately by the fibre optic through the total internal reflection (TIR) mechanism and finally detected by a photomultiplier tube (PMT), which is also fitted inside the black box. The photon detector is connected to a computer, where the light is digitalized and analyzed.

A few key points have been determined in the construction of the above CFOB: For immuno-CFOS: (1) the immobilization of antibody on the solid phase of fibre optic; (2) the optimization of the protocol to improve the S/N ratio and sensitivity. For geno-CFOS: (1) the design of proper oligonucleotides probes and probes validation; (2) integration of the probes into the CFOB environment.

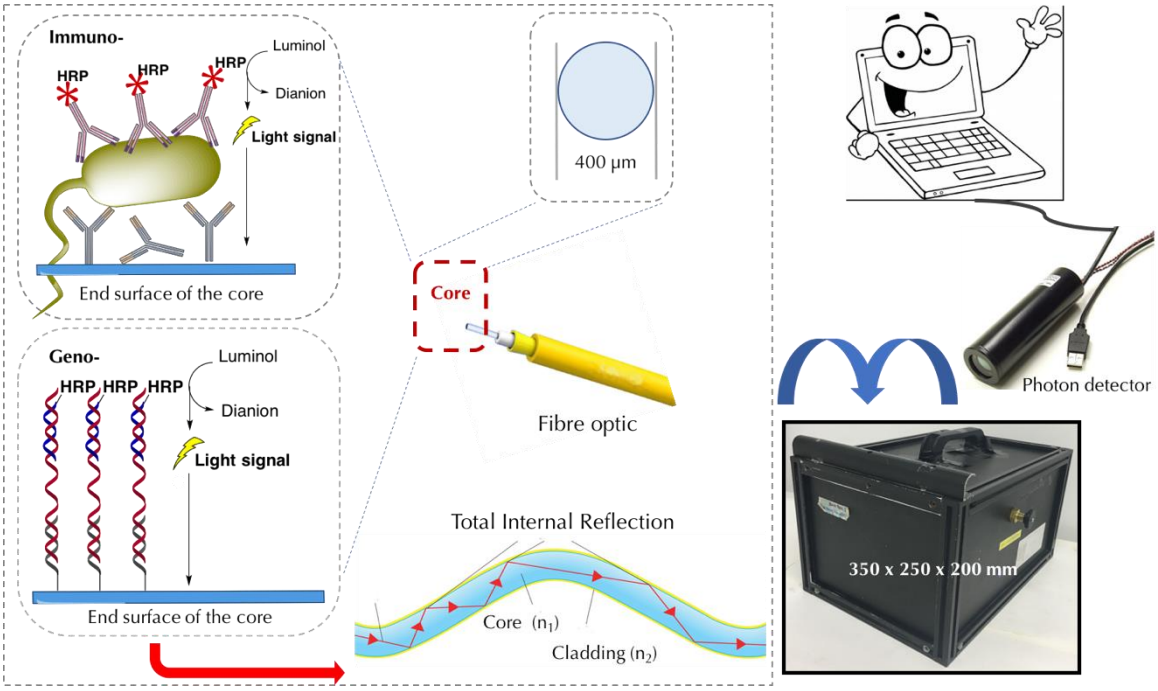

Figure 1.1 Construction of an immuno- or geno-CFOS.

1.2 Hypothesis

Based on the problems and the reviewed previous work, the following hypotheses are proposed under this project:

Hypothesis #1: An aliphatic silane diazirine can be used as a bifunctional crosslinker to immobilize antibody in the aqueous buffer solution onto the fibre optic surface by UV activation and maintain its immunoactivity. The hypothesis is based on the facts that, upon UV activation at 340 - 370 nm, which is not harmful to the protein structures at different levels, the diazirine molecule transforms to a carbene intermediate which inserts into various chemical bonds on the side chains of the antibodies as illustrated in **Figure 1.2**. The silane moiety on the other end is able to connect to the hydroxyl groups on the silica-based fibre surface.

Hypothesis #2: The combination of the better stability and proximity of covalent binding and the higher immobilization efficiency of the diazirine crosslinker will bring higher sensitivity of an immuno-CFOS compared to the traditional 96-well ELISA method and the immuno-CFOS constructed by glutaraldehyde silane method. The hypothesis is based on the facts that, the covalent binding method used for capture antibody immobilization on optical fibre is more stable and bring closer proximity of the light signal generation than the physical absorption used in the 96-well ELISA method. On the other hand, the carbene intermediates react with a broader range of functional groups in a considerably shorter time than the chemical silane tails do, which will lead to more efficient antibody binding.

Hypothesis #3: The sandwich structure formed by the NH_2-modified 24 base ssDNA capture probe, target sequence and the HRP-linked 24 base ssDNA detection probe on the end face of the fibre optic (shown in **Figure 1.1**) will enable the geno-CFOS to perform the sensing ability to HAV cDNA and RNA in high specificity and sensitivity due to the following suppositions: (1) the unique region of the HAV target sequence; (2) the enhanced selectivity by the combination of two probes targeting at different target regions, which makes the complementarity degree to 48 base-pairs, leading to a stronger and more specific hybridization.

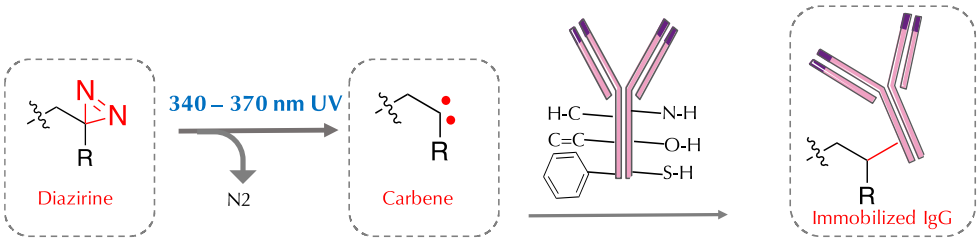

Figure 1.2 Antibody immobilization mechanism of diazirine.

1.3 Objectives and scope

This work targets at developing and improving the immuno- and geno-CFOSs for rapid, sensitive and specific detections of *E. coli* and HAV respectively. To achieve this goal, a few sub-objectives are established that are correlated to the specific work done in the results chapters.

1. To synthesize silane-diazirine and to confirm its photoimmobilization ability of antibody in aqueous conditions by UV activation.
2. To confirm that the immunoactivity of the antibody is maintained after the UV induced immobilization by silane diazirine.
3. To explore the optimum diazirine functionalization route.
4. To optimize the immunosensor performance by selecting the type of diazirine (aliphatic vs. aromatic) and the diazirine UV activation condition.
5. To evaluate the performance of the immuno-CFOS constructed by diazirine by (1) the parameters in the calibration curves comparing with previous methods; (2) the specificity test using polyclonal and monoclonal antibodies.
6. To design the ssDNA probes and primers and to validate the ssDNA probes by the traditional PCR-based method.
7. To explore the optimum immobilization and working conditions for the geno-CFOS.
8. To explore the genosensor performance by evaluating the calibration curves and specificity.

The scope of the thesis includes: the device used in this project is based on the CFOB concept as described in **Figure 1.1.** The chemiluminescent signal generation is based on the oxidation of luminol with the presence of HRP as a catalyst once the full biostructure is formed. The fibre optic used is silica based fibre which transmits light

via the total internal reflective (TIR) mechanism. The work in the project is mainly performed on the tip of the fibre optic with a diameter of 400 µl, which is divided into two major parts: in the immunosensor part, a new UV-induced capture antibody immobilization method using silane diazirine crosslinker will be investigated from its synthesis, functionalization conditions and efficiency. The target analyte is laboratory *E. coli* strains. In the genosensor part, new probes targeting at the RNA and cDNA sequences of HAV will be designed and integrated into the genosensor platform by a series of optimization work. The final performances of the immuno- and geno-CFOSs will be evaluated by the calibration curves and specificity tests.

1.4 Dissertation overview

This dissertation comprises of 8 chapters:

Chapter 1 presents the hypothesis, provides a rationale for the research and outlines the objectives and scope.

Chapter 2 reviews the previous related work concerning environmental pathogens monitoring, the current *E. coli* and HAV detection methods, immuno- and geno-CFOSs, antibody immobilization methods, the working mechanism of diazirine and its applications on protein-based molecule immobilization.

Chapter 3 discusses the strategy and rationale for materials and methods employed. Experimental details can also be found in this section.

Chapter 4 elaborates the silane-diazirine synthesis and characterization, followed by the confirmation of its antibody immobilization ability through UV activation.

***Chapter* 5** compares the two diazirine functionalization routes together with a few selection work of the biological materials used.

Chapter 6 discusses the optimization of the protocol based on the optimum route from Chapter 5 and devaluates the immunosensor performances.

Chapter 7 presents the construction of genosensor for HAV detection including probe design and validation, protocol optimization, sensor calibration and specificity evaluation.

Chapter 8 concludes and summarizes the major findings of the project and suggests future work. It also addresses the extent of the verification of the hypothesis and the fulfillment of the designed targets.

1.5 Findings and outcomes/originality

This project has led to several novel outcomes by:

1. Developing a diazirine-mediated antibody immobilization method on the silica-based fibre optics in aqueous buffer.
2. Establishing an optimized sensitive chemiluminescent immuno-sensor for *E. coli* cells detection.
3. Designing a set of sensitive and specific ssDNA probes targeting at HAV RNA sequence.
4. Constructing a portable chemiluminescent genosensor for HAV detection.

References

[1] Ramírez-Castillo, F. Y.; Loera-Muro, A.; Jacques, M.; Garneau, P.; Avelar-González, F. J.; Harel, J.; Guerrero-Barrera, A. L., *Pathogens* **2015,** *4* (2), 307-334.

[2] Alhamlan F, A.-Q. A., Al-Ahdal M *The Journal Of Infection In Developing Countries* **2015,** *9* (02), 128-135.

[3] Ho, J.-a. A.; Hsu, H.-W.; Huang, M.-R., *Analytical biochemistry* **2004,** *330* (2), 342-349.

[4] Organization, W. H., *Progress on sanitation and drinking water: 2015 update and MDG assessment*. World Health Organization: **2015**.

[5] Harris, L. M.; Goldin, J. A.; Sneddon, C., *Contemporary water governance in the global south: Scarcity, marketization and participation*. Routledge: **2015**.

[6] Bitton, G., *Microbiology of drinking water production and distribution*. John Wiley & Sons: **2014**.

[7] Soller, J.; Embrey, M.; Tuhela, L.; Ichida, A.; Rosen, J., *Journal of Environmental Management* **2010,** *91* (11), 2329-2335.

[8] Ahmed, A.; Rushworth, J. V.; Hirst, N. A.; Millner, P. A., *Clinical microbiology reviews* **2014,** *27* (3), 631-646.

Chapter 2

Literature Review

The historical and contemporary work related to the scope of the thesis is reviewed in this chapter. It first overviews the background information of environmental monitoring and then goes to the details of waterborne pathogens detection with the focus on the current detection methods of E. coli and HAV. The third part starts with the background of biosensors, with the key points of biosensors being addressed. The specific studies on the immunosensor and the DNA-based array are then presented including the technique development and a few examples of applications. The fourth part reviews the immobilization techniques with emprise on the diazirine method. At last, the gaps between the literature and the thesis are established.

2.1 Environmental monitoring

Urbanization, industrialization, and population growth are creating increasing burden on the environment by resource consumption and concomitant pollutants deposition[1]. Studies have shown that the expanding of human activities are greatly changing the air, soil, water and biota in unexpected ways [2-3], which in turn lead to an increasing concern in protecting the environment. The main attentions were focused on the concept of environmental monitoring, which is the recurring and systematic measurement of the physical, chemical and biological variables in order to reveal the current state and establish trends in the environment. The results of the monitoring will be reviewed and analyzed for the environmental impact assessments, particularly in the circumstances where the human activities may carry harmful effects on the environment. This information is fundamental for researchers, decision-makers, and the community, to take necessary actions to preserve and sustain a healthy environment for future generations.

Environmental monitoring is a very broad issue and it demands a multi-disciplinary scientific effort. The monitoring programmes are generally implemented in four major phases [4]:

1. *Frame the problem*: define the problems and clarify the objectives; develop a conceptual model of the system and identify management policy action(s).
2. *Design the monitoring actions*: select and develop the data collection and analysis, components based on 1.
3. Implement the monitoring and analysis the data
4. Learn to improve the monitoring process or revise 1, 2 and 3.

An inappropriate decision on the selection of the components or methods in any of the above steps may lead to failure of the monitoring programme. One of the crucial elements, which is also the focus of the thesis, is the development of the detection method. The basic requirements for a good measurement should be repeatable, biased and likely to produce a large number of zero values [4]. Details in the selection of the measurement methods will be discussed in the specific applications in the following sections

2.2 Waterborne pathogens monitoring

The environmental water monitoring is based on several guidelines that specify the categories, species and the concentration limits of the determined pollutants. The water hazard includes physical, chemical and biological properties changes and the presence of health-risk contaminants [4]. The biological risk mainly comes from the waterborne pathogens which have been identified into bacteria (538 species), viruses (208 types), parasitic protozoa (57 species), and several fungi and helminths species [5].

Currently, there is no single method able to collect and analyze a water sample for all the pathogens of interest [6]. The challenges of the detection methods such as differences in physical properties between the major pathogen groups, low concentration of pathogens and the presence of inhibitors from the sample [6]. The culture based techniques are most extensively used for pathogens detection in water are there are also a number of molecular methods available including immunoassay and PCR-based techniques.

2.2.1 *E. coli* detection

Escherichia coli (*E. coli*) is a gram-negative, facultatively anaerobic, rod-shaped, coliform bacterium of the genus *Escherichia* that is a common inhabitant in the lower part of the intestines of warm-blooded animals [7]. Most *E. coli* strains are harmless and are expelled into the environment within fecal matter. *E. coli* survives in water for 4 - 12 weeks, depending on environmental conditions (temperature, chemical contents and microflora, etc.) [8]. In many countries, drinking and recreation water safety regulations are based on the presence of the fecal indicator bacteria [9]. Even not perfectly matching the indicator criteria [8], non-pathogenic *E.coli* is still regarded as the most reliable indicator as it was found to correlate better with the potential presence of its illness strains like O157:H7 or other pathogens causing enteric disease [8], and the detection methods for *E. coli* are relatively easy and inexpensive [10].

Despite the extensive use of culture-dependent detection methods, they are limited by the low sensitivity, specificity and a large time-commitment to obtain reliable results [10]. On the other hand, the immunoassay method, mainly ELISA, is easier, faster and less expensive, hence it is generally performed before going into polymerase chain

reaction (PCR) based methods [11]. Even though the lower detection limit (LDL) of conventional ELISA for *E. coli* is generally in the range of 10^5 to 10^7 CFU/ml [12], various modifications have been done to improve the sensitivity of the strategies based on the ELISA principles: a functional nanoparticle-enhanced ELISA could detect 68 cells/mL of *E. coli* O157 : H7 [12]; a combination of magnetic microparticles and AuNP method gives detection limit of 10^2 CFU/mL of *E. coli* O157:H7 [13]. Immunoarray-based biosensor methods have also been noted: a paper striped chemiluminescent immunosensor (LDL: 1 × 10 CFU/mL) [14]; an SPR detection using polyclonal and monoclonal antibodies to *E. coli* O157:H7 (LDL: 10^4 CFU/mL) [15]; an amperometric immunosensor for the detection of *E. coli* (LDL: 10 CFU/ml) [16]; an indirect optical biosensor using anti-*E. coli* O157:H7 antibodies with fluorescent labeling (LDL: 360 cells/mL) [17].

2.2.2 HAV detection

Hepatitis A virus (HAV) infection is responsible for around half of the total number of hepatitis infections diagnosed worldwide [18], presenting a major public health problem in many parts of the world [19]. HAV is a virus classified in the *Hepatovirus* genus within the *Picornaviridae* family [18]. It is a nonenveloped virus containing a positive-sense, single-stranded RNA genome of 7.5 kb which is polyadenylated at the 3′ end and has a polypeptide (VPg) attached to the 5′ end [20]. Studies show it has an estimated infectious dose of 10 - 100 particles [18]. HAV infection is a self-limiting disease [21-22]. The signs of infection usually don't appear until a few weeks after exposures and in most cases, resolve within six months. The symptoms may include: fatigue, nausea, vomiting, abdominal discomfort, low-grade fever, joint pain and jaundice. The symptoms are typically more severe in older children and adults than in children less than six years old, in whom 70% of cases are asymptomatic [23-24]. Although rare, cases of acute liver failure and death may happen, particularly in the elderly and in patients with pre-existing liver diseases [23, 25-29]. In the environment, HAV can survive for more than one month [30] and is reported to be resistant to many physical and chemical pressures [31-35]. This has enabled HAV to play a significant role in many outbreaks worldwide [18-19, 23, 25, 27, 36-38] with 1.4 million new cases reported every year according to World Health Organization [22]. In most cases, HAV is transmitted via the fecal-oral

route [23, 39], mainly through ingestion of contaminated water and/or food, particularly shellfish, fruits and salad [30].

In view of the morbidity and economic losses to human society, it is important to have a fast, sensitive and reproducible preventive method for timely detection of HAV in water and food samples. Traditional virus infectivity assays and immunoassays have been found to be unsuitable for HAV detection as they require long incubation times and the presence of virus in the samples is generally of limited quantity [23, 39]. Instead, nucleic acid-based detection techniques have become the most popular methods for HAV detection due to their accuracy and sensitivity, such as with reverse transcriptase polymerase chain reaction (RT-PCR) (LDL: 0.15PFU [40]), real-time quantitative PCR (RT-qPCR) (LDL: 1PFU[41]; 0.05 infectious unit and 10 copies of a synthetic single-stranded RNA[42]; 0.5 infectious units of HAV and 40 copies of a synthetic transcript [43]; HAV 5×10^2 $TCID_{50}$ g^{-1} [44]) or nested real-time quantitative PCR (LDL: 0.2 PFU [45]; 0.1 PFU [46]; 1 $TCID_{50}$/10 g [47]).

2.3 Biosensors

Biosensors are compact devices that integrate the bio-receptor and transducer to provide selective analytical information of one or more target analyte [48-49]. The modern concept of a biosensor owns much to the idea of Leland C. Clark Jr., known as the father of biosensors, and his co-workers in 1962 with the development of an enzyme-based biosensor that monitored the blood glucose level by producing an electrical signal [50]. Since the invention of Clark, its simplicity, convenience and accuracy in detection have drawn increasing attentions, resulting in a fast growth of biosensor research. There are many ways that a biosensor can be used: qualitative (pregnancy lateral flow test), quantitative or semi-quantitative (glucose level test or contaminations in food), can either give trend information or accurate numbers, on which appropriate decision making can be based [51-52]. Nowadays, a few biosensors for medical diagnosis, for example, glucose and pregnancy tests are already commercialized with a huge market potential [51]. Food, agriculture, medicine, environment and defense services are also potential areas for commercial biosensors, where considerable academic research has been concentrated [53]. According to a recent market report, the global biosensor market is estimated at USD 12.9 billion in 2014 and is expected to reach USD 22.5 billion by

2020. Growing at a CAGR of 10.7%, optical biosensors, in particular, will likely emerge as the fastest growing segment in the biosensor market by 2020 [54].

Although the biosensors have been refined in different ways during the recent decades, the core of the working principle, as illustrated in **Figure 2.1**, remains the same: every biosensor is composed of a bio-recognition element and a transducing element. The bio-element interacts very specifically with certain substances through biochemical mechanisms and the change of the biomolecule is subsequently transformed through the transducer to a measurable signal, which has a given relationship with the concentration of the target analyte [55]. Biosensors can be classified according to the transducing elements involved. Most of the transduction methods fall in one of the five main categories: optical, gravimetric, piezoelectric, magnetic and electrochemical [56-57]. Each type of biosensors cooperates with a variety of bio-entities which are specific to the analyte of interest [57]. Another important issue in biosensor is the immobilization method coupling the two components together, which is a key to its performance [56]. The most commonly used immobilization techniques are physical adsorption [58], membrane entrapment [59], matrix entrapment [60-61], inter molecular cross-linking [62] and covalent binding [63-65]. Other factors that affect the biosensor function may be the chemical and/or physical conditions (pH, ion strength, temperature and impurities), thickness and stability of the materials [52, 66].

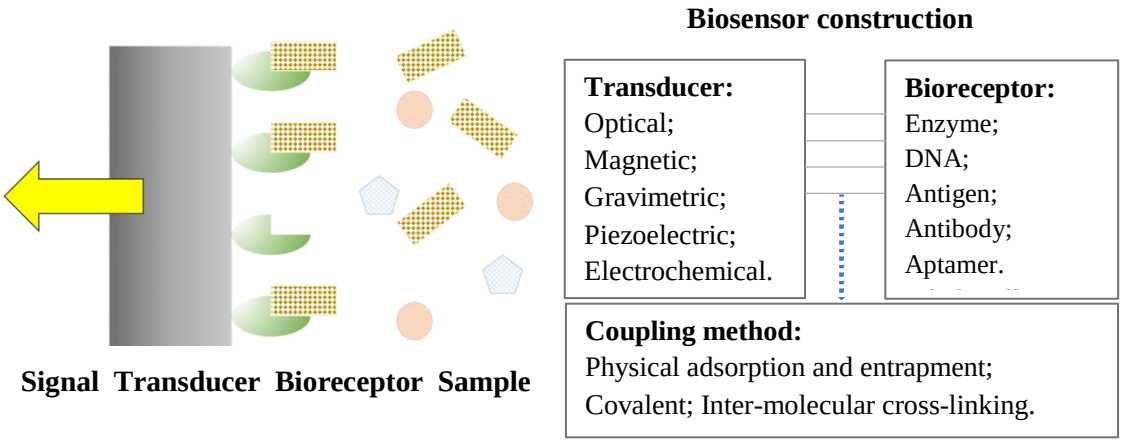

Figure 2.1 Working principles and the core elements of a biosensor.

2.3.1 Fibre optic biosensors

As its name signifies, silica fibre optic biosensor is the type that utilizes silica-based fibre optic as the transducer, which is a highly flexible, transparent, dielectric and hair-thin strand. A fibre optic is mainly consisting of: (1) a glass (silica) core as the light carrier; (2) a layer of glass cladding which limits the light rays in the core by total internal reflection (TIR); (3) an outer jacket that protects the fiber from physical or chemical damages during handling. The chemical and physical natures of the glass core enable the immobilization of a variety of biospecific recognition elements onto the surface including enzyme [67], immunomolecules [68-69], microorganisms [70-72] and DNA probes [73] using a number of methods based on the appealing of different conditions, allowing for various biological activities happening on the detection interface. Also, during light propagation, the FO carrier is immune to the interferences coming from electrical and magnetic sources or extreme environmental temperatures thus allowing for remote detection [74]. In addition, FO is particularly favoured for portable device development due to its flexibility and the ability to be miniaturized [74].

2.3.2 Immuno-CFOS

The fibre optic immunosensor model proposed in this project as shown in Section 1.1 has been already applied for the detections of *brucella* cells [75], cholera antitoxin [76], dengue virus IgM antibody [69], West Nile virus IgG antibodies [77], Ebola virus antibodies [78], Crimean-Congo Hemorrhagic fever IgG antibodies [68], Rift Valley fever virus IgG antibodies [79] and ovarian and breast cancer-associated antigens autoantibodies [80]. The immobilized capture agents were either the antigens or antibodies based on the detection purpose and samples. Both the capture and detection can be in direct and indirect formats. In these studies and applications, the FOISs generally have lower detection limits and higher sensitivities than the traditional chemiluminescent or colorimetric ELISA [81]. Within the FOISs, most of the capture agents are immobilized through the silanes bearing various chemical reactive tails including –CHO, –NHS, epoxy and benzophenone groups, in which, the FOISs constructed by photoinducible benzophenone crosslinking method showed better sensing ability [82].

Table 2.1 Recent examples of DNA-hybridization array based biosensors

	Target	Signal transduction	Method	LDL	Ref
1	Influenza H7N9	EC[a]	ssDNA capture probe supported by a tetrahedral nanostructure on gold electrode	100 fM	83
2	Influenza H5N1	EC	combination of gold nanoparticles, graphene and flower-like VS_2 modified glassy carbon electrode as platform	52 fM	84
3	Influenza H1N1	EC	AuNPs modified carbon electrode	0.1 pM	85
4	Hepatitis B virus (HBV)	EC	gold nanorods (AuNRs) as amplification element on gold electrode	2 pM	86
5	*Salmonella*	EC	lable-free impedimetric detection on nanoporous glassy carbon electrode	0.15 pM	87
6	Human papilloma virus (HPV)	EC	graphene/Au nanorod/polythionine (G/Au NR/PT) modified glassy carbon electrode for signal enhancement	40.3 fM	88
7	Oral cancer overexpressed 1 (ORAOV1)	EC	combination of the nicking endonuclease assisted target recycling and the immobilization-free electrochemistry as signal amplification method	0.35 pM	89
8	Acute promyelocytic leukemia (APL)	EC	a dual-probe DNA biosensor taking advantage of Y junction structure and restriction endonuclease assisted cyclic enzymatic amplification	47 fM	90
9	Lung cancer cell (H460)	FRET[b]	combination of endonuclease MscI and a single base extension reaction	5.3 aM	91
10	*Neisseria meningitides*	EC	flower-like ZnO nanostructures modified platinized silicon substrate	5 ng/μL	92
11	*Mycobacterium tuberculosis*	EC	template assisted electrochemical deposition technique was used for the synthesis of gold nanotubes array	0.05 ng/μL	93
12	P53 tumor suppressor gene	ECL[c]	combination of amplification methods of nicking endonuclease assisted target recycling and hyperbranched rolling circle amplification	0.02 fM	94
13	Breast cancer overexpressed c-erbB-2 oncogene	UCL[d]	ExoIII-assisted target cycles and long-range self-assembly DNA concatamers as dual signal amplification elements	40 aM	95
14	*Escherichia coli* O157:H7	EC	HRP-mimicking G-quadruplex/hemin DNAzyme wrapped GOx nanocomposites as tag	0.01 nM	96
15	*Klebsiella pneumoniae carbapenemase* (KPC)	EC	AuNPs and graphene modified glassy carbon electrode	0.2 pM	97
16	Thermolabile hemolysin	EC	single-walled carbon nanotubes–carboxyl-functionalized graphene oxide-based sensing platform	72.1 fM	98
17	Human immunodeficiency virus type 1 (HIV-1)	SERS[e]	SERS-based lateral flow assay; colourimetry	0.24 pg/mL	99
18	*Erwinia carotovora* *Rhazictonia solani*	liquid-crystal	liquid-crystal (LC)-filled transmission electron microscopy (TEM) grid cell coated with the cationic surfactant dodecyltrimethylammonium bromide (DTAB)	0.05 nM	100

a. EC (electrochemistry)

b. FRET (fluorescence resonance energy transfer)

c. ECL (electrochemilumin-escence)

d. UCL (upconversion luminescence)

e. SERS (surface-enhanced Raman scattering)

2.3.3 DNA-hybridization array based biosensor

The specific DNA CFOB model shown in Section 1.1 has not been as extensively studied yet except for a preliminary work on the DNA of *Brettanomyces bruxellensis* [73], the optimized condition has led to a satisfactory signal/noise ratio but the sensor calibration is lacking. However, biosensors using DNA or RNA sequence hybridization have been studied for pathogen detection in various platforms [101-102]. The well-known specific hydrogen bonding behaviours between NA strands are the main working basis of the DNA detection method. Because of such simplicity, and a sensitive and variable technological foundation provided by the genomic sequences analysis, DNA hybridization technique is even more frequently used in a diagnostic laboratory than the direct sequencing method [102], especially in the detection of pathogens and the differentiation of genetic variations (**Table 2.1**).

In order to bring a high S/N ratio, there are also various factors should be well controlled in the process including ionic strength, working temperature, ssDNA probe sequence design and concentration [103]. The choice of the signal transducers should also be carefully selected in order to adapt to specific applications [102].

2.3.4 Chemiluminescence as the signal generation mechanism

There are a few signal generation methods used for biosensors including fluorescence, electrochemistry, electrochemiluminescence (ECL), chemiluminescence (CL), colorimetry, surface plasmon resonance (SPR) and so on. The CL mechanism seems to be the most suitable model to be incorporated with the fibre optic biosensor context due to a few attractive advantages such as they working in the absence of a light source; avoiding light scattering and the ability for trace analysis, which allow CL method processing high sensitivity, wide calibration range, simplicity in instrument setup and the possibility for miniaturization [104-105].

The luminol-H_2O_2 reaction mixture with HRP catalyst is the most widely used CL mechanism. The chemical reaction yields 6-aminophthalate in a singlet excited state, which emits photons at 425 nm during relaxation [106-108] which are imaged or recorded over a defined decay time between 1 s and some minutes by the use of a CCD camera or a PMT [105]. The direct proportionality of the light intensity to the number of HRP is

used for analytical purposes. The overall quantum yield of the CL reaction is 0.001 to 0.1 [109] and can be enhanced by the use of p-iodophenol (PIP) [110], 4-(1-imidazolyl)phenol [111], or other p-phenol derivatives [112] and multi-HRP labels [113]. A constant, preferably relatively higher temperature must be maintained, as the change of the temperature affects the diffusion coefficient of the reaction product and the activity of the HRP enzyme thus leading to a variance of light signals [114-115].

2.4 Immobilization strategies on fibre optic

One of the greatest challenges that define the performance of an optical fiber biosensor is the immobilization of the receptor molecules onto the surface of fibre optic [81-82]. Covalent binding has been favoured in this context due to its stability, that the bonded molecule is firmly attached to the proximity of the solid surface and therefore more robust towards environmental and processing conditions [67].

2.4.1 Silanization as a general method for surface activation

Silanization has been the most extensively employed surface activation procedure to introduce a variety of reactive chemical groups onto the silica-based surfaces [74, 82], making them ready to accommodate the biomolecules of interests. Silanes are a group of bifunctional coupling reagents as shown in **Figure 2.2**, with one end being constituted by hydrolysable groups, usually 1~3 units of alkoxy or chloro groups, which then form siloxane bonds with the hydroxyl groups on the fiber core surface; the other end commonly bearing reactive chemical tails such as -SH, -CHO, -NH2, -COOH [67, 69, 82] or epoxy [68] which bind to biomolecules.

Several commonly used functional silane with respective chemical groups on antibody backbones are presented in **Table 2.2**.

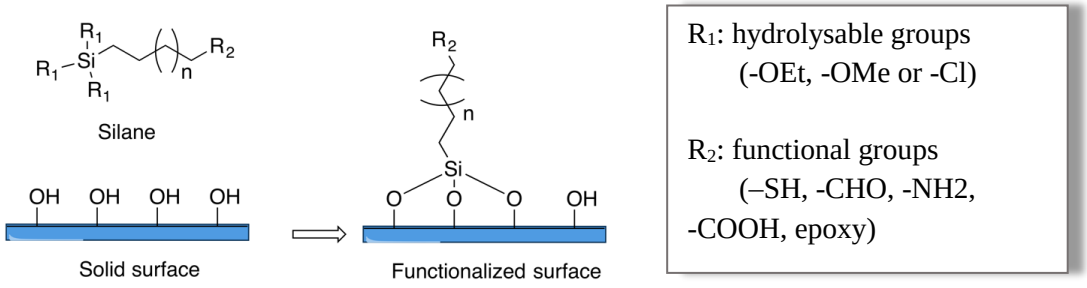

Figure 2.2 Silane for crosslinking reactions.

Table 2.2 Functional groups on antibody (Ab) backbones that are available for crosslinking with functional tails of silane

Ab Functional Groups	Location and distribution	React with silane tails (R_2)
–NH_2	numerous lysine residues over the entire antibody, and the N-terminus of each polypeptide chain [116]	-CHO [117]; epoxy [118]; NHS [119-121]; -COOH [116]
–SH	cysteine residues over the entire antibody (cycteins are not as abundant as lysine [122]); reduction from disulfide bonds	Maleimide [116, 123]; -SH [124]
–CHO	carbohydrate residue after oxidation from Fc region of IgG	-NH_2 [117]
-COOH	carboxyl-terminal	EDC-NHS [125]

2.4.2 Photoinducible crosslinkers

Amongst many methods for covalent crosslinking on solid substrates, the group of photoinducible crosslinkers have been favoured recently, such as aryl azides [126-128] benzophenone [82, 129-131] and diazirine moieties [132-134]. The major advantages of these approaches are (1) the greater efficiency due to highly reactive activated intermediates [135] (which are nitrenes, ketyl radicals and carbenes, respectively, **Figure 2.3**); (2) the much tidier procedures compared with the traditional chemical approaches [136]. Furthermore, benzophenone and diazirines can be irradiated under longer UV wavelengths [131, 137], which is not harmful to the native structures or the biological activities of protein-based biomolecules such as antibodies, some antigens and enzymes, which are essential for the function of a bio-array [137-139].

As an early attempt to make use of the photoinducible molecules as the crosslinkers on a solid surface, silane-benzophenone hetero-crosslinkers were first synthesized and characterized by Pruker and co-workers in 1999 [129] followed by a lot of work in exploring their abilities in protein immobilization [75, 82, 131]. In a particular study on the immobilization strategies of *Brucella* particles on optical fibers, it has shown a superior adaptability over traditional covalent binding methods in the construction of chemiluminescent immunosensors [82] by lowering detecting limit, improving sensitivity and maintaining the function of biomolecules. Until now, the use of the diazirine

moieties as new members of PIC group in biosensors remains relatively unexplored [137, 140]. Their most common utilization is in photoaffinity labeling in biological applications, which have however suggested that it could be more effective than benzophenone in photocrosslinking for solid surface fabrication [138-145].

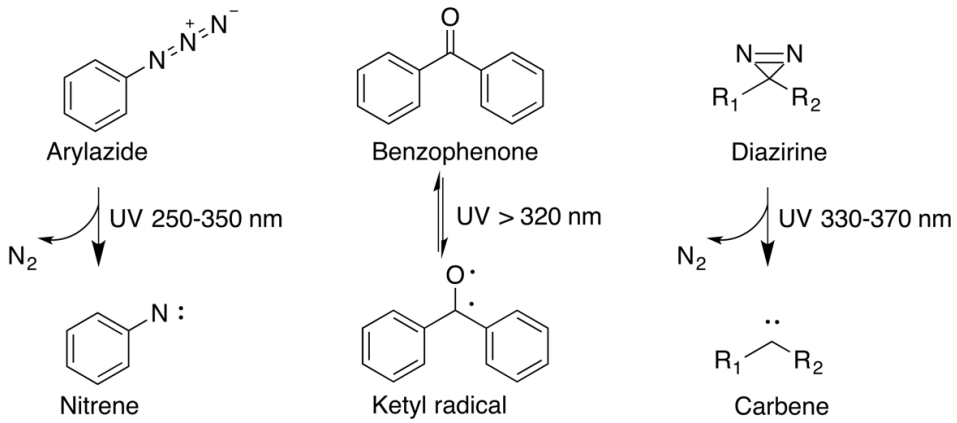

Figure 2.3 Most common photoinducible crosslinkers and their active intermediate under UV irradiation.

2.4.3 Diazirine for protein crosslinking

Being first synthesized in 1960 [146-147] and their structures being confirmed in 1962 [148-149], diazirines hadn't gained too much attentions until they were identified as potential photoprobes in the 1970s by Jeremy Knowles and co-workers [150-151]. These three-membered ring systems consist of two double bonded nitrogen atoms and an sp^3 hybridized carbon [143]. Highly reactive carbene can be easily generated with the extrusion of one N_2 molecule in the exposure of UV light at 330 - 370 nm [137], which not only reacts with C-H bond like benzophenone does, but also with O-H, N-H [137], X-H (X = heteroatom) [138] C=C and aromatic systems [143] (**Figure 2.4**) and thus expanding the number of reactive sites on the target protein side chains.

2.4.3.1 Generation of carbene: molecular orbital explanation

During the formation of carbene upon excitation, the two σ bonds between the sp^3 C atom and the two N atoms are broken and the two bonding electrons in each bond are reallocated into the newly formed free N_2 molecule and the carbene. This process is commonly explained by the orbital theories: in a ground state diazirine ring, the

HOMOs are the two nonbonding orbitals from the nitrogen atoms, each of which contains two electrons [152]. Upon absorption of quantum at 330 - 370 nm, these electrons are excited to the higher anti-bonding orbitals of the ring, decreasing the bond order and causing partial dissociation of the two N-C bonds [153]. Later relaxation of the excited state results in a complete dissociation of a free N_2 molecule and the formation of a carbene at the formally sp^3 carbon [153].

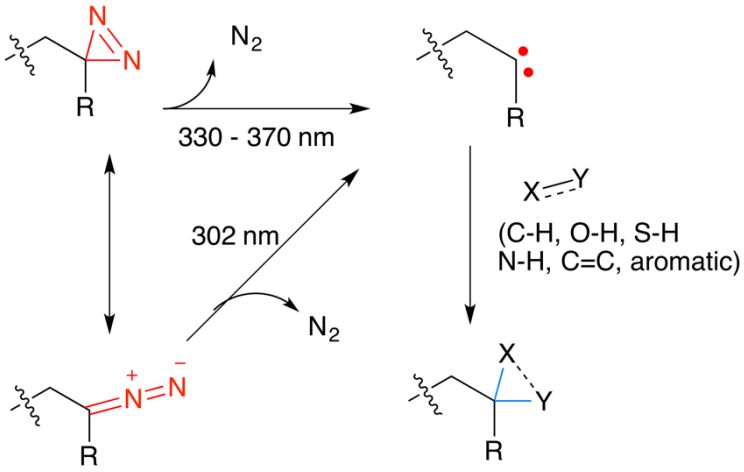

Figure 2.4 The general mechanism of diazirine-diazo isomerization, carbene generation and insertion reactions.

2.4.3.2 Triplet and singlet carbenes

The photolysis of a diazirine may lead to the formation of two different states of carbenes as shown in **Figure 2.5**: singlet, where the two electrons are spin-paired in one orbital; and triplet, where the electrons are distributed in two different orbitals [154]. The singlet carbenes are more advantageous for the purpose of crosslinking, because they usually insert more rapidly (the rate constants are found to be 10^7 - 10^9 L mol^{-1} s^{-1}) with almost any type of bonds (O-H, C=C, aromatic and even C-H) in the near proximity [141]. However, triplet carbenes are believed to be the more stable states due to the lower Coulombic repulsions between the two electrons (Hund's law). The energy gap between the two states was reported to be 8 to 10 kcal/mol [155-158]. Some substituents with electron donating nature are capable to reduce this energy gap by delocalizing their electrons to the empty p orbitals, for example, methyl and phenyl groups can reduce

the energy gap to 2 to 4 kcal/mol [159] with the triplet carbenes still being the ground state. The small energy gap resulted in a rapid equilibration between the two carbene states and the highly reactive singlet carbenes are predominant in most insertion process as evidenced by a few studies involving aromatically substituted diazirine species [160-161].

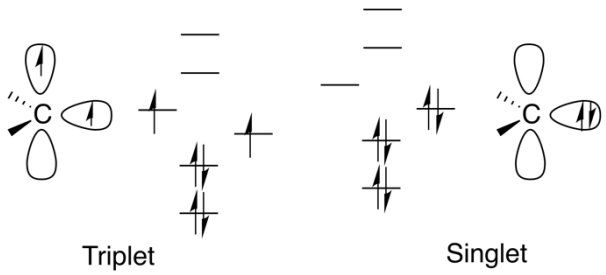

Figure 2.5 Orbital occupancy of triplet and singlet carbenes.

2.4.3.3 Carbene vs. diazo

Another important feature during the photo-irradiation is the non-inevitable isomerization process which generates the linear diazo compound (**Figure 2.6**). Diazo is much less reactive and with a much longer lifetime than a carbene, so it is not favoured for the crosslinking purpose [141]. Some studies suggest a second boosting irradiation at 302 nm as diazo is also able to generate carbene at this wavelength [139], which however is harmful to most protein or DNA based biomolecules thus not practical in such conditions.

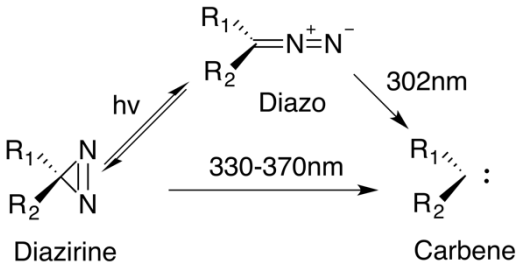

Figure 2.6 Simplified scheme of the formation of diazo and carbene from a diazirine compound.

2.4.3.4 RIES mechanism

The diazirine mechanisms are still not thoroughly understood and studies have been putting forward new theories in addition to the old ones [141, 162]. Recent studies have shown that the photolysis pathways lead to more complicated alkene products either by 1,2-H shift [163-167] or 1,2-C shift [163] concerted with the loss of N_2, indicating the existence of other intermediates. Some proposals include carbene-alkene complex (CAC) and the excited diazirine which undergoes rearrangement in the excited state (RIES) [163]. The latter condition is more convincing as being supported by both computational and spectroscopic evidence [141]. There are three possible types of non-radiative deactivation of the excited state according to the studies including the formation of carbene, formation of diazo and direct yield of alkenes [163-167]. (**Figure 2.7**)

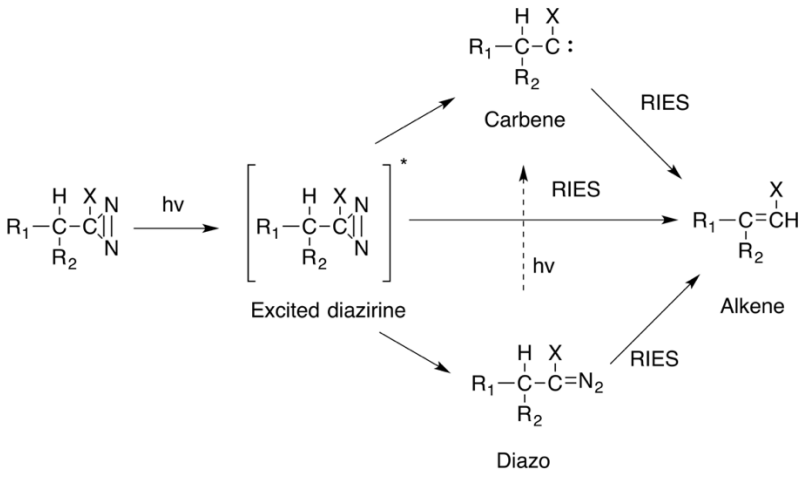

Figure 2.7 Pathways of diazirine RIES photolysis. The final product is an alkene compound formed by diazirine species bearing a halogen group.

2.4.3.5 Aromatic vs. aliphatic diazirines

Typically, the relative ratio of the mentioned photolysis intermediates and products depends on the nature of the substituents on the diazirine carbon center, with a general trend that the aromatic substituents bringing more carbenes and more singlet carbenes than aliphatic ones do [168-172]. Furthermore, the incorporation of a -CF_3 group to an aromatic diazirine is found to be more effective in preventing the generated carbene from going rearrangement [168-169]. Hence, the majority work of diazirine photolabeling and immobilization were carried out by 3-aryl-3-(trifluoromethyl) diazirines [173].

However, the large size of aromatic diazirine is not favoured during application [138-139] and its relatively more hydrophobic nature is not compatible with aqueous conditions [141], however, which is very important for macro-biomolecules to maintain their structures and functions.

2.4.3.6 Application of diazirine in the immobilization of protein on solid support

The utilization of diazirine in biomolecule immobilization on solid phase support is relatively less explored than benzophenone due to the facts that (1) the diazirine is relatively a new member as the photocrosslinker and (2) the newly generated carbene species can be quenched by water molecule if the target functional bonds are not present in the molecular vicinity during the carbene lifetime in microsecond scale [174]. Some pioneer work has been done with a few biomolecules in various procedures, in the context of this thesis, the research related to protein-based biomolecules, especially antibodies are summarized in **Table 2.3.** In which, most of the procedures are carried out by the trifluoromethyl-aryl-diazirine in dry conditions and the immobilized proteins are the fragments of antibodies. The substrates include polystyrene, silicon, SiO_2 and carbon nanotube.

2.5 Thesis vs. literature

This section put the thesis in the literatures context and shows the awareness of the gaps.

2.5.1 Photoinducible silane diazirine vs. chemically activated silane

The common chemically activated silane immobilization strategies described in Section 2.4.1 and **Table 2.2** bear a few drawbacks: (1) they only react to very limited numbers of functional groups [137], thus lowering the immobilization efficiency; (2) they are usually subjected to a series of chemical treatments [68], which not only make the procedure more complicated but also introduce more uncertainties that affect the binding affinity [131, 175]. The photoinducible silane diazirine approach is potentially able to make up the mentioned deficiency due to the facile activation, short lifetime and powerful insertion ability of the carbene intermediate.

2.5.2 Diazirine vs. other PICs

Diazirines are in general more stable in the ambient environment and the activation efficiency is higher than benzophenones [138-139]. Comparing to azide, diazirine requires longer UV wavelength which is transparent to biomolecules.

2.5.3 Silane diazirine vs. previous diazirine immobilization strategies

From the summary list in **Table 2.3**, it is noticed that, on one hand, the ability of diazirine in protein-based biomolecules immobilization was confirmed. On the other hand, most of the illumination processes were conducted in dry conditions to prevent the quenching effect of water, which is not ideal for antibodies applications as there is a high risk of denaturation. In addition, most of the applications utilized aromatic diazirines. With a hydrophobic nature, it is not compatible with aqueous conditions. However, a very recent work in enzyme immobilization on MWCNT/GC electrode involved an aliphatic diazirine which is easily obtained from suppliers, and it was conducted in aqueous condition [137], where the diazirine was integrated with pyrrole which was then deposited on the solid surface by electropolymerization. This work has inspired the concept of the combination of aliphatic diazirine and silane as a new and more adaptable heterobifunctional crosslinker for the modification of silica optical fibres. Furthermore, providing the sophisticated carbene mechanism described in 2.4.3.1 ~ 2.4.3.4, to what extent that the diazirine would serve its crosslinking function remains to answer by the outcome of the project.

2.5.4 The immunosensor vs. current *E. coli* detection methods

The focus of the immunosensor is the development of a silane diazirine as a new immunemolecules crosslinker and the evaluation of its efficiency by comparing with common detection/ crosslinking method. The author expects that the results can help to apply this method on the immobilization application of other protein-based biomolecules. *E. coli* is selected as a model analyte as the materials are easily accessible and the standard is well established.

Moreover, the application of biosensors in *E. coli* detection is becoming more popular due to the simplicity, portability, accuracy and cost efficiency. Comparing with the

reported methods in 2.2.1, the chemiluminescent fibre optic immunosensor is more simply constructed and the optical mechanism is able to give quantitative results and is generally more sensitive, by improving the immobilization method, the author hopes it would further improve the sensitivity of a portable detection device.

Table 2.3 Applications of diazirine as a crosslinker for biomolecules immobilization

	Immobilized biomolecules	Methods	Substrate	Remarks	Ref
1	anti-AFP[a] antibody; F(ab') and $F(ab')_2$ fragments of anti-PSA[b] antibody	T-BSA[c] mediated; Dried condition.	polystyrene	The immunologically activities remained after UV exposure; BSA stabilized molecular cooperativity;	176
2	amino acids: synthetic peptide: Anti-PSA F(ab'), $F(ab')_2$ fragments.	Heterobifunctional crosslinker (MAD[d]) mediated; Dried condition.	polystyrene; glass	Selective and oriented photoimmobilization of Fab fragments bearing thiol groups on solid support can be achieved through various procedures mediated by MAD heterocrosslinker.	177
3	anti-PSA whole antibody and F(ab') fragments	Aryl-diazrine grafted silicon surface; Dried condition.	silicon chips	Immobilization of antibodies through aryl-diazirine grafted silicon surface is possible.	136
4	anti-PSA $F(ab')_2$ fragments	T-BSA mediated; Dried condition.	TiO_2/SiO_2 waveguides	F(ab')2 fragments coverage on TiO_2/SiO_2 surface is achieved by T-BSA mediated method and retained immunoacitivity in ELISA procedure	178
5	myoglobin, streptavidin, trypsin, antibodies	liposomes formed by PED[e] in aqueous media.	liposomes	Either the liposome nor the immobilized proteins were altered by UV irradiation.	179-180
6	PSA antibody	sulfo-SDAD[f] grafted on EGPA[g]-modified surface	SiO_2/Si	The antibodies were successfully immobilized on the surface.	134
7	laccase, glucose oxidase	NHS-diazirine derived poly(pyrrole–diazirine)films; aqueous solution spotted	MWCNT/GC[h] electrode	The enzyme was efficiently immobilized on the MWCNT, and the resulting amperometric biosensor exhibited high biological activities.	137

a. Anti-AFP (Anti-Alpha-Foetoprotein)

b. Anti-PSA (Anti-Prostate-Specific Antigen)

c. T-BSA (Trifluoromethyl–aryl–diazirine functionalized BSA)

d. MAD (N-[m-[3-(trifluoromethyl)diazirin-3-yl]phenyl]-4-maleimidobutyramide)

e. PED (N'-(1,2-Dimyristoyl-sn-glycero-3-phosphoethyl)-N-[m-[3-(trifluoromethyl)diazirin-3-yl]phenyl]thiourea)

f. Sulfo-SDAD (Sulfo-NHS-SS-Diazirine)

g. EPGA (Ethylene glycol protected amine)

h. MWCNT/GC (Multiwalled carbon nanotubes/glassy carbon)

2.5.5 The genosensor vs. current HAV detection methods

Despite the highly sensitive detection ability, PCR-based detection tools (2.2.2) are limited by the requirement of heavy lab equipment, well-trained personnel, a relatively high cost and sometimes being affected by the potential presence of the polymerase inhibitors. To further improve the detection method in the potential field-operations, which would be more effective for early warning, DNA fibre optic genosensors emerge as a promising candidate attributed to their various attractive advantages: (1) they offer the solid phase DNA probes, being highly specific, sensitive, cheap and easy to synthesize; (2) the unique features of fibre optics provide the possibility for further equipment miniaturization and offer the flexibility as a dispatchable tool for most sites; (3) the absence for the need of PCR eliminates the usual inhibitive effect of polyphenol compounds to DNA polymerases reactions; (4) it is independent of thermal-cycler equipment and the operation is simpler hence not requiring well-trained lab personnel.

References

[1] Pepper, I. L.; Rensing, C.; Gerba, C. P., *Environmental Monitoring & Characterization* **2004,** *7* (2), 263–280.

[2] Wiersma, G. B.; Wiersma, G. B., *Crc Press* **2004,** *7* (3), 115-120.

[3] Stern, P. C.; Young, O. R.; Druckman, D., *Global environmental change : understanding the human dimensions*. National Academy Press: **1992**; p 25-28.

[4] Reynolds, J. H.; Knutson, M. G.; Newman, K. B.; Silverman, E. D.; Thompson, W. L., *Environmental Monitoring & Assessment* **2016,** *188* (7), 1-25.

[5] Bitton, G., *Microbiology of drinking water production and distribution*. John Wiley & Sons: **2014**.

[6] Straub, T. M.; Chandler, D. P., *Journal of Microbiological Methods* **2003,** *53* (2), 185-197.

[7] Tenaillon, O.; Skurnik, D.; Picard, B.; Denamur, E., *Nat Rev Micro* **2010,** *8* (3), 207-217.

[8] Edberg, S. C.; Rice, E. W.; Karlin, R. J.; Allen, M. J., *Symp Ser Soc Appl Microbiol* **2000,** (29), 106S-116S.

[9] Soller, J.; Embrey, M.; Tuhela, L.; Ichida, A.; Rosen, J., *Journal of Environmental Management* **2010,** *91* (11), 2329-35.

[10] Ramírez-Castillo, F. Y.; Loera-Muro, A.; Jacques, M.; Garneau, P.; Avelar-González, F. J.; Harel, J.; Guerrero-Barrera, A. L., *Pathogens* **2015,** *4* (2), 307-334.

[11] Priyanka, B.; Patil, R. K.; Dwarakanath, S., *The Indian Journal of Medical Research* **2016,** *144* (3), 327-338.

[12] Shen, Z.; Hou, N.; Jin, M.; Qiu, Z.; Wang, J.; Zhang, B.; Wang, X.; Wang, J.; Zhou, D.; Li, J., *Gut Pathogens* **2014,** *6* (1), 14.

[13] Kim, H.-S.; Oh, B.-K., *BioChip Journal* **2014,** *8* (1), 1-7.

[14] Park, S.; Min, J.; Kim, Y.-K., *International Journal of Environmental Analytical Chemistry* **2012,** *92* (6), 655-664.

[15] Taylor, A. D.; Yu, Q.; Chen, S.; Homola, J.; Jiang, S., *Sensors and Actuators B: Chemical* **2005,** *107* (1), 202-208.

[16] Abu-Rabeah, K.; Ashkenazi, A.; Atias, D.; Amir, L.; Marks, R., *Biosensors and Bioelectronics* **2009,** *24* (12), 3461-3466.

[17] Ho, J.-a. A.; Hsu, H.-W.; Huang, M.-R., *Analytical biochemistry* **2004,** *330* (2), 342-349.

[18] Sánchez, G., *Hepatitis A virus in food: detection and inactivation methods*. Springer: New York, **2013**.

[19] Chen, C. M.; Chen, S. C. C.; Yang, H. Y.; Yang, S. T.; Wang, C. M., *Journal of Viral Hepatitis* **2016,** *23* (11), 940-945.

[20] Leying, H.; Lu, N.; Newton, N.; Wolfelschneider, A.; Young, K.; Zimmermann, D., HAV detection. Google Patents: 2013.

[21] Kasper, D.; Jameson, J.; Hauser, S.; Loscalzo, J.; Fauci, A.; Longo, D., *Harrison's Principles of Internal Medicine 19/E (Vol.1 & Vol.2)*. McGraw-Hill Education: **2015**.

[22] Hepatitis A. http://www.who.int/mediacentre/factsheets/fs328/en/ (accessed 26 November).

[23] Yong, H. T.; Radu, S., *International Food Research Journal* **2009,** *16* (4), 455-467.

[24] Malani, P. N., *JAMA* **2010,** *304* (18), 2067-2071.

[25] Collier, M. G.; Tong, X.; Xu, F., *Hepatology* **2015,** *61* (2), 481-485.

[26] Siegl, *PRAXIS* **2003,** *92* (40), 1659-1673.

[27] Lee, S.-D., *Journal of Gastroenterology and Hepatology* **2000,** *15*, G94-G99.

[28] Ly, K. N.; Klevens, R. M., *Journal of Infectious Diseases* **2015,** *212* (2), 176-182.

[29] Ciocca, M., *Vaccine* **2000,** *18*, S71-S74.

[30] Normann, A.; Jung, C.; Vallbracht, A.; Flehmig, B., *Journal of medical virology* **2004,** *72* (1), 10-16.

[31] Scholz, E.; Heinricy, U.; Flehmig, B., *Journal of General Virology* **1989,** *70* (9), 2481-2485.

[32] Biziagos, E.; Passagot, J.; Crance, J.-M.; Deloince, R., *Applied and environmental microbiology* **1988,** *54* (11), 2705-2710.

[33] Siegl, G.; Weitz, M.; Kronauer, G., *Intervirology* **1984,** *22* (4), 218-226.

[34] Bidawid, S.; Farber, J.; Sattar, S.; Hayward, S., *Journal of Food Protection®* **2000,** *63* (4), 522-528.

[35] Arnal, C.; Crance, J.; Gantzer, C.; Schwartzbrod, L.; Deloince, R.; Billaudel, S., *Zentralblatt fur Hygiene und Umweltmedizin= International journal of hygiene and environmental medicine* **1998,** *201* (3), 279-284.

[36] Spada, E.; Genovese, D.; Tosti, M. E.; Mariano, A.; Cuccuini, M.; Proietti, L.; Di Giuli, C.; Lavagna, A.; Crapa, G. E.; Morace, G., *Journal of hepatology* **2005,** *43* (6), 958-964.

[37] Pavoni, E.; Dalzini, E.; Monastero, P.; Galuppini, E.; Meletti, F.; Bertasi, B.; Daminelli, P.; Losio, M.; Varisco, G., *The European Journal of Public Health* **2016,** *26* (suppl 1), ckw174. 037.

[38] Pal, S.; Juyal, D.; Sharma, M.; Kotian, S.; Negi, V.; Sharma, N., *Indian journal of medical microbiology* **2016,** *34* (2), 233.

[39] Sánchez, G.; Bosch, A.; Pintó, R., *Letters in applied microbiology* **2007,** *45* (1), 1-5.

[40] Kingsley, D. H.; Richards, G. P., *Applied and Environmental Microbiology* **2001,** *67* (9), 4152-4157.

[41] El Galil, K. H. A.; El Sokkary, M.; Kheira, S.; Salazar, A. M.; Yates, M. V.; Chen, W.; Mulchandani, A., *Applied and environmental microbiology* **2005,** *71* (11), 7113-7116.

[42] Costafreda, M. I.; Bosch, A.; Pintó, R. M., *Applied and Environmental Microbiology* **2006,** *72* (6), 3846-3855.

[43] Jothikumar, N.; Cromeans, T.; Sobsey, M. D.; Robertson, B., *Applied and environmental microbiology* **2005,** *71* (6), 3359-3363.

[44] Di Pasquale, S.; Paniconi, M.; De Medici, D.; Suffredini, E.; Croci, L., *Journal of virological methods* **2010,** *163* (1), 96-100.

[45] Hu, Y.; Arsov, I., *Letters in applied microbiology* **2009,** *49* (5), 615-619.

[46] Hu, Y.; Arsov, I., *Food and Environmental Virology* **2014,** *6* (3), 189-195.

[47] Croci, L.; De Medici, D.; Morace, G.; Fiore, A.; Scalfaro, C.; Beneduce, F.; Toti, L., *International Journal of Food Microbiology* **1999,** *48* (1), 67-71.

[48] Turner, A.; Karube, I.; Wilson, G. S., *Biosensors: fundamentals and applications*. Oxford University Press: **1987**.

[49] Banica, F.-G., *Chemical sensors and biosensors: fundamentals and applications*. John Wiley & Sons: **2012**.

[50] Clark, L. C.; Lyons, C., *Annals of the New York Academy of Sciences* **1962,** *102* (1), 29-45.

[51] Bahadır, E. B.; Sezgintürk, M. K., *Analytical Biochemistry* **2015,** *478*, 107-120.

[52] Kissinger, P. T., *Biosensors and Bioelectronics* **2005,** *20* (12), 2512-2516.

[53] Turner, A. P. F., *Chemical Society Reviews* **2013,** *42* (8), 3184-3196.

[54] Thomes, A. *Global Market Study on Biosensor: Asia-Pacific to Witness Highest Growth by 2020*; New York City, 2014-10-28, 2014.

[55] Mohanty, S. P.; Kougianos, E., *Ieee Potentials* **2006,** *25* (2), 35-40.

[56] Monošík, R.; Streďanský, M.; Šturdík, E., *Acta Chimica Slovaca* **2012,** *5* (1), 109-120.

[57] Mehrotra, P., *Journal of Oral Biology and Craniofacial Research* **2016,** *6* (2), 153-159.

[58] Nanduri, V.; Sorokulova, I. B.; Samoylov, A. M.; Simonian, A. L.; Petrenko, V. A.; Vodyanoy, V., *Biosensors and Bioelectronics* **2007,** *22* (6), 986-992.

[59] Pancrazio, J. J.; Bey Jr, P. P.; Cuttino, D. S.; Kusel, J. K.; Borkholder, D. A.; Shaffer, K. M.; Kovacs, G. T.; Stenger, D. A., *Sensors and Actuators B: Chemical* **1998,** *53* (3), 179-185.

[60] O'Connor, S. M.; Andreadis, J. D.; Shaffer, K. M.; Ma, W.; Pancrazio, J. J.; Stenger, D. A., *Biosensors and Bioelectronics* **2000,** *14* (10), 871-881.

[61] Gupta, R.; Chaudhury, N., *Biosensors and Bioelectronics* **2007,** *22* (11), 2387-2399.

[62] Nenkova, R.; Ivanova, D.; Vladimirova, J.; Godjevargova, T., *Sensors and Actuators B: Chemical* **2010,** *148* (1), 59-65.

[63] Schuhmann, W.; Lammert, R.; Uhe, B.; Schmidt, H.-L., *Sensors and Actuators B: Chemical* **1990,** *1* (1-6), 537-541.

[64] Williams, R.; Blanch, H., *Biosensors and Bioelectronics* **1994,** *9* (2), 159-167.

[65] Azmi, M. M.; Tehrani, Z.; Lewis, R.; Walker, K.-A.; Jones, D.; Daniels, D.; Doak, S.; Guy, O., *Biosensors and Bioelectronics* **2014,** *52*, 216-224.

[66] Polyak, B.; Bassis, E.; Novodvorets, A.; Belkin, S.; Marks, R. S., *Sensors and Actuators B: Chemical* **2001,** *74* (1), 18-26.

[67] Sassolas, A.; Blum, L. J.; Leca-Bouvier, B. D., *Biotechnology advances* **2012,** *30* (3), 489-511.

[68] Algaar, F.; Eltzov, E.; Vdovenko, M. M.; Sakharov, I. Y.; Fajs, L.; Weidmann, M.; Mirazimi, A.; Marks, R. S., *Analytical chemistry* **2015,** *87* (16), 8394-8398.

[69] Atias, D.; Liebes, Y.; Chalifa-Caspi, V.; Bremand, L.; Lobel, L.; Marks, R. S.; Dussart, P., *Sensors and Actuators B: Chemical* **2009,** *140* (1), 206-215.

[70] Eltzov, E.; Marks, R. S.; Voost, S.; Wullings, B. A.; Heringa, M. B., *Sensors and Actuators B: Chemical* **2009,** *142* (1), 11-18.

[71] Hakkila, K.; Green, T.; Leskinen, P.; Ivask, A.; Marks, R.; Virta, M., *Journal of Applied Toxicology* **2004,** *24* (5), 333-342.

[72] Polyak, B.; Bassis, E.; Novodvorets, A.; Belkin, S.; Marks, R., *Water Science and Technology* **2000,** *42* (1-2), 305-311.

[73] Cecchini, F.; Manzano, M.; Mandabi, Y.; Perelman, E.; Marks, R. S., *Journal of Biotechnology* **2012,** *157* (1), 25-30.

[74] Marazuela, M.; Moreno-Bondi, M., *Analytical and Bioanalytical Chemistry* **2002,** *372* (5-6), 664-682.

[75] Liebes, Y.; Marks, R. S.; Banai, M., *Sensors and Actuators B: Chemical* **2009,** *140* (2), 568-576.

[76] Marks, R. S.; Bassis, E.; Bychenko, A.; Levine, M. M., *Optical Engineering* **1997,** *36* (12), 3258-3264.

[77] Herrmann, S.; Leshem, B.; Landes, S.; Rager-Zisman, B.; Marks, R. S., *Talanta* **2005,** *66* (1), 6-14.

[78] Petrosova, A.; Konry, T.; Cosnier, S.; Trakht, I.; Lutwama, J.; Rwaguma, E.; Chepurnov, A.; Mühlberger, E.; Lobel, L.; Marks, R., *Sensors and Actuators B: Chemical* **2007,** *122* (2), 578-586.

[79] Sobarzo, A.; Paweska, J. T.; Herrmann, S.; Amir, T.; Marks, R. S.; Lobel, L., *Journal of Virological Methods* **2007,** *146* (1–2), 327-334.

[80] Salama, O.; Herrmann, S.; Tziknovsky, A.; Piura, B.; Meirovich, M.; Trakht, I.; Reed, B.; Lobel, L. I.; Marks, R. S., *Biosensors and Bioelectronics* **2007,** *22* (7), 1508-1516.

[81] Eltzov, E.; Marks, R. S., *IEEE instrumentation & measurement magazine* **2009,** *12* (5), 10-16.

[82] Liebes, Y.; Amir, L.; Marks, R. S.; Banai, M., *Talanta* **2009,** *80* (1), 338-345.

[83] Dong, S.; Zhao, R.; Zhu, J.; Lu, X.; Li, Y.; Qiu, S.; Jia, L.; Jiao, X.; Song, S.; Fan, C., *ACS applied materials & interfaces* **2015,** *7* (16), 8834-8842.

[84] Fang, L.-X.; Cao, J.-T.; Huang, K.-J., *Journal of Electroanalytical Chemistry* **2015,** *746*, 1-8.

[85] Falcone, N.; She, Z.; Chen, C.; Dong, B.; Yi, D.; Kraatz, H.-B., *Analytical Methods* **2017,** *9* (10), 1643-1649.

[86] Shakoori, Z.; Salimian, S.; Kharrazi, S.; Adabi, M.; Saber, R., *Analytical and bioanalytical chemistry* **2015,** *407* (2), 455-461.

[87] Tabrizi, M. A.; Shamsipur, M., *Biosensors and Bioelectronics* **2015,** *69*, 100-105.

[88] Huang, H.; Bai, W.; Dong, C.; Guo, R.; Liu, Z., *Biosensors and Bioelectronics* **2015,** *68*, 442-446.

[89] Tan, Y.; Wei, X.; Zhao, M.; Qiu, B.; Guo, L.; Lin, Z.; Yang, H.-H., *Analytical chemistry* **2015,** *87* (18), 9204-9208.

[90] Wang, K.; Lei, Y.; Zhong, G.-X.; Zheng, Y.-J.; Sun, Z.-L.; Peng, H.-P.; Chen, W.; Liu, A.-L.; Chen, Y.-Z.; Lin, X.-H., *Biosensors and Bioelectronics* **2015,** *71*, 463-469.

[91] Tang, W.; Zhu, G.; Liang, L.; Zhang, C.-y., *Analyst* **2015,** *140* (17), 5936-5943.

[92] Tak, M.; Gupta, V.; Tomar, M., *Biosensors and Bioelectronics* **2014,** *59*, 200-207.

[93] Torati, S. R.; Reddy, V.; Yoon, S. S.; Kim, C., *Biosensors and Bioelectronics* **2016,** *78*, 483-488.

[94] Yang, L.; Tao, Y.; Yue, G.; Li, R.; Qiu, B.; Guo, L.; Lin, Z.; Yang, H.-H., *Analytical chemistry* **2016,** *88* (10), 5097-5103.

[95] Lan, J.; Liu, Y.; Li, L.; Wen, F.; Wu, F.; Han, Z.; Sun, W.; Li, C.; Chen, J., *Scientific reports* **2016,** *6*.

[96] Li, Y.; Deng, J.; Fang, L.; Yu, K.; Huang, H.; Jiang, L.; Liang, W.; Zheng, J., *Biosensors and Bioelectronics* **2015,** *63*, 1-6.

[97] Pan, H.-z.; Yu, H.-w.; Wang, N.; Zhang, Z.; Wan, G.-c.; Liu, H.; Guan, X.; Chang, D., *Journal of biotechnology* **2015,** *214*, 133-138.

[98] Yang, L.; Li, X.; Yan, S.; Wang, M.; Liu, P.; Dong, Y.; Zhang, C., *Analytical Methods* **2015,** *7* (12), 5303-5310.

[99] Fu, X.; Cheng, Z.; Yu, J.; Choo, P.; Chen, L.; Choo, J., *Biosensors and Bioelectronics* **2016,** *78*, 530-537.

[100] Khan, M.; Khan, A. R.; Shin, J.-H.; Park, S.-Y., *Scientific reports* **2016,** *6*, 22676.

[101] Leung, A.; Shankar, P. M.; Mutharasan, R., *Sensors and Actuators B: Chemical* **2007,** *125* (2), 688-703.

[102] Du, Y.; Dong, S., *Analytical Chemistry* **2017,** *89* (1), 189-215.

[103] Chen, J.-C.; Shih, J.-L.; Liu, C.-H.; Kuo, M.-Y.; Zen, J.-M., *Analytical chemistry* **2006,** *78* (11), 3752-3757.

[104] Cai, S.; Tian, X.; Sun, L.; Hu, H.; Zheng, S.; Jiang, H.; Yu, L.; Zeng, S., *Analytical chemistry* **2015,** *87* (20), 10542-10546.

[105] Seidel, M.; Niessner, R., *Analytical and bioanalytical chemistry* **2014,** *406* (23), 5589-5612.

[106] Mirasoli, M.; Michelini, E., *Analytical and bioanalytical chemistry* **2014,** *406* (23), 5529.

[107] Roda, A.; Mirasoli, M.; Dolci, L. S.; Buragina, A.; Bonvicini, F.; Simoni, P.; Guardigli, M., *Analytical chemistry* **2011,** *83* (8), 3178-3185.

[108] Roda, A.; Guardigli, M.; Michelini, E.; Mirasoli, M.; Pasini, P., Peer reviewed: analytical bioluminescence and chemiluminescence. ACS Publications: 2003.

[109] Roda, A.; Pasini, P.; Mirasoli, M.; Michelini, E.; Guardigli, M., *TRENDS in Biotechnology* **2004,** *22* (6), 295-303.

[110] Thorpe, G. H.; Kricka, L. J., *Methods in Enzymology* **1986,** *133*, 331-353.

[111] Dotsikas, Y.; Loukas, Y. L., *Analytica chimica acta* **2004,** *509* (1), 103-109.

[112] Garcia Sánchez, F.; Navas Diaz, A.; Gonzalez Garcia, J., *Journal of luminescence* **1995,** *65* (1), 33-39.

[113] Marquette, C. A.; Blum, L. J., *Analytical and Bioanalytical Chemistry* **2006,** *385* (3), 546-554.

[114] Lengger, S.; Otto, J.; Elsässer, D.; Schneider, O.; Tiehm, A.; Fleischer, J.; Niessner, R.; Seidel, M., *Analytical and bioanalytical chemistry* **2014,** *406* (14), 3323-3334.

[115] Schuetz, A. J., Winklmair, Michael, Weller, Michael G., Niessner, Reinhard, In *Stabilization of horseradish peroxidase (HRP) for use in immunochemical sensors*, Chemical, Biochemical and Environmental Fiber Sensors IX, Munich, Germany, May 30, 1997; Lieberman, R. A., Ed. SPIE, Proceedings: Munich, Germany, 1997; p 332.

[116] Trilling, A. K.; Beekwilder, J.; Zuilhof, H., *Analyst* **2013,** *138* (6), 1619-1627.

[117] Yuan, Y.; Yin, M.; Qian, J.; Liu, C., *Soft Matter* **2011,** *7* (16), 7207-7216.

[118] Kusnezow, W.; Hoheisel, J. D., *Journal of Molecular Recognition* **2003,** *16* (4), 165-176.

[119] Didar, T. F.; Foudeh, A. M.; Tabrizian, M., *Analytical chemistry* **2011,** *84* (2), 1012-1018.

[120] Campbell, G. A.; Mutharasan, R., *Analytical sciences* **2005,** *21* (4), 355-357.

[121] Maraldo, D.; Rijal, K.; Campbell, G.; Mutharasan, R., *Analytical Chemistry* **2007,** *79* (7), 2762-2770.

[122] Yu, Q.; Wang, Q.; Li, B.; Lin, Q.; Duan, Y., *Critical Reviews in Analytical Chemistry* **2015,** *45* (1), 62-75.

[123] Billah, M. M.; Hodges, C. S.; Hays, H. C. W.; Millner, P. A., *Bioelectrochemistry* **2010,** *80* (1), 49-54.

[124] Neves‐Petersen, M. T.; Snabe, T.; Klitgaard, S.; Duroux, M.; Petersen, S. B., *Protein science* **2006,** *15* (2), 343-351.

[125] Dixit, C. K.; Vashist, S. K.; MacCraith, B. D.; O'kennedy, R., *nature protocols* **2011,** *6* (4), 439-445.

[126] Chen, G.; Ito, Y.; Imanishi, Y.; Magnani, A.; Lamponi, S.; Barbucci, R., *Bioconjugate Chemistry* **1997,** *8* (5), 730-734.

[127] Rodríguez, M. C.; Rivas, G. A., *Talanta* **2009,** *78* (1), 212-216.

[128] Liu, L.-H.; Yan, M., *Accounts of chemical research* **2010,** *43* (11), 1434.

[129] Prucker, O.; Naumann, C. A.; Rühe, J.; Knoll, W.; Frank, C. W., *Journal of the American Chemical Society* **1999,** *121* (38), 8766-8770.

[130] Rozsnyai, L. F.; Benson, D. R.; Fodor, S.; Schultz, P. G., *Angewandte Chemie International Edition in English* **1992,** *31* (6), 759-761.

[131] Leshem, B.; Sarfati, G.; Novoa, A.; Breslav, I.; Marks, R. S., *Luminescence* **2004,** *19* (2), 69-77.

[132] Caelen, I.; Gao, H.; Sigrist, H., *Langmuir* **2002,** *18* (7), 2463-2467.

[133] Clemence, J.-F.; Ranieri, J. P.; Aebischer, P.; Sigrist, H., *Bioconjugate chemistry* **1994,** *6* (4), 411-417.

[134] Kim, W.-J.; Kim, A.; Huh, C.; Park, C. W.; Ah, C. S.; Kim, B. K.; Yang, J.-H.; Chung, K. H.; Choi, Y. H.; Hong, J., *Applied Surface Science* **2012,** *261*, 880-889.

[135] Suchanek, M.; Radzikowska, A.; Thiele, C., *Nature methods* **2005,** *2* (4), 261-268.

[136] Sundarababu, G.; Gao, H.; Sigrist, H., *Photochemistry and photobiology* **1995,** *61* (6), 540-544.

[137] Papper, V.; Gorgy, K.; Elouarzaki, K.; Sukharaharja, A.; Cosnier, S.; Marks, R. S., *Chemistry–A European Journal* **2013,** *19* (29), 9639-9643.

[138] Dubinsky, L.; Krom, B. P.; Meijler, M. M., *Bioorganic & medicinal chemistry* **2012,** *20* (2), 554-570.

[139] Preston, G. W.; Wilson, A. J., *Chemical Society Reviews* **2013,** *42* (8), 3289-3301.

[140] Ghiassian, S.; Ismaili, H.; Lubbock, B. D. W.; Dube, J. W.; Ragogna, P. J.; Workentin, M. S., *Langmuir* **2012,** *28* (33), 12326-12333.

[141] Das, J., *Chemical Reviews* **2011,** *111* (8), 4405-4417.

[142] Hashimoto, M.; Hatanaka, Y., *European journal of organic chemistry* **2008,** *2008* (15), 2513-2523.

[143] Blencowe, A.; Hayes, W., *Soft Matter* **2005,** *1* (3), 178-205.

[144] Li, Z.; Wang, D.; Li, L.; Pan, S.; Na, Z.; Tan, C. Y. J.; Yao, S. Q., *Journal of the American Chemical Society* **2014,** *136* (28), 9990-9998.

[145] Li, Z.; Hao, P.; Li, L.; Tan, C. Y. J.; Cheng, X.; Chen, G. Y. J.; Sze, S. K.; Shen, H.-M.; Yao, S. Q., *Angewandte Chemie International Edition* **2013,** *52* (33), 8551-8556.

[146] Paulsen, S., *Angewandte Chemie* **1960,** *72* (21), 781-782.

[147] Schmitz, E.; Ohme, R., *Angewandte Chemie* **1961,** *73* (6), 220-221.

[148] Pierce, L.; Dobyns, S. V., *Journal of the American Chemical Society* **1962,** *84* (13), 2651-2652.

[149] Schmitz, E.; Ohme, R.; Schmidt, R. D., *Chemische Berichte* **1962,** *95* (11), 2714-2717.

[150] Smith, R. A.; Knowles, J. R., *Journal of the Chemical Society, Perkin Transactions 2* **1975,** (7), 686-694.

[151] Smith, R. A.; Knowles, J. R., *Journal of the American Chemical Society* **1973,** *95* (15), 5072-5073.

[152] Mueller-Remmers, P. L.; Jug, K., *Journal of the American Chemical Society* **1985,** *107* (25), 7275-7284.

[153] Yamamoto, N.; Bernardi, F.; Bottoni, A.; Olivucci, M.; Robb, M. A.; Wilsey, S., *Journal of the American Chemical Society* **1994,** *116* (5), 2064-2074.

[154] Bethell, D.; Stevens, G.; Tickle, P., *Journal of the Chemical Society D: Chemical Communications* **1970,** (13), 792b-794.

[155] Richards, C. A.; Kim, S.-J.; Yamaguchi, Y.; Schaefer, H. F., *Journal of the American Chemical Society* **1995,** *117* (40), 10104-10107.

[156] Dewar, M. J. S.; Haddon, R. C.; Weiner, P. K., *Journal of the American Chemical Society* **1974,** *96* (1), 253-255.

[157] Lucchese, R. R.; Schaefer, H. F., *Journal of the American Chemical Society* **1977,** *99* (20), 6765-6766.

[158] Lengel, R. K.; Zare, R. N., *Journal of the American Chemical Society* **1978,** *100* (24), 7495-7499.

[159] Borden, W. T.; Gritsan, N. P.; Hadad, C. M.; Karney, W. L.; Kemnitz, C. R.; Platz, M. S., *Accounts of Chemical Research* **2000,** *33* (11), 765-771.

[160] Weber, T.; Brunner, J., *Journal of the American Chemical Society* **1995,** *117* (11), 3084-3095.

[161] Brunner, J., [34] Photochemical labeling of apolar phase of membranes. In *Methods in Enzymology*, Academic Press: 1989; Vol. Volume 172, pp 628-687.

[162] Wang, J.; Kubicki, J.; Peng, H.; Platz, M. S., *Journal of the American Chemical Society* **2008,** *130* (20), 6604-6609.

[163] Brinker, U. H., *Advances in Carbene Chemistry*. Elsevier: **2001**; Vol. 3.

[164] Liu, M. T., *Chemical Society Reviews* **1982,** *11* (2), 127-140.

[165] Modarelli, D. A.; Morgan, S.; Platz, M. S., *Journal of the American Chemical Society* **1992,** *114* (18), 7034-7041.

[166] Toscano, J. P.; Celius, T. C., The Photochemistry of Diazirines. In *CRC Handbookof Organic Photochemistry and Photobiology, Volumes 1 & 2, Second Edition*, CRC Press: 2003.

[167] Zhang, Y.; Kubicki, J.; Platz, M. S., *Organic Letters* **2010,** *12* (14), 3182-3184.

[168] Brunner, J.; Senn, H.; Richards, F., *Journal of Biological Chemistry* **1980,** *255* (8), 3313-3318.

[169] Erni, B.; Khorana, H. G., *Journal of the American Chemical Society* **1980,** *102* (11), 3888-3896.

[170] Bonneau, R.; Liu, M. T. H., *Journal of the American Chemical Society* **1996,** *118* (30), 7229-7230.

[171] Akasaka, T.; Liu, M. T. H.; Niino, Y.; Maeda, Y.; Wakahara, T.; Okamura, M.; Kobayashi, K.; Nagase, S., *Journal of the American Chemical Society* **2000,** *122* (29), 7134-7135.

[172] Wakahara, T.; Niino, Y.; Kato, T.; Maeda, Y.; Akasaka, T.; Liu, M. T. H.; Kobayashi, K.; Nagase, S., *Journal of the American Chemical Society* **2002,** *124* (32), 9465-9468.

[173] Kumar, A. B.; Anderson, J. M.; Manetsch, R., *Organic & biomolecular chemistry* **2011,** *9* (18), 6284-6292.

[174] Sigrist, H.; Collioud, A.; Clemence, J.-F.; Gao, H.; Luginbuehl, R.; Saenger, M.; Sundarababu, G., *Optical Engineering* **1995,** *34* (8), 2339-2348.

[175] Eigler, F. S.; Georger, J.; Bhatia, S. K.; Calvert, J.; Shriver-Lake, L. C.; Bredehorst, R., Immobilization of active agents on substrates with a silane and heterobifunctional crosslinking agent. Google Patents: 1991.

[176] Gao, H.; Kislig, E.; Oranth, N.; Sigrist, H., *Biotechnology and Applied Biochemistry* **1994,** *20* (2), 251-263.

[177] Collioud, A.; Clemence, J. F.; Saenger, M.; Sigrist, H., *Bioconjugate Chemistry* **1993,** *4* (6), 528-536.

[178] Gao, H.; Sänger, M.; Luginbühl, R.; Sigrist, H., *Biosensors and Bioelectronics* **1995,** *10* (3), 317-328.

[179] Saenger, M.; Borle, F.; Heller, M.; Sigrist, H., *Bioconjugate Chemistry* **1992,** *3* (4), 308-314.

[180] Sänger, M.; Sigrist, H., *Sensors and Actuators A: Physical* **1995,** *51* (1), 83-88.

Chapter 3

Experimental Methodology

Section 3.1 illustrates the rationale of the experiments based on the logic flow to the hypotheses verification. Section 3.2 covers the overview of the biosensor construction protocols used in this thesis. Section 3.3 describes the details of the experiments and set-up in each results chapter. The optimization, immobilization efficiency and the sensor performances are determined by the RLU values in the black box operation as it provided directly information on the final outcome caused by the experiments' variables. The synthesis of the silane-diazirine molecules was confirmed by the 1H and 13C NMR technique as they showed the unique peaks in the products for identification purpose. The diazirine absorption was also measured by UV-VIS spectrophotometer as it provided the direct information on the wavelengths absorbed by the molecule which was helpful in selecting the UV source. The surface characterization was carried out by SEM-EDX as it enabled visualization and element analysis of the fibre surface, monitoring the changes of the surface by each treatment. In the genosensor part, the traditional qPCR was used as a reference technique to validate the ssDNA probes and the dot-blotting method was conducted first to confirm the hybridization of the designed target.

3.1 Rationale of strategy

The experiments were designed to verify the proposed hypotheses. The logic flow of the strategy is illustrated in the following charts in **Figure 3.2** and **Figure 3.3**. An explanatory figure of the symbols appearing in the above logic charts is displayed in **Figure 3.1**.

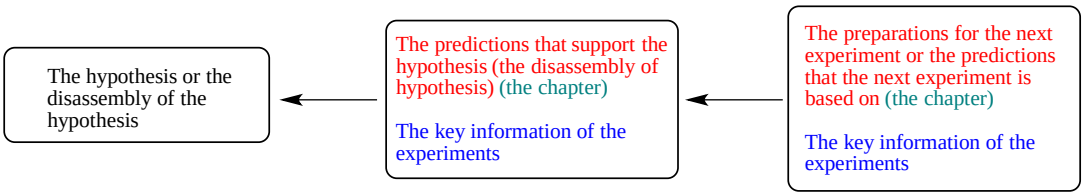

Figure 3.1 An explanatory figure of the symbols appearing in the charts in **Figure 3.2** and **Figure 3.3**.

3.2 Overview of the protocols

A black box developed by Prof. Robert S. Marks' group (Ben-Gurion University of the Negev, Beer Sheva, Israel) was used as the detection device and its general construction. Its detection principle has been illustrated in **Figure 1.1** in Chapter 1. Herein each step of the surface modification is described for immuno- (**Figure 3.4**) and geno-(**Figure 3.4**) CFOSs. The major effort was put into the modification of the end face of the tip of the fibre optic (SFS400/440/590/880B, Fiberguide), each fibre was cut into a piece of 35 cm in length, the near-end surface was ensured to be left smooth by a diamond cutter (SADI-ATI, HCG400) and was washed with MeOH/HCl (1:1, v:v) for 20 minutes and activated with piranha solution (30% H_2O_2: 95% H_2SO_4, 1:3, v/v). The later modifications varied with the experiment objectives [1-2].

Note: The reagents for the common steps were labeled with the names and producers, for alternative experiment steps or optimization experiments, the reagents' names/recipes/structures and producers will be mentioned in the specific sections. Unless noted, the same procedure uses the same reagent(s) and the details will not be referred again.

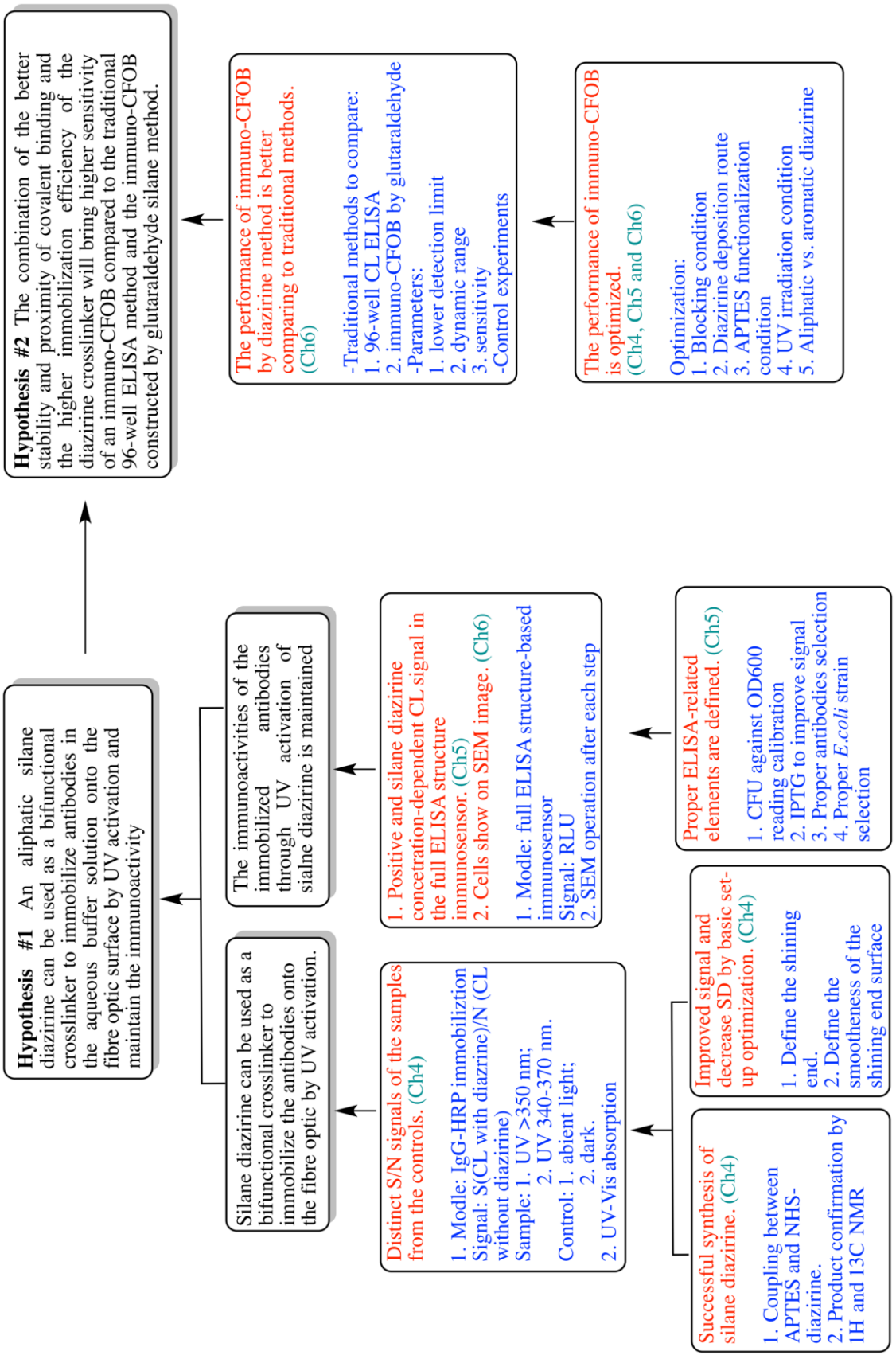

Figure 3.2 The logic chart for H1 and H2 and the experiments information of immuno-CFOS construction in Chapter 4, 5 and 6.

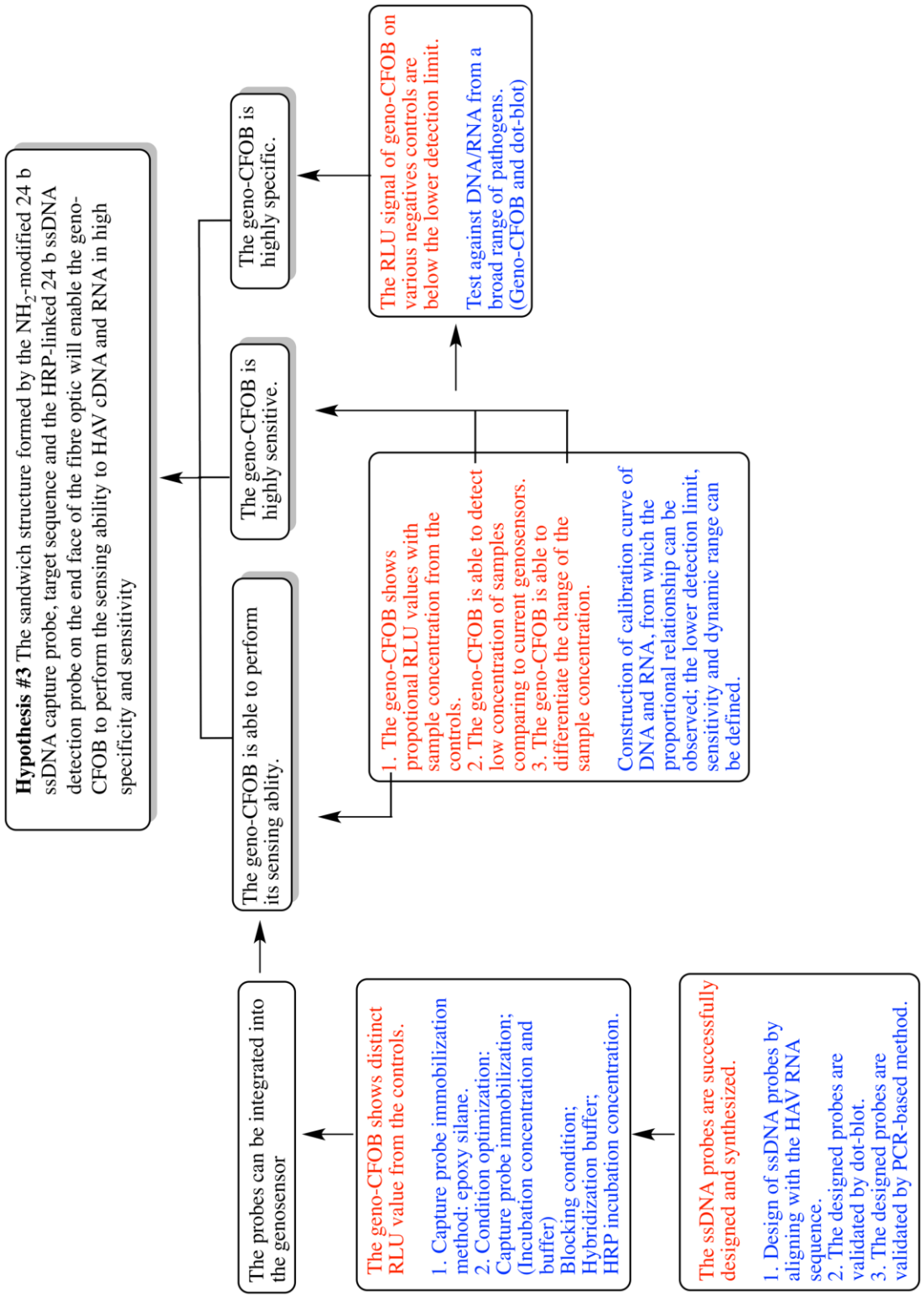

Figure 3.3 The logic chart for H3 and the experiments information of geno-CFOS construction in Chapter 7.

3.2.1 FO modification for immuno- CFOS: adapt ELISA onto FO

The protocol of the modification of the fibre optic for immuno- FOC is described in **Figure 3.4**. The protocol is composed of 4 parts:

Surface functionalization: (1) Piranha activation; (2) Silanization using APTES (Sigma); (3) Diazirine functionalization;

Capture antibody immobilization: (4) UV induced carbene generation and subsequent antibody immobilization; (5) Blocking;

Analyte capture: (6) *E. coli* capture; (7) Detection antibody incubation;

Signal generation: (8) Substrate exposure that generates chemiluminescence (BioRad, Clarity™ and Clarity Max™ Western ECL Blotting Substrates).

Alternative procedures in each step for optimization or comparison purpose will be mentioned in specific sections.

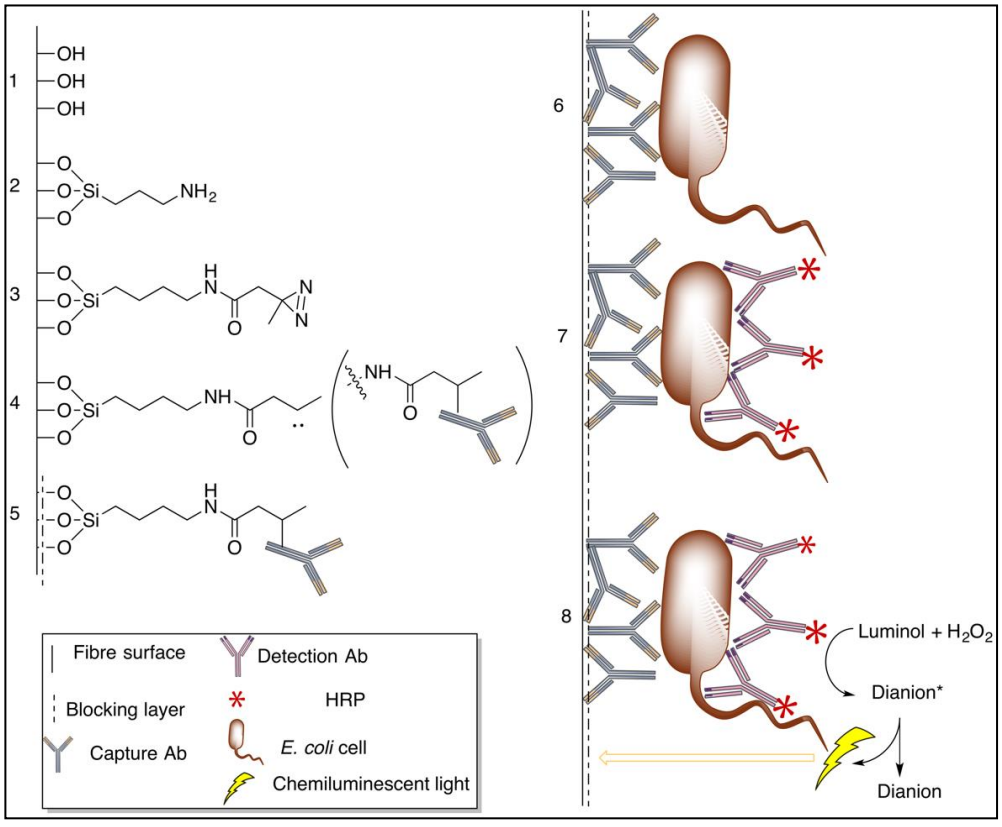

Figure 3.4 Schematic illustration of the modification on the end surface of fibre optic and the working mechanism of the immuno-CFOS for *E. coli* detection.

3.2.2 FO modification for geno-CFOS: adapt DNA hybridization onto FO

The protocol of the modification of the fibre optic for geno-CFOS is described in **Figure 3.5.** The protocol is composed of 5 parts:
Surface functionalization: (1) Piranha activation; (2) Silanization using epoxy silane (Sigma); (3) Chemical treatments to convert epoxy to –CHO layer;
Capture probe immobilization: (4) Capture probe incubation; (5) Blocking;
Hybridization: (6) Hybridization of capture probe (immobilized on fibre tip), target HAV cDNA or RNA sequence and detection probe;
HRP linkage: (7) Avidin-HRP (Sigma) linkage through avidin-biotin binding;
Signal generation: (8) Substrate exposure that generates chemiluminescence.

Each part having alternative procedures for optimization or comparison purpose will be mentioned in specific sections.

3.3 Experimental details in each chapter

The major contributions of each chapter, experiment settings and rationales are described in this part.

3.3.1 Synthesis and the proof-of-art for immobilization (Chapter 4)

Chapter 4 serves as proof of concept to confirm the antibody immobilization ability of the silane diazirine. The objective of Chapter 4 is two-fold: to synthesize silane-diazirine and to confirm the ability of silane diazirine to immobilize the antibodies in aqueous conditions by UV activation.

3.3.1.1 Silane-diazirine synthesis

3-(3-methyl-3H-diazirin-3-yl)-N-(3-(triethoxysilyl)propyl)propanamide (silane-diazirine) was synthesized by a coupling reaction between succinimidyl 4,4'-azipentanoate (NHS-diazirine or SDA, Thermo Scientific Pierce; 4×50mg), and (3-Aminopropyl)triethoxysilane (APTES, Sigma; 208 μl) with Diisopropyl ethyl amine (DIPEA, Sigma; 1:1wrt APTES) in anhydrous dimethyl sulfoxide (DMSO, Sigma; 5ml) solution. The mixture was allowed to react in a glass vial covered with aluminum foil with continuous mixing. TLC in DCM analysis was performed every 30 minutes until

reaction completion. Vacuum distillation was done next to purify the silane-diazirine. 13C-NMR and 1H-NMR were conducted to confirm the successful synthesis (Bruker 400 MHz NMR spectrometer).

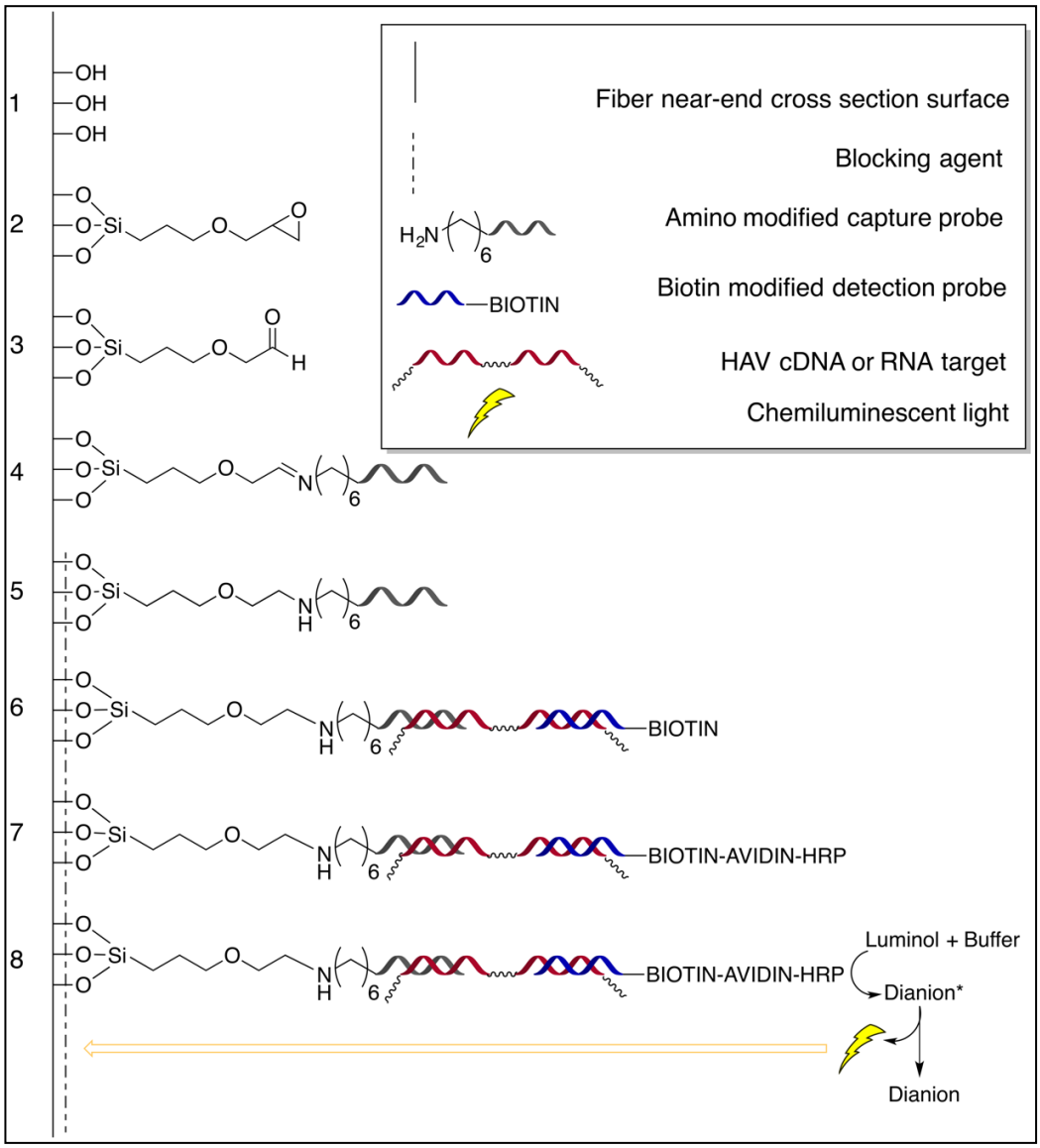

Figure 3.5 Schematic illustration of the modification on the fibre optic and working mechanism of the geno-FOCB for HAV detection.

3.3.1.2 Evaluating the ability of silane diazirine in HRP-IgG immobilization

The prepared silane-diazirine was dissolved in toluene (Sigma) at 1%, 5%, 10% (v/v) concentrations and soaked with the piranha-activated near-end of fibre overnight. Then the fibres were washed with toluene 2 times and 0.1% PBST (PBS (tablet from Sigma): 137 mM NaCl, 2.7 mM KCl and 10 mM phosphate buffer solution, pH 7.4 at 25 °C;

Tween 20 (Sigma), 0.1% v/v in PBS) for 3 times. Then the fibre was soaked in anti-*E. coli* HRP-IgG (Virostat, 1004) solution PBS in 1/10, v/v. The photoimmobilization was archived by UV irradiation from the far-end of the fibre for 15 minutes followed by 0.1% PBST washing for 5 times and the near-end of a single fibre optic was inserted into a lightproof tube with 120 µl of peroxide buffer. Then 120 µl luminol solution was added immediately before taking measurements by a photomultiplier tube (PMT) detector (Sensetech) in a confined black box. 5 fibres were used for each treatment and the signal for each fibre was recorded as an average of 10 readings after the signal reached the maximum range. The light signal was interpreted as relative light unit (RLU).

As the objective is only to confirm that the IgG is attached, only HRP-IgG instead of the full ELISA structure was introduced on the modified platform. The S/N values were used for evaluation, where the S values were from the fibres with diazirine treatment, N values were from the fibres without diazirine treatment. Experiment groups utilized the Max 303 Xenon light source (300 W) (Asahi Spectra) as the UV source with filters at 340 - 370 nm and > 350 nm. Control groups included the ambient light condition and dark condition.

3.3.1.3 UV-vis absorbance

The UV-vis absorbance of SDA solution was recorded by Lambda 950 UVVIS spectrophotometer and presented by the software PerkinElmer UV WinLab. SDA was dissolved in DMSO in the concentration of 0.5 mM, pure DMSO was used as a reference.

3.3.1.4 Set-up optimization

The format of UV shining and the effect of the roughness of the far-end surface of fibre optic were also optimized to improve the signal. The UV were shined in two formats: one is shining directly at the near-end, by placing the bottom of the 200 µl PCR tube with Ab solution and fibre near-end at 1 cm apart from the light source at an angle of 45˚. The other way is shining through the fibre optic as the fibre is designed for light transmission at 190 -1250 nm which includes the desired range. The shining lasted for 15 minutes.

The next optimization is the roughness of the far-end. The smooth surface was obtained by the same cutting procedure of the near-end. The rough surface was random cut by scissors.

3.3.2 Diazirine functionalization routes (Chapter 5)

Based on the outcome of Chapter 4, Chapter 5 went further to confirm that the immunoactivity of the antibody is maintained after UV induced silane diazirine immobilization and to explore the optimum diazirine functionalization route.

3.3.2.1 Diazirine functionalization routes for selection

In the route selection step, diazirine was deposited on the fibre near-end in two different routes: Route A is the same as described in 3.3.1.2. Route B is shown in **Figure 3.6**, where the fibre bundles were immersed in an APTES solution at 60 ˚C for 4 hours, then washed with ethanol thrice and allowed to dry under N_2 flow. Then the diazirine solution was made by mixing SDA and DIPEA (mole ratio 1:1) in anhydrous DMSO and stirred overnight in dark with the fibre optic bundles immersed in the mixture solution. At the end of the reaction, fibres were taken out and rinsed with DMSO and PBS and stored in PBS until use. In both routes, silane diazirine was in concentration of 1% and 10% while amino silane was in the concertation of 1%, 10%, 50% and 100% (v/v in toluene).

3.3.2.2 Two models for functionalization routes evaluation

Two models were used in the evaluation. The first one is the IgG-HRP model as in 3.3.1.2 with only IgG-HRP being attached. The second model is the full ELISA model: the fibre near-end deposited with diazirine was soaked in rabbit anti-*E. coli* polyclonal IgG (capture antibody) (Virostat, 1001) solution in PBS (1:10, v/v). The photoimmobilization was achieved by irradiation from the far-end of the fibre for 15 minutes, followed by a blocking step with 5% (w/v) skim milk solution in 0.1% PBST. *E. coli* capture was performed by incubating with *E. coli* dilutions for 2 hours. Then the fibre was immersed in anti-*E. coli* polyclonal HRP-IgG (Virostat, 1004) in the same concentration and volume for 1 hour. The luminescence generation and recording

followed the description in 3.3.1.2. The fibers were washed with 0.1% PBST thrice between each step mentioned above and all the incubation steps took place at 37 ºC.

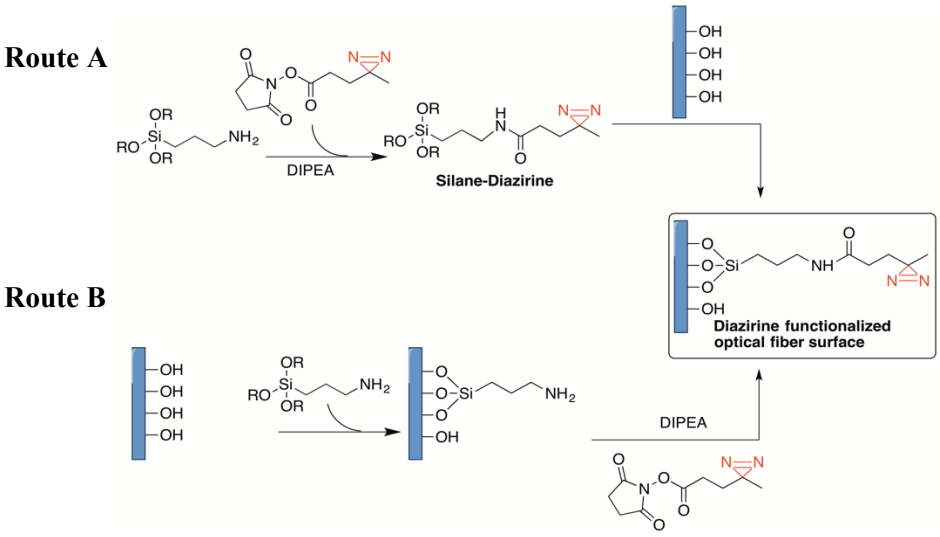

Figure 3.6 Diazirine functionalization routes.

3.3.2.3 Maintenance of the bacterial model analyte

Escherichia coli RM443 strain DPD2794 was pre-cultured overnight in DifcoTM Luria-Bertani Broth (LB) at 37 ºC and refreshed in LB with 0.5 mM IPTG for 2.5 hours at 37 ºC until it reached a logarithmic phase.

3.3.2.4 Supplementary experiments for diazirine functionalization route comparison

Prior to the full ELISA assay in 3.3.2.2, a few supplementary experiments were conducted to optimize the signal and prepare for the next experiments. Experiments in 3.3.2.4.1 to 3.3.2.4.3 were performed in 96-well ELISA plates (Nunc Maxisorp^{TM} Microplate).

3.3.2.4.1 Selection of bacteria strains and HRP-antibody

Different strains of *E. coli* bacteria process different serotypes [3-4] on the surface of the cell membrane which are the target of specific antibodies. With the availability of the *E. coli* strains in the lab, the following strains of DPD 2794 (derived from RM443 [5]

which is originated from K-12 [3]), wild-type ATCC 25922 and B strain were compared to select the most compatible strains in the antibodies system. The HRP-antibodies for selection were from rabbit (Virostat 1004) and goat sources (Virostat 1094). The selections were based on the conventional chemiluminescent ELISA method: Rabbit anti-*E. coli* polyclonal IgG was diluted in PBS solution in 1/50 volume ratio and 100 µl of the solution was placed into each relevant well in a 96-well Maxisorp™ plate before incubating at 4 ºC overnight. This was followed by a blocking step with 5% (w/v) skim milk solution in 0.1% PBST. *E. coli* dilutions were added into respective wells and the incubation took 2 hours to process. HRP modified anti-*E. coli* IgG was then added in the same volume and concentration as that of the capture antibody and allowed to incubate for an additional 1 hour. 100 µl buffer and luminol solutions were added separately and immediately before chemiluminescent recording by the Luminoskan™ Ascent Microplate Luminometer. The wells were washed with 0.1% PBST thrice between each of the steps mentioned above and all the incubation steps took place at 37 ºC. The final response and standard deviation of each array were calculated as an average of the maximum readings of triplicate wells and the result was reported as relative light unit (RLU).

The control groups include: without blocking, without capture Ab, without bacteria and without HRP-IgG.

3.3.2.4.2 The effect of IPTG

Isopropyl-β-D-thiogalactoside (IPTG) is an effective inducer of protein expression in the concentration range of 100 µM to 3.0 mM [6], the author noted that in a few immunosensor-based *E. coli* detection methods, IPTG was added to promote the immune interactions, so the effect of IPTG was also explored to improve the signal. IPTG (Roche) was added to the refreshment incubation mixture in the concentrations of 0.5 mM and 1 mM, 0 mM was for negative control.

3.3.2.4.3 The calibration of CFU of *E. coli* cells against the OD600 reading

The bacteria strain DPD 2794 was grown overnight in 10 ml LB medium supplemented with 50 µl kanamycin in a rotary thermo-shaker at 120 rpm at 37°C. 100 µl overnight culture was diluted with 10 ml LB medium without antibiotics and put in 37°C

incubator. The OD600 reading and viability test were performed every 30 minutes starting from the beginning of the refreshment. Triplet dropping 20 µl of each dilution up to 10^{-9} was placed onto labeled area of agar plates (DifcoTM Luria-Bertani). The number of colonies was counted in each dropping area after overnight culture at 37°C.

3.3.3 Immunosensor optimization and evaluation (Chapter 6)

Chapter 6 optimized the selected chemical modification route from the outcome of Chapter 5, and the immunosensor to *E. coli* was evaluated based on the comparison with conventional ELISA and another fibre optic immunosensor constructed by glutaraldehyde crosslinker method.

3.3.3.1 Protocol optimization

3.3.3.1.1 APTES incubation temperature

The fibre optic silica core was exposed by stripping off the outer layers, and then cut into 7 mm length pieces, washed by acid and activated by piranha solution. The fibre pieces were then immersed in APTES for 4 hours at temperatures of 30 ºC, 60 ºC, 90 ºC, 120 ºC and 150 ºC, followed by washing by DMSO and socking in 5 10-fold serial DMSO dilutions with cyanine-3 NHS-ester (Lumiprobe, 3/1000, v/v) for 5 hours. The fluorescent dye-functionalized fiber pieces were washed by sonicating in DMSO and rinsed with DMSO. The fluorescent signal was recorded by fluorescence spectrophotometer (Agilent, Cary Eclipse system).

3.3.3.1.2 Irradiation light intensities and UV exposure time

Two kinds of UV sources were used and compared in this study according to the recommendations of the product manual of SDA [7], one was a Max 303 Xenon light source (300 W) (Asahi Spectra) (referred as MAX 303) capped with a single-band bandpass filter (FF01-356/30-25, Semrock), the final UV output is in the range of 340 - 370 nm with a power of 200 mW/cm^2 measured at 365 nm and the other source was the ENF-280C (8 W) hand-held UV lamp (referred as UV 365) at 365 nm with a power of 1090 µW/cm^2. The fibre near-end deposited with diazirine was soaked in antibody

solution in PBS (1:10, v/v). The photoimmobilization was archived by irradiation from the far-end of the fibre for 5, 10, 20, 30, 40, 50 and 60 minutes.

3.3.3.1.3 Different silane spacer arm lengths or(and) diazirine types

Four types of surface grafted with 4-atom and 7-atom silane and aliphatic and aromatic diazirine were prepared and compared. They are referred as 4-Ali, 4-Ar, 7-Ali and 7-Ar as described in **Figure 3.7.**

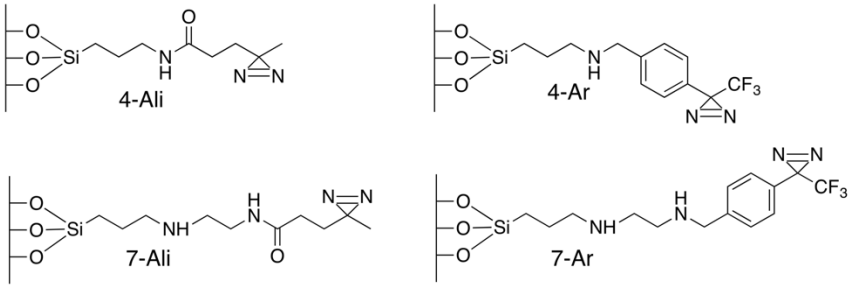

Figure 3.7 Surface grafted with 4 or 7 atoms spacer arm silane with aliphatic or aromatic diazirine.

Preparation of 4-atom silane covered surface was achieved by APTES modification at 90 ºC.

Preparation of 7-atom silane covered surface. 7-atom silane coverage was formed by the reaction between piranha activated fibre optic with [3-(2-Aminoethylamino)propyl]trimethoxysilane (Sigma) by immersing the near-end tip in 100% silane solution at 90 ºC for 4 hours and rinsing with methanol and DMSO.

Preparation of 4-Ali and 7-Ali was achieved by the reaction between the -NH2 covered fibre surface with SDA as described in 3.3.2.1 Route B.

Preparation of 4-Ar and 7-Ar. For introducing the aromatic diazirine onto the surface, 3-[4-(Bromomethyl)phenyl]-3-(trifluoromethyl)-3H-diazirine (Ar-Dia, TCI) was mixed with triethylamine (Sigma) mixture in DMSO in molar ratio of 1:1[8-10], which is allowed to react for 4 hours and the fibres were rinsed with DMSO and then PBS.

3.3.3.2 Surface characterization by scanning electron microscope (SEM)

A surface analysis was carried out after each step of fibre modification shown in **Figure 3.4**. by scanning electron microscope (SEM) (JOEL JSM - 6360LV) equipped with energy dispersive X - ray spectrometer (EDS). The image area was coated with gold plasma at 20 mA for 60 seconds.

3.3.3.3 Evaluation of the immunosensor constructed by diazirine method

The calibration (including lower detection limit and dynamic range) and the specificity of the immunosensor constructed by diazirine method were evaluated.

3.3.3.3.1 Maintenance of the bacterial model analyte and other antigens

Escherichia coli RM443 strain DPD2794 was pre-cultured overnight in LB medium at 37 °C before being incubated with 0.5 mM IPTG in fresh LB for 2.5 hours at 37 °C. The refreshed culture was then made into a series of analyte dilutions with bacterial concentrations ranging from 6.44 $*10^8$ CFU/ml down to an estimated 6.44 CFU/ml in PBS solution containing 1% (w/v) skim milk. *E. coli* strains K-12, B and ATCC 25922 were prepared in the same condition. *Salmonella enteritidis*, *Micrococcus luteus* and *Staphylococcus aureus* antigen samples were the bacteria culture diluted in PBS with skim milk solution. *Brucella* was diluted from inactivated cell suspensions (Bio-Rad). LPS from *Vibrio cholera* (Sigma), Hepatitis A VP3 antigen (Virostat) and Hepatitis B e antigen (Virostat) were diluted in PBS with skim milk solution too.

3.3.3.3.2 Calibration

The calibration evaluation of the diazirine constructed immunosensor (referred as FOBS-AmDia) was based on the comparison with the conventional 96-well chemiluminescent ELISA (referred as CL-ELISA) and another immunosensor constructed by a traditional glutaraldehyde crosslinking method (FOBS-AmDia) as described in **Figure 3.8**

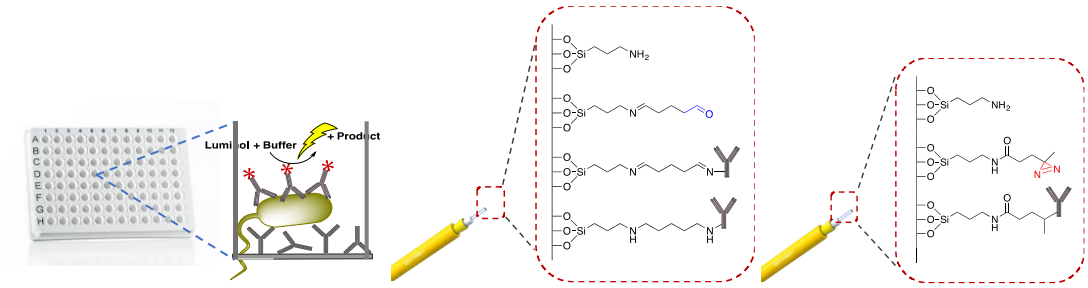

Figure 3.8 Detection methods for comparison: from left to right: CL-ELISA, FOBS-AmGlu and FOBS-AmDia.

The CL-ELISA method was conducted as described in 3.3.2.4.

The FOBS-AmGlu method was conducted as described below: the APTES treated fibre optic was soaked in PBS solution with 10% (v/v) glutaraldehyde (Sigma) solution while stirring at room temperature for 2 hours and rinsed with DI water. Antibody immobilization was achieved by overnight incubation with antibody PBS solutions at 4 °C followed by blocking with 5% skim milk at 40 °C and then incubating with 0.6 mM NaH_3BCN (Sigma) solution to reduce any Schiff base.

The FOBS-AmGLu method followed the protocol in **Figure 3.4** and was performed following the optimized conditions.

The calibration curve was generated by plotting the RLU values against the log(CFU/ml) values of the *E. coli* dilutions, from where the lower detection limit values and dynamic ranges are extracted.

3.3.4 Genosensor construction (Chapter 7)

Chapter 7 aims at developing an HAV genosensor. The specific ssDNA probes were designed and validated by the PCR/qPCR technique and integrated into the fibre optic genosensor system. The conditions were optimized before the calibration curves plotting for cDNA and RNA and specificity test.

3.3.4.1 Microorganisms preparation

Samples of RNA extracted from pure cultures of HAV (HAV4, HAV5, HAV6) were used to produce cDNA samples by reverse transcription (RiboClone® cDNA Synthesis

System, Promega) and the concentration was recorded by NanoPhotometer® (Implen, 7122 version 2.3.1). HAV cDNA and norovirus cDNA were then used as a positive sample and negative sample, respectively, in the probes optimization. DNA or RNA strands or proteins extracted from bacterial and viral samples, *Escherichia coli, Campylobacter lari DSM 11375, Pseudomonas aeruginosa, Aeromonas sobria, Listeria monocytogenes, Lactobacillus bulgaricus, Legionella pneumophila, Vibrio 14379, Lactococcus lactis, Morganella morganii, Proteus vulgaris, Bacillus subtilis, Staphylococcus aureus Pseudomonas putida*, Norovirus G1, Norovirus G2, Dengue virus and South Bay virus, were used as negative controls in probes' specificity test.

3.3.4.2 Oligonucleotide sequences

Primers for PCR and qPCR. Two sets of primers were designed by aligning sequences retrieved from the NCBI online repository with the ClustalW software, optimized using Primer3 [11] and tested with the Primer-Blast tool.

Set 1: outer primers: (forward, 5'-ACTTGATACCTCACCGCCGTTTGC-3') and (reverse 5'-AGTCCTCCGGCGTTGAATGG-3'); inner primers: (forward 5'-CGGGGTCAACTCCATTA-3') and (reverse 5'-CGCCGCTGTTACCCTATCC-3'). Set 2: outer primers: (forward 5'- GGACTTGATACCTCACCGCC-3') and (reverse 5'-CAAACACCACATAAGGCCCCA-3'). Inter primers: (forward 5'-GGGGTCAACTCCATGATTAGCA-3') and (reverse 5'-GGTTTCACCCGTAGCCTACC-3').

Probes for dot blot and fibre optic biosensors. Oligonucleotide probes for HAV were designed by aligning the selected regions of the HAV RNA sequence available from GenBank. The oligonucleotides sequences were obtained from Integrated DNA Technologies, Pte. Ltd. The first probe (capture probe) is a 24-base ssDNA sequence (5'-TCTTAACAACTCACCAATATCCGC-3'). For fibre optic biosensing, the 5' end was modified with a -NH_2 group with a 6-carbon spacer. For dot blotting, the 5' end was labeled with digoxigenin. The 24-base second probe (detection probe) (5'-CCAATTTAGACTCCTACAGCTCCA-3'), was modified with a biotin at the 3' end. A 24-base ssDNA complementary to the first probe was synthesized as the positive control in the dot blotting test.

3.3.4.3 Nested qPCR

PCR and qPCR conditions. The first run PCR, involving primers Set 2, was performed according to the following steps: 1 cycle pre-denaturation at 95 °C for 2 min followed by 30 cycles denaturation at 95 °C for 45 sec, annealing at 56 °C for 45 sec, extension at 72 °C for 45 sec and finally 1 cycle of extension at 72 °C for 7 min. The reaction mixture containing 1 µL template was used in a final volume of 50 µL with 1X Colorless GoTaq® Reaction Buffer, 1.25 U GoTaq® G2 DNA Polymerase, 1 µL dNTP mix (10 mM), and 1 µL of each primer (10 µM). Following PCR the product was analyzed in a 1% (w/v) agarose gel with a loading of 5µl of resulting synthesized DNA.

Several sets of 10-fold serial dilutions of the standardized cDNA were prepared to build the qPCR standard curve using the following reaction conditions: 1 cycle activation at 95 °C for 2 min, followed by 40 cycles denaturation at 95 °C for 15 sec, annealing/extension at 60 °C for 60 sec, and 1 cycle melt curve at 60-95 °C. The reaction mixture consisted of GoTaq® qPCR Master Mix 1X, 1 µL each of HAVIF-274 and HAVIR-412 primers at 10 µM and 10 µL DNA template from the first run.

3.3.4.4 Dot blotting

Synthetic ssDNA as the positive sample was used to test the probes. The target DNA sequences were denatured in a thermal cycler (Biorad, T100) at 95 ºC for 10 min, and 1 µl from each was spotted onto a positively charged nylon membrane (Sigma). RNA samples were directly spotted without heating. The spotted membrane was exposed to UV at 254 nm for 10 min to allow for nucleic acid cross-linking. The surface was pre-hybridized in pre-warmed DIG Easy Hyb™ (Roche) buffer with shaking. Then it was incubated overnight in 10 ml DIG Easy Hyb™ (Roche) buffer containing 10 µl denatured dig-probe (68ºC, 10min) at 35 ºC. The membrane was washed twice with SSC 2X with 0.1% (w/v) SDS for 5 min, twice with SSC 0.5X with 0.1% (w/v) SDS for 15 min, and once with 1X washing buffer (Roche) for 5 min. Then it was blocked using 10 ml maleic buffer 1X with 10% (v/v) blocking solution (Roche) before incubating the membrane in antibody solution (10 ml blocking buffer with 0.02% (v/v) Anti-Digoxigenin-AP (Roche)), each for 30 min under 35 ºC. The membrane was washed twice with washing buffer for 15 min under 35 ºC then neutralized with detection buffer 1X (Roche) for 5 min at 35 ºC. In the final colouring stage, the

membrane was treated with 10 ml detection buffer with 2% (v/v) NBT/BCIP solution (Roche) and kept in a dark box. It was checked every 15 min for the development of any coloured dots until no more dot(s) appeared.

3.3.4.5 Fibre optic genosensor assay

The preparation of the fibre optic genosensor followed the protocol in **Figure 3.5**. Some steps were subjected to a few optimization experiments with details stated below.

Immobilization of -NH_2 modified capture probe. The -NH_2 modified capture probe was denatured at 95 ºC to avoid double-stranded complexing then dissolved in incubation buffer. Chemically modified fibre optic ends were then exposed to the probe solutions with concentrations ranging from 6 to 48 ng/µl in TBS solution (25 mM Tris, 150 mM NaCl, 2 mM KCl, pH7.4) with or without 1% (w/v) bovine serum albumin at 4 ºC. Other buffers tested in this section were: PBS (Sigma, 10 mM phosphate buffer, 2.7 mM potassium chloride and 137 mM sodium chloride, pH 7.4); HEPES (diluted from stock solution from Thermo Fischer, 20 mM, pH 7.4); PBS + $NaBCNH_3$ (Sigma, 0.3 M); NaOAc (diluted from stock solution from Sigma, 30 mM, pH 5.2) + $NaBCNH_3$ and Borax (100 mM boric acid, 75 mM NaCl, 25 mM sodium tetraborate, pH 8.1).

Blocking. After overnight incubation, the fibre bundles were washed with TBST (0.1% (v/v) Tween 20 in TBS) five times and then incubated in blocking conditions for 1.5 hours at 40 ºC then washed five times again with TBST followed by incubation with 0.3 M $NaBCNH_3$ in TBS buffer for 40 min at 40 ºC. The different blocking conditions were: 1%, 3% and 5% (w/v) BSA, 5% (w/v) skim milk and 1 M glycine in 0.1% (v/v) TBST.

Hybridization. The hybridization mixture was prepared by mixing 24 ng/µl detection probe and nucleic acid sequence in hybridization buffer and incubated with fibre optic tips under 35 ºC for 2 hours. The buffers tested were: Church buffer (0.5 M Na_2HPO_4, 0.5 M NaH_2PO_4, 1% (w/v) SDS and 10 mM EDTA, pH 7.5; all reagents mentioned above were supplied by Sigma); Church + 1% (w/v) BSA, TBS pH 7.4, PBS pH 7.4, 0.1% (v/v) PBST pH 7.4, TBS pH 7.4 + 1% (w/v) SDS + 10mM EDTA; Borax + 1% (w/v) SDS + 10 mM EDTA.

Avidin-HRP linkage. Avidin-HRP (Sigma) was dissolved in 0.1% (w/v) PBST with 1% (w/v) BSA in various concentrations: 1/500, 2/500, 5/500 and 12/500 (v/v) and incubated with fibre bundles for 1 hour under shaking at room temperature. Then the fibres were washed 5 times with 0.1% (v/v) PBST.

Chemiluminescent light measurement. The near-end of a single fibre optic was inserted into a lightproof tube with 120 µl of peroxide buffer. Then 120 µl luminol solution was added immediately before taking measurements by a photomultiplier tube (PMT) detector in a confined black box. 5 fibres were used for replication and the signal for each fibre was recorded as an average of 10 readings after the signal reached the maximum range. The light signal was interpreted as relative light intensities (RLU).

References

[1] Algaar, F.; Eltzov, E.; Vdovenko, M. M.; Sakharov, I. Y.; Fajs, L.; Weidmann, M.; Mirazimi, A.; Marks, R. S., *Analytical chemistry* **2015,** *87* (16), 8394-8398.

[2] Liebes, Y.; Amir, L.; Marks, R. S.; Banai, M., *Talanta* **2009,** *80* (1), 338-345.

[3] Bachmann, B. J., *Escherichia coli and Salmonella: cellular and molecular biology, 2nd ed. ASM Press, Washington, DC* **1996**, 2460-2488.

[4] Wang, L.; Wang, Q.; Reeves, P. R., The variation of O antigens in gram-negative bacteria. In *Endotoxins: Structure, Function and Recognition*, Springer: 2010; pp 123-152.

[5] LaRossa, R. A.; Majarian, W. R.; Van Dyk, T. K., Highly sensitive method for detecting environmental insults. Google Patents: 1997.

[6] Hansen, L. H.; Knudsen, S.; Sørensen, S. J., *Current Microbiology* **1998,** *36* (6), 341-347.

[7] Scientic, T. Instructions (Amine - reactive diazirine crosslinkers). https://tools.thermofisher.com/content/sfs/manuals/MAN0011635_AmineReactive_Diazirine_CrsLnk_UG.pdf (accessed 10th June).

[8] Leshem, B.; Sarfati, G.; Novoa, A.; Breslav, I.; Marks, R. S., *Luminescence* **2004,** *19* (2), 69-77.

[9] Sundarababu, G.; Gao, H.; Sigrist, H., *Photochemistry and photobiology* **1995,** *61* (6), 540-544.

[10] Saenger, M.; Borle, F.; Heller, M.; Sigrist, H., *Bioconjugate Chemistry* **1992,** *3* (4), 308-314.

[11] Rozen, S.; Skaletsky, H., *Bioinformatics methods and protocols* **1999**, 365-386.

Chapter 4

Synthesis of Silane-diazirine and its Ability in Antibody Immobilization in Aqueous Solution

This chapter shows proof-of-concept that (1) silane-diazirine can be chemically synthesized by the coupling reaction of amino silane and NHS-diazirine and (2) silane-diazirine functionalized on the fibre optic is able to capture antibodies in the aqueous condition under UV activation. The synthesis of the new silane was confirmed by 1H and 13C NMR and the photoimmobilization ability was confirmed by the direct use of HRP-linked antibody, which shows distinct signal under UV irradiation at 340-370 nm compared to the controls. The set-up optimization including the direction of the incoming UV light and the roughness of the end surface of the fibre were conducted to reduce the SD values.

4.1 Rationale and introduction

The objective of this chapter is to synthesize silane-diazirine and to confirm its photoimmobilization ability of antibody in aqueous conditions by UV activation.
By synthesizing and storing silane-diazirine molecule, it can simplify the procedures of each time when we need to use it. NHS (N-Hydroxysuccinimide) ester is the most common agent to create activated carboxylic groups [1], which has been proved highly efficient to conjugate with primary amine [1] with the release of NHS and formation of an amide bond. The previous approach has successfully obtained a pyrrole-diazirine using NHS- and amine chemistry [2] using a commercially available NHS-diazirine [3-4]. If the silane bears NH_2 tail, it is able to link NHS-diazirine as well as shown in **Figure 4.1**.

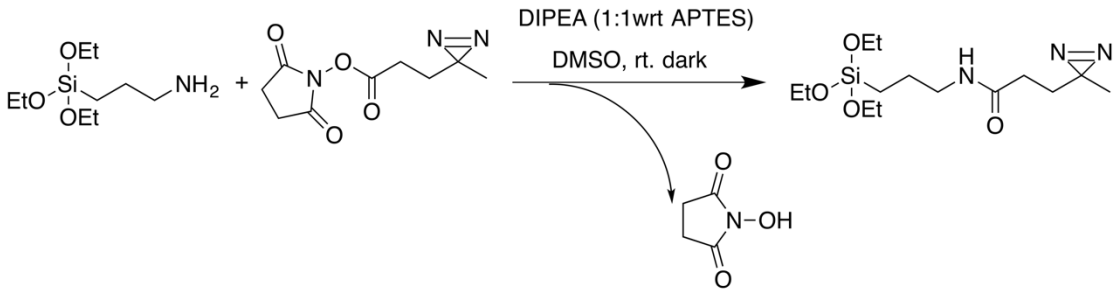

Figure 4.1 Schematic description of the synthesis of silane-diazirine by coupling of amino silane (APTES) and NHS-diazirine.

In previous studies, diazirine moieties have been used to immobilize protein-based enzymes [2] on solid support surface through UV irradiation without impairing its biological functions in the construction of biosensors. The antibody is also protein-based macromolecule. Thus, if the diazirine is present on the surface of fibre optic, antibody molecules can be photoimmobilized under UV exposure. For convenience in the preliminary experiments, HRP-linked IgG molecules were immobilized directly, so that the catalytic reaction leading to chemiluminescent signal can be immediately performed after the immobilization step.

4.2 Results and discussions

4.2.1 Synthesis and characterization of silane-diazirine

Silane-diazirine was synthesized by the coupling reaction of NHS-Diazirine and (3-aminopropyl)triethoxysilane followed by vacuum distillation. ^{1}H and ^{13}C NMR spectrum were recorded and presented below. The reaction was conducted in DMSO, so the sample of reaction mixture (0.2 mL) was mixed with 0.2 mL DMSO (d6) for ^{1}H (**Figure 4.2**) and ^{13}C (**Figure 4.3**) spectra recording. As a comparison, the spectra of starting material APTES was also recorded in DMSO (d6).

Table 4.1 NMR peaks assignment to corresponding hydrogens and carbons

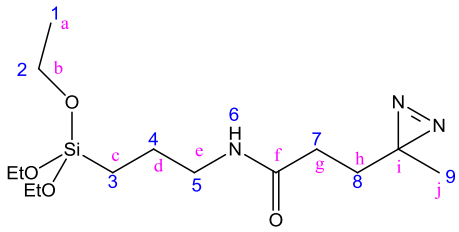

1H spectrum				13C spectrum	
H	δ (ppm)	Split	Integration	**C**	δ (ppm)
1	1.09	t	9	**a**	18.66
2	3.69	q	6	**b**	58.14
3	0.49	t	2	**c**	7.81
4	1.39	m	2	**d**	30.20
5	Around 3.4 (interfered by H_2O)	-	-	**e**	41.74
6	7.77	m	1	**f**	170.95
7	1.51	t	2	**g**	45.02
8	1.90	t	2	**h**	25.90
9	0.93	s	3	**i**	26.26
				j	23.15

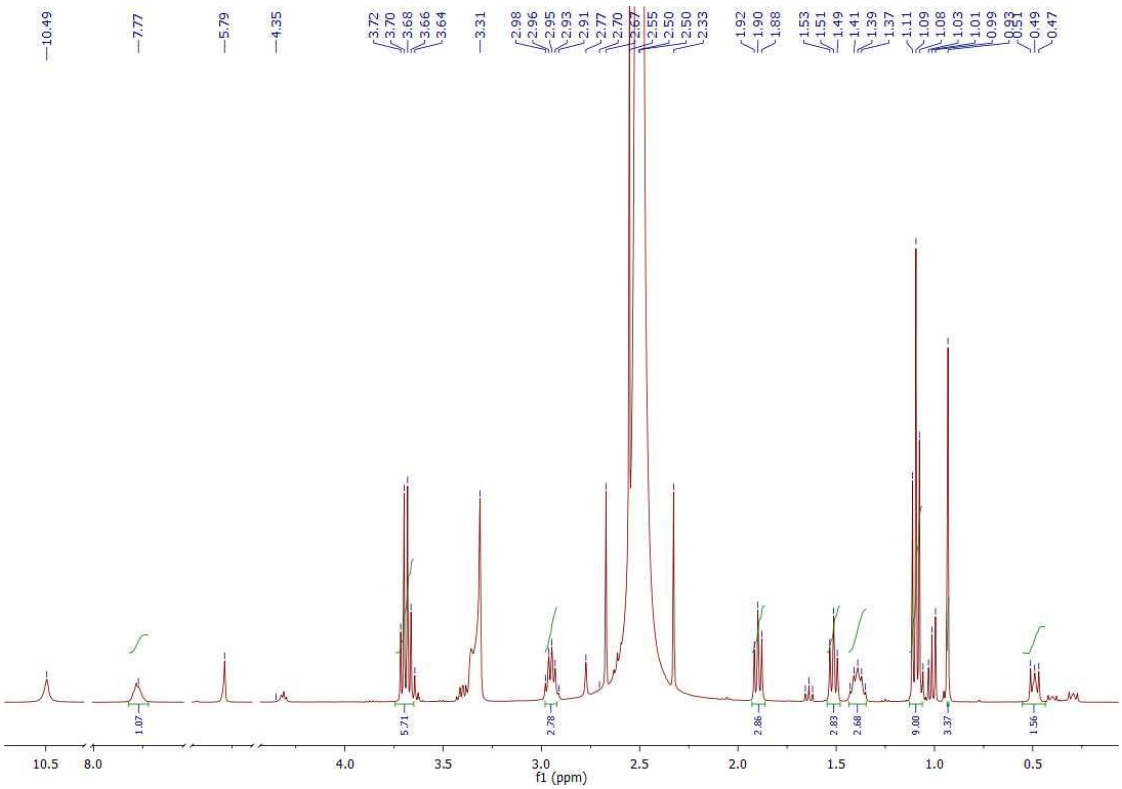

Figure 4.2 ^{1}H NMR spectrum of silane-diazirine.

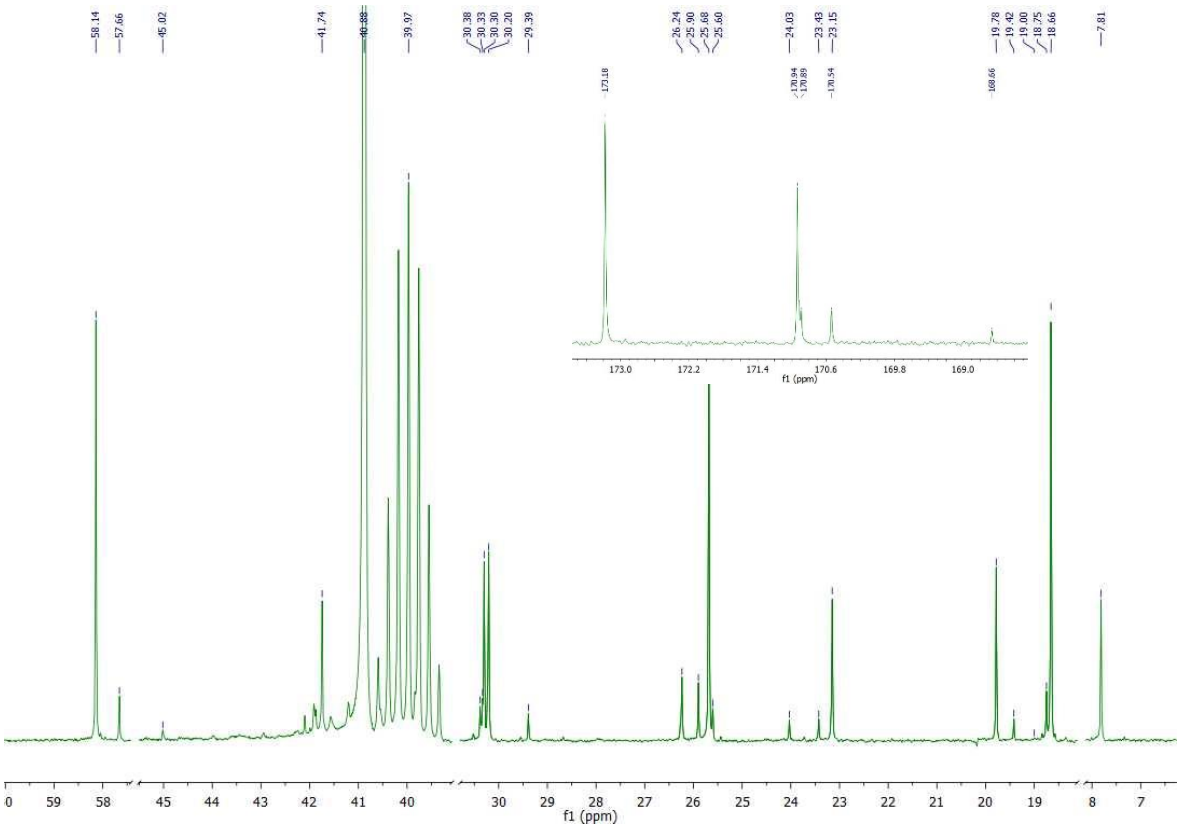

Figure 4.3 ^{13}C NMR spectrum of silane-diazirine.

In the area of carbonyl carbon region, the 173.20 ppm peak belongs to C=O carbon of NHS-succinimide [5], which, together with a broad singlet peak in 1H spectra at 10.54 ppm, corresponding to the -O**H**, indicated the release of NHS-succinimide from the reaction system. The 170.96 ppm comes from the newly formed amide bond [6]. In a comparison with APTES and reaction mixture as shown in **Figure 4.4**, all the corresponding peaks were observed to shift as shown in **Table 4.2**. The **C**H_2-NH_2 carbon peak disappeared and a new peak was shown at 41.74, showing a change in chemical environment due to the formation of –**C**H_2-NH-CO bond.

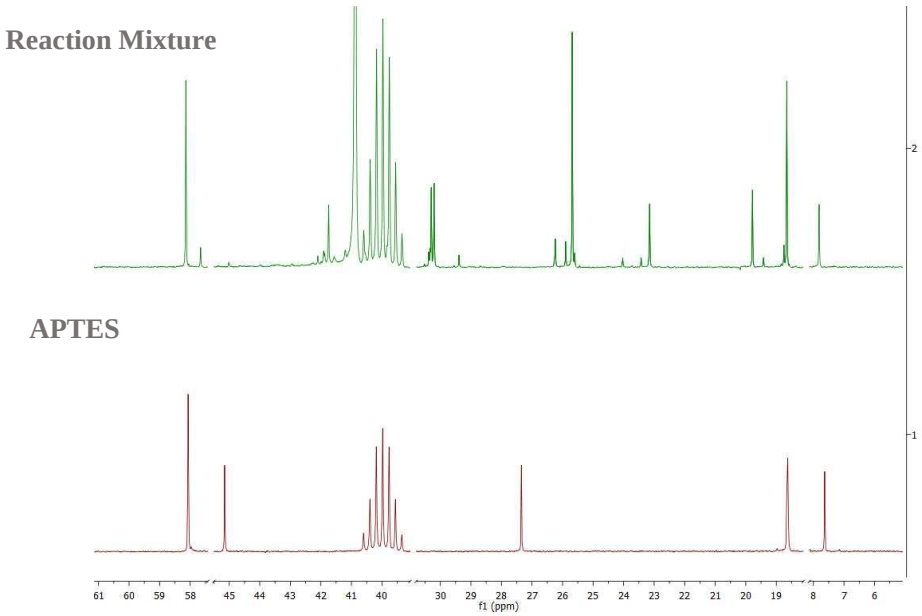

Figure 4.4 Comparison of reaction mixture and APTES ^{13}C spectrum.

Table 4.2 Comparison of reaction mixture and APTES ^{13}C spectrum

Carbon Atom	**δ_1 (ppm)**	**δ_2 (ppm)**
($\mathbf{C}D_3)_2SO$	39.98 (septet)	39.97 (septet)
$CH_3\mathbf{C}H_2OSi$	18.63	18.66
$\mathbf{C}H_2OSi$	58.07	58.14
$Si\mathbf{C}H_2$	7.63	7.81
$Si\mathbf{C}H_2CH_2$	27.35	30.20
$\mathbf{C}H_2NH_2$	45.15	41.74

On the other hand, small peaks found at 56.50 ppm, 19.00 ppm belong to the trace amount of EtOH (literature data 56.07 ppm and 18.51 ppm [7]). Thus, the decomposition

of $(EtO)_3Si$ was noticed by hydrolysis. Water peak was also observed at 3.3 ppm in ^1H spectra.

The diazirine quaternary carbon (**C**NN) signal was reported as a weak peak at around 60 ppm [6], which is not obvious in the present ^{13}C spectra. So ^{13}C DEPT NMR was conducted to distinguish the quaternary C atom. As shown in **Figure 4.5**, in the upfield region, the peak at 26.26 ppm in the normal 13C spectra below was absent in the DEPT spectra above, while all other peaks were present in both spectra. In addition, all the carbonyl C peaks were absent in the DEPT spectra. Thus, the peak at 26.26 ppm can be confirmed to be the diarizing quaternary carbon.

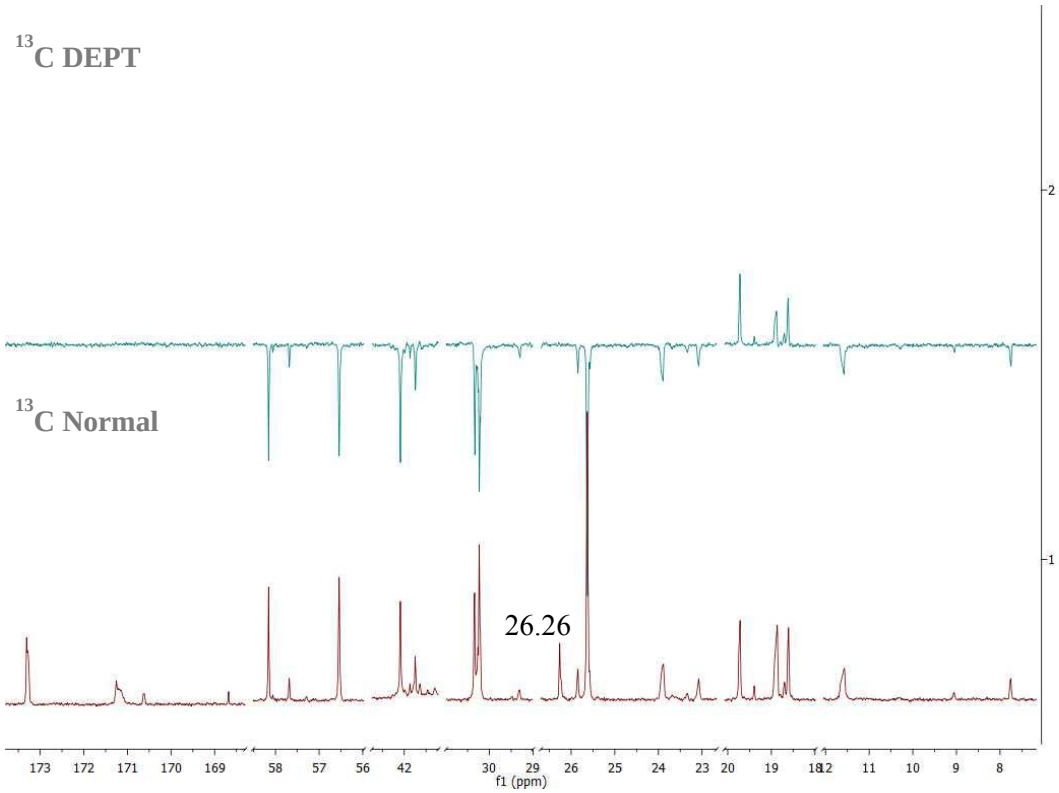

Figure 4.5 ^{13}C DEPT NMR spectrum.

4.2.2 Application of newly synthesized silane-diazirine in the immobilization of antibodies on optical fibre surface

In order to test the immobilization ability of the newly synthesized silane-diazirine, it was deposited on the surfaces of fibre optics, and then used to immobilize an HRP-attached IgG antibody, directly leading to the generation of chemiluminescent light, which is proportional to the number of immobilized HRP-IgG molecules. The UV-Vis

absorbance measurement in **Figure 4.6 (B)** shows that the absorbance of diazirine in DMSO solution happens at 300 - 385 nm, with the highest at 350 nm. The light out of that range was rejected by the compound. Thus, the UV light at 340 - 370 nm and > 350 nm were chose for the photoimmobilization test. Ambient light and dark conditions were set as control groups. As shown in the results in **Figure 4.6 (A),** the distinct S/N values of the positive groups from the control groups show the successful attachment of HRP-IgG on the fibre optic: The best results were obtained by UV irradiation at 340 - 370 nm and > 350 nm in 10% (v/v) silane-diazirine concentrations (S/N: 4.31 and 3.32, respectively) with respective dark condition signal (S/N: 1.08). Regarding the concentration of the silane, the highest concentrations always significantly increased the signal, which may imply the connection site for silane has not been saturated on the surface, which will be further explored in later sections. On the other hand, the low signal under ambient light condition (1.02, 0.64, 1.24) has confirmed the stability of NHS-silane under visible light.

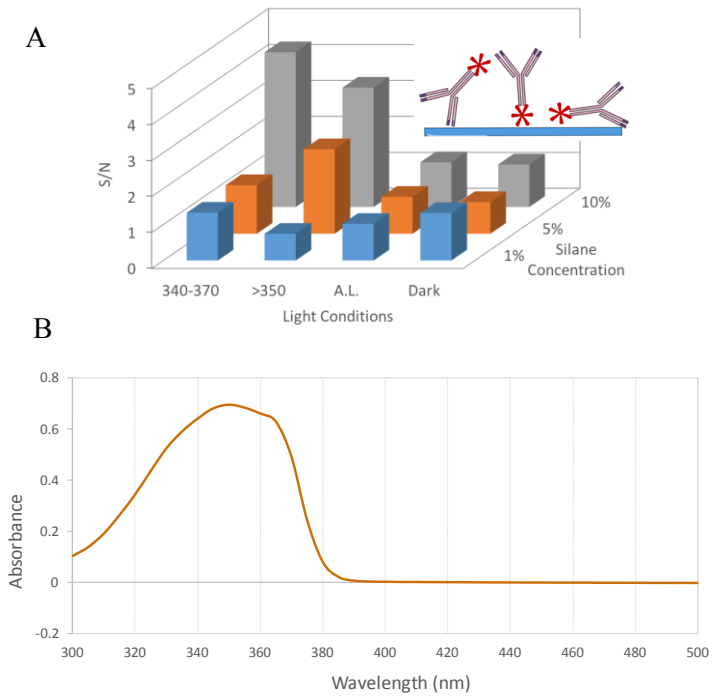

Figure 4.6 A: S/N values of the RLU signal from the immobilized HRP-IgG by silane-diazirine. The values were calculated as the ratio of the obtained RLU signal of each fibre to the RLU signal from the group without diazirine functionalized fibre. Different UV wavelengths: 340 - 370 nm, >350 nm, ambient light (A.L.) and dark conditions were tested in 1%, 5%, 10% (v/v) silane concentrations in toluene. B: UV-vis absorbance recording of the diazirine compound.

4.2.3 Set-up optimization

From the results in **Figure 4.7**, it can be easily observed that the S/N value was much higher if the light shined from the far-end than from the near-end. This is in accordance with expectation, as here the fibre optic collects and transfers the light to the site where the photo reaction happens, ensuring the steady supply of the photo for the reaction. While if the light directly shined at the near-end, it places more unstable factors to the light supply: the angle of the light source, the interference from the tube and from the antibody solutions and the distance of the light source. On the other hand, in theory, the roughness of the far-end shouldn't affect the results as illustrated by the Snell Law, only the angle of the incoming light matters. However, as guided by these two comparative tests, the later experiments will be conducted with light shining from the smooth far-end surface of the fibre.

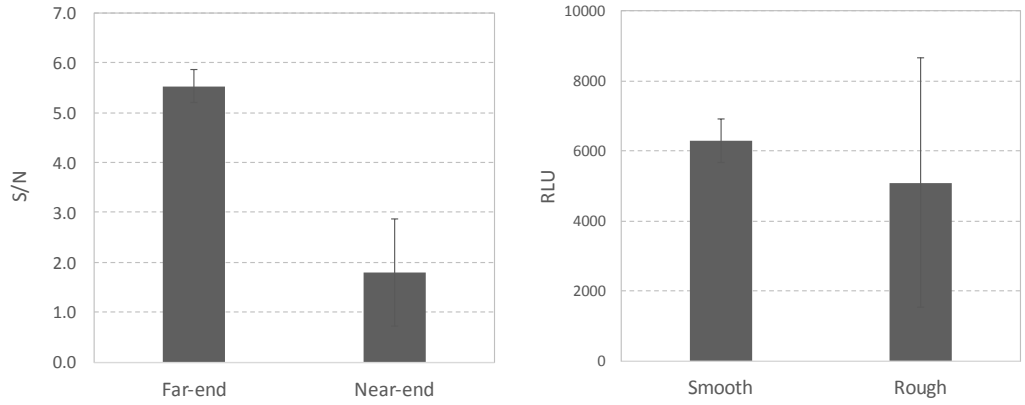

Figure 4.7 Results of the set-up optimization, left: the point where the UV light was placed at. The far-end means the non-functionalized end of the fibre strand, the light comes in from this end and propagates to the near-end surface to induce the photo-reaction; while the near-end means the functionalized end, the UV shined directly at this end from outside of the tubes containing antibody solution. Right: the roughness of the far-end where the light comes from.

4.3 Conclusions

Both the ^{1}H and ^{13}C spectrum showed the successful synthesis of the silane-diazirine by the coupling of APTES and NHS-diazirine. However, the product was not stable in

trace presence of moisture. Application of the newly synthesized silane-diazirine showed its best immobilization ability of HRP-linked antibodies under UV at 340 - 370 nm and > 350 nm by a light source at 200 mW/cm^2 (measured at 365 nm).

References

[1] Hermanson, G. T., *Bioconjugate Techniques*. Elsevier Science: **2013**.

[2] Papper, V.; Gorgy, K.; Elouarzaki, K.; Sukharaharja, A.; Cosnier, S.; Marks, R. S., *Chemistry–A European Journal* **2013,** *19* (29), 9639-9643.

[3] INSTRUCTIONS: Amine-Reactive Diazirine Crosslinkers. https://tools.thermofisher.com/content/sfs/manuals/MAN0011635_AmineReactive_Diazirine_CrsLnk_UG.pdf (accessed 1 May, 2017).

[4] Gomes, A. F.; Gozzo, F. C., *Journal of mass spectrometry* **2010,** *45* (8), 892-899.

[5] Sigma-Aldrich N-Hydroxysuccinimide product-FTNMR http://www.sigmaaldrich.com/catalog/product/fluka/56480?lang=en&region=IL (accessed 10Feb).

[6] Chou, C.; Uprety, R.; Davis, L.; Chin, J. W.; Deiters, A., *Chem. Sci.* **2011,** *2* (3), 480-483.

[7] Gottlieb, H. E.; Kotlyar, V.; Nudelman, A., *The Journal of organic chemistry* **1997,** *62* (21), 7512-7515.

Chapter 5

Comparison of the Diazirine Functionalization Routes on Fibre Optic Surface

This chapter compares the immobilization efficiency of two diazirine functionalization routes: one-step silane-diazirine as in Chapter 4 and two-step functionalization of APTES and NHS-diazirine. Two schemes were used in the experiments. The two-step functionalization route showed much higher immobilization efficiency in both schemes and was thus selected for further device construction. This chapter also shows that the immunoactivity of antibody was retained after UV photoimmobilization. In addition, a few supplementary experiments were also presented for signal improvement in the ELISA assay.

5.1 Rationale and introduction

The objectives of this chapter are:

1. To confirm the immunoactivity of the antibody is maintained after UV induced immobilization by silane diazirine.

The diazirine moieties can be induced by UV light at 330 - 370 nm and the lifetime of the carbene intermediates are within microseconds [1], which shouldn't destroy the functional protein structure of an antibody. Thus, the immunoactivity of the antibody would be preserved after the photoimmobilization on the fibre optic surface.

2. To explore the optimum diazirine functionalization route.

Results in Chapter 4 has shown that there is high risk for silane-diazirine (**Figure 3.6 Route A**) to undergo hydrolysis by the trace amount of water present during the synthesis, storage and handling process, and the photo-deterioration is inevitable during the whole process. In the two-step functionalization process as shown in **Figure 3.6 B**, the functional groups were used one at a time: the fresh hydrolyzable -OEt groups on silane reacted with the -OH groups on the fiber surface with much less chances of hydrolysis or crosslink with each other; and the diazirine groups were involved in the later stage of the process, the risk of photo-deterioration was reduced too. Thus, it is hypothesized that the two-step diazirine functionalization procedure is more effective than the direct functionalization procedure.

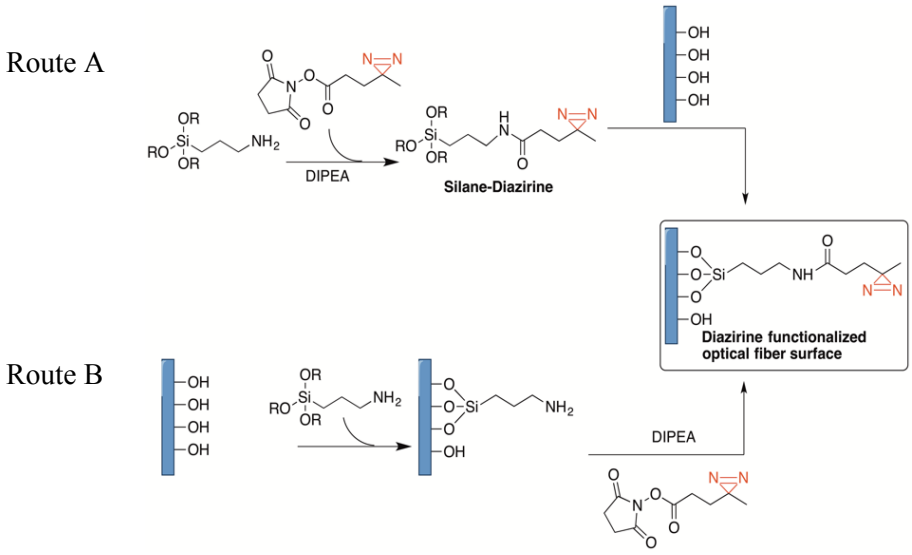

Figure 3.6 Diazirine functionalization routes.

There are two bio-assay involved to test the hypotheses. One employs the HRP-linked antibody as in Chapter 4, one is a full micro-ELISA assay using real *E. coli* cells as the analyte. The first objective requires the full ELISA assay and the second one is achieved in both assay.

The results from the full ELISA are based on several pre-experiments including (1) the calibration of the cell population against the OD 600 values in order to obtain the cell population from the OD 600 measuring; (2) the addition of IPTG to maximize the signal; (3) the selection of the suitable *E. coli* strain; (4) the selection of the suitable HRP-Ab as the detection antibody; (5) the optimum blocking condition.

5.2 Results and discussions

5.2.1 Diazirine functionalization route comparison

Two diazirine functionalization routes were compared in this section: the silane-diazirine molecule used as a one-step method as described in Chapter 4 (Route A) and a sequential addition of -NH_2 tailed silane and NHS-diazirine (Route B) on the fiber surface. The efficiency was evaluated by the RLU signals in two schemes as described in 5.1.

The results from the comparative experiments are summarized in **Figure 5.1.** In both schemes, Route B showed significant advantage as reflected by the higher RLU signal. In the HRP-IgG scheme, the RLU was proportional to the concentration of the silane with the maximum signal being brought by 100% silane in both routes. In the full ELISA assay, Route B with 50~100% silane concentration was the better method as it achieved the highest RLU response. The RLU signals in full ELISA assay were generally lower than the ones in the HRP-IgG only scheme in an order of 2. This is because, in the first scheme, the HRP performs its catalytic function regardless of the orientation of the immobilized protein. While in the second scheme, (1) only the capture antibodies in the correct orientation are able to catch the analyte; (2) the surface antigens on the cells are in certain amount that limits the numbers of detection antibodies (with HRP attached) too. On the other hand, the results in Scheme 2 further proved that the protein molecules were not only successful immobilized but also its

ability of interacting with the antigens were preserved, which is essential for the function of a immunosensor.

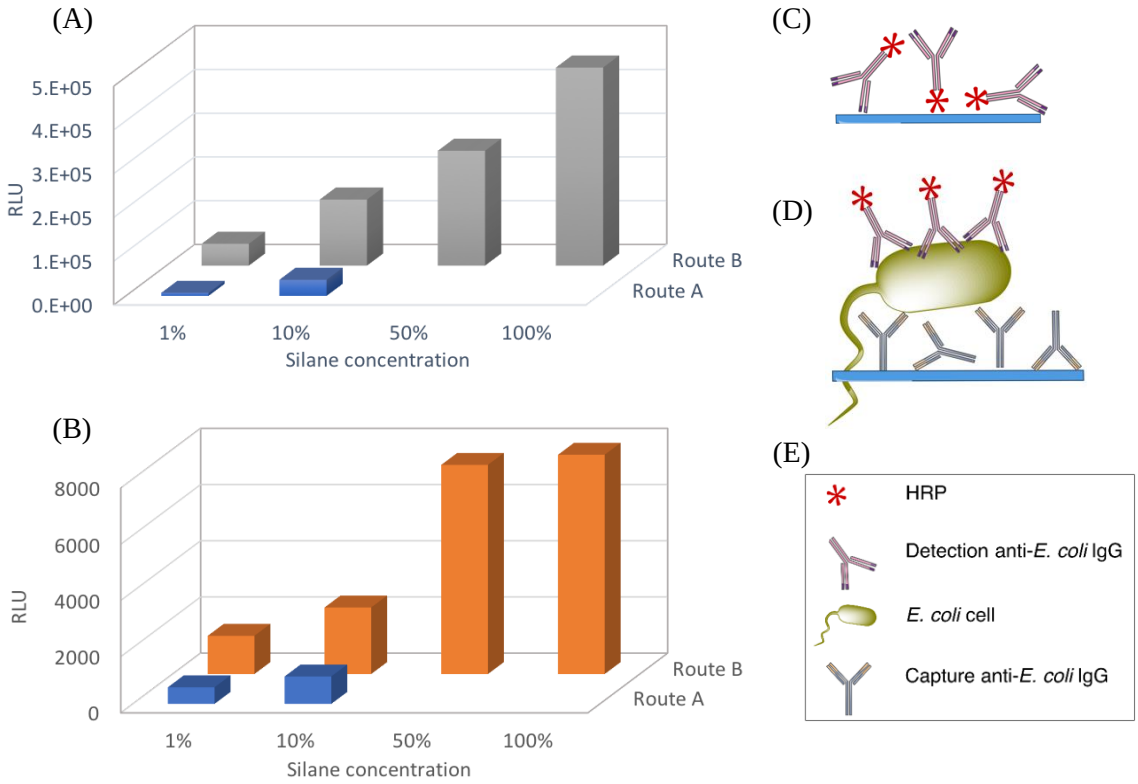

Figure 5.1 (A): RLU report of the two routes of diazirine functionalization using model in (C). (B): RLU report of the two routes of diazirine functionalization using model in (D). In (A) and (B), the silane or silane-diazirine were dissolved in toluene in 1%, 10%, 50% and 100% (v/v) concentrations. (C): the HRP-antibodies are directly immobilized by photoimmobilization. (D): the ELISA-like structure. (E): legend in (C) and (D).

Route A was initially considered to offer more convenience as the newly synthesized silane-diazirine may be stored for further one-step functionalization procedure. However, the main problems are that the ethoxy group is highly hydrolysable and these groups crosslink with each other in the presence of trace moisture. The side product from condensation of the silane molecules was observed based on the presence of the unique alcohol carbon peak at 56.50 ppm and 19 ppm. This might explain the low efficiency of Route A, as part of the hydrolyzable -OEt groups had been locked into the condensation process. Moreover, the light sensitive diazirine was involved in the earlier steps of the process, which placed more risk of light exposure.

Thus, the synthesis silane-diazirine was successful, however, with the absence of proper preservation method of the new silane-diazirine, the later experiments were following Route B, despite the disadvantage of a more time-consuming protocol. Yet the preparation time can be shortened by elevating the temperature of silane installation as there is no concern of damage to diazirine group anymore.

5.2.2 Supplementary experiments for diazirine functionalization route comparison

Prior to the full ELISA assay, a few supplemental experiments were conducted to optimize the signal and prepare for the next experiments. Experiments in 5.2.2.1 to 5.2.2.4 were performed in 96-well ELISA plates.

5.2.2.1 Selection of bacteria strains and HRP-antibody used in the ELISA assay

The ELISA assay in the experiments involved indirect capture, where the detection surface was covered by a layer of capture antibody that selectively binds and captures the surface antigens on *E. coli* cells; and direct detection, where the HRP-linked detection antibody was incubated with the antigen. The 'match' between the presence of the antigens on the surface and the specificity of the antibodies defines the final signal. By selecting the suitable bacteria strains and the antibodies would improve the signal. As shown from **Figure 5.2** and **Figure 5.3,** *E. coli* strain DPD 2794 and HRP-linked rabbit anti-*E. coli* were selected in the ELISA assay.

5.2.2.2 The effect of IPTG

The addition of IPTG was considered to induce the expression of surface antigen and thus enhancing the final signal. IPTG in the concentrations of 0.5 mM and 1 mM were tested and compared with the non-IPTG group. The signal was recorded by luminometre until the maximum reading had been reached, which was then used to plot against the CFU/ml values of the bacteria cells from the calibration curve in **Figure 5.4.** It is observed that in general, the addition of IPTG helped to enhance the signals. Thus, In the later experiments, the IPTG in concentration of 0.5 mM were used in cell culture.

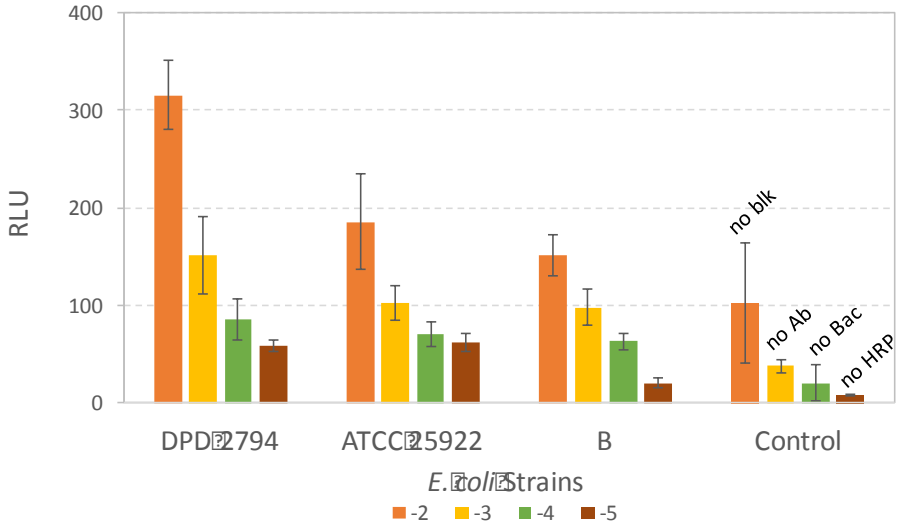

Figure 5.2 Selection of bacteria strains. -2, -3, -4, -5 stands for the cells diluted in 1/100, 1/1000, 1/10000 and 1/100000. The control experiments are performed in the 1/1000 dilution.

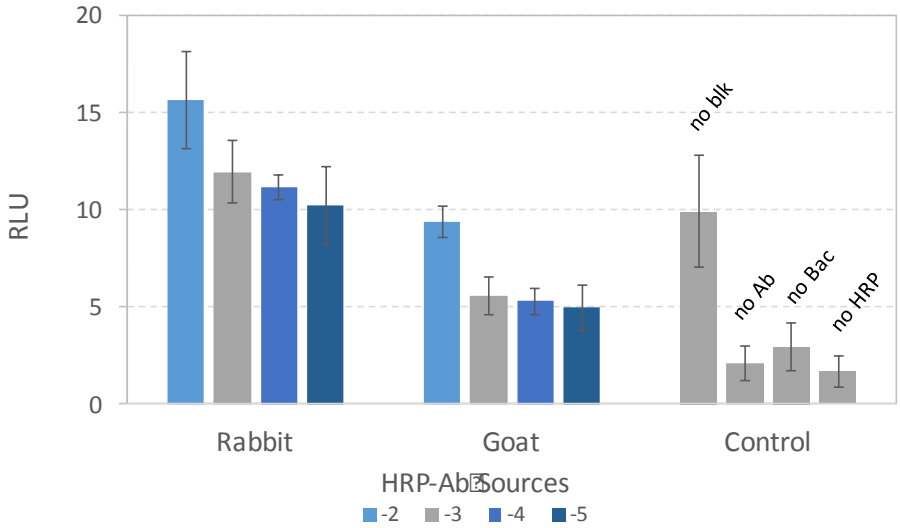

Figure 5.3 Selection of detection antibody. -2, -3, -4, -5 stands for the cells diluted in 1/100, 1/1000, 1/10000 and 1/100000. The control experiments are performed in the 1/1000 dilution.

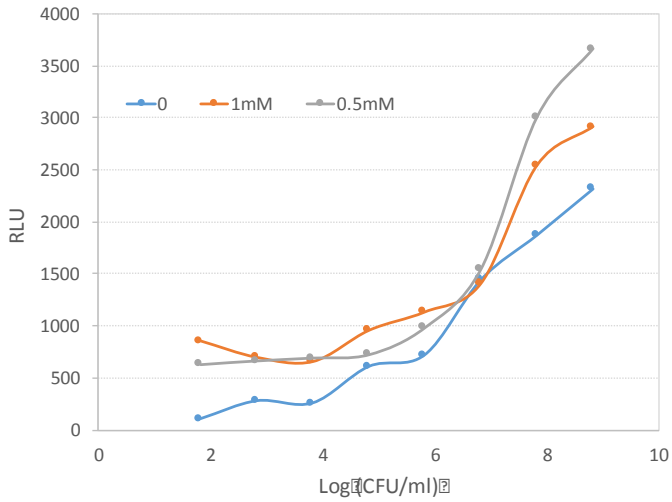

Figure 5.4 The effect of addition of IPTG.

5.2.2.3 The calibration of CFU of *E. coli* cells by the OD600 reading

The cell growth curve was generated by the dropping method in which 20 µl for each drop was pipetted onto the agar plate (in triplet multiplication). The growing phase occurred around OD600 = 0.24 (around 1.0×10^8 cells/ml), 2 hours after the refreshment under 37°C. The calibration curve was extracted along the interested OD600 range covering 0.2 to 0.6, where the cell colonies formation and OD600 values fit in a linear relationship. The growth rate of DPD 2794 was observed to be much slower than other reported *E. coli* strains [2]. However, the experiment only aimed to study the relationship between OD600 values and bacteria populations for later bacteria count calculation, as long as a linear relationship was obtained, it indicates that the total biomass measured by optical density is contributed from the live cells, the calibration curve obtained is valid [2-4]. Literature shows similar results between dropping and spreading method by using glass spreader for non-cluster formation bacteria (*E. coli*) [2], however it suggests using glass spreader instead of plastic one for spreading method. On the other hand, dropping method provides less chance for contamination and it is faster for operation, hence the author recommends this method under the experimental condition and purpose within the study.

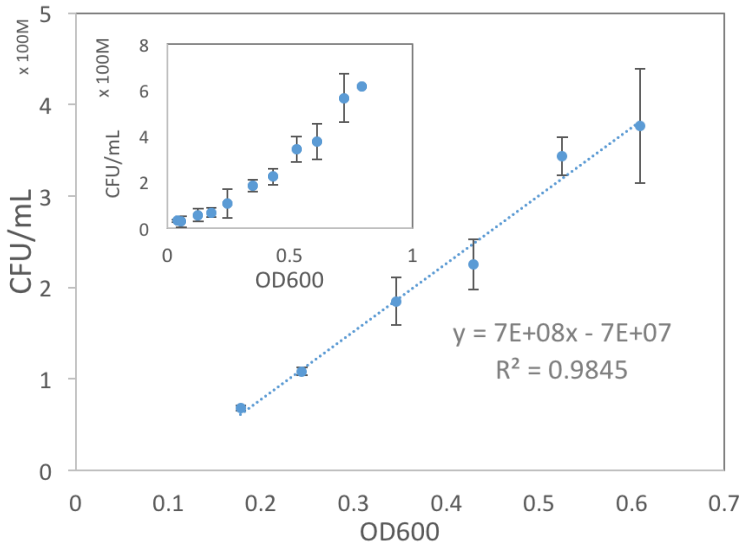

Figure 5.5 Calibration Curve of DPD2794 strain CFU counts against OD600 reading.

5.3 Conclusions

Herein the direct and two-step diazirine functionalization routes were compared based on their chemiluminescence outcome. The direct route provides convenience in the operation however is limited by the moisture and light sensitive nature of the compound. The two-step route resulted in better performance in both schemes and is selected for the construction and optimization of the immunosensor in the later experiments. It also confirmed that the immunoactivity of the capture antibodies was retained after UV irradiation, which is the foundation of a immunosensor to function.

References

[1] Sigrist, H.; Collioud, A.; Clemence, J.-F.; Gao, H.; Luginbuehl, R.; Saenger, M.; Sundarababu, G., *Optical Engineering* **1995,** *34* (8), 2339-2348.

[2] Barbosa, H.; Rodrigues, M.; Campos, C.; Chaves, M.; Nunes, I.; Juliano, Y.; Novo, N., *Journal of microbiological methods* **1995,** *22* (1), 39-50.

[3] Sezonov, G.; Joseleau-Petit, D.; D'Ari, R., *Journal of Bacteriology* **2007,** *189* (23), 8746-8749.

[4] Yamamoto, T.; Koyama, Y.; Matsumoto, M.; Sonoda, E.; Nakayama, S.; Uchimura, M.; Paveenkittiporn, W.; Tamura, K.; Yokota, T.; Echeverria, P., *Journal of Infectious Diseases* **1992,** *166* (6), 1295-1310.

Chapter 6

Optimization and Evaluation of the *E. coli* Immunosensor Constructed by Silane Diazirine

*Following chapter 5, this chapter adopted the two-step diazirine functionalization route and further optimized the key steps including the APTES coverage, blocking condition, UV irradiation condition and types of diazirine. Later the performance of the immunosensor was evaluated by comparative studies with traditional 96-well plate ELISA and another immunosensor constructed by the commonly used glutaraldehyde crosslinker. The immunosensor by diazirine method has shown superior adaptability over the other two methods in detection limit (6.44 * 10^2 CFU/ml) and dynamic range (6.44 *10^5 to 6.44 *10^8 CFU/ml, r^2 = 0.98; 6.44 *10^2 to 6.44 *10^5, r^2 = 0.92). A panel of control experiments were also conducted to verify the data above. Finally, the specificity was tested by covering various related antigens. Polyclonal and monoclonal antibodies showed the specificity in different degrees, where the polyclonal may detect the specifies sharing the similar serotypes and the monoclonal was able to not only recognize E. coli but also differentiate different strains in the same species.*

6.1 Rationale and introduction

The objectives of this chapter include:

1. To optimize the immunosensor performance by selecting the type of diazirine (aliphatic vs. aromatic) and the diazirine UV activation condition.

The coupling between the antibodies and the solid surface is the key factor of the performance of a biosensor [1-4]. A better antibody immobilization enables maximum access to the analyte and allows efficient interactions at the proximity of the transducer surface. The crucial crosslinker used for antibody coupling in this study is diazirine and improvement of the its photo-activation process can greatly promote the antibody immobilization and hence the performance of the biosensor.

As described in 2.4.3.5, proper substituted aromatic diazirines render more carbene species under UV exposure and the aromatic substituents promote the generation of more singlet state carbenes that are more active in the insertion reaction and the $-CF_3$ group helps to keep the carbenes from undergoing rearrangement. As an attempt to improve the immobilization efficiency, diazirine species with aromatic substituents were introduced and compared with the aliphatic diazirine.

Many studies have suggested that diazirine requires relatively short irradiation period [5-7], which may reduce the risk of damage of the biomolecule due to the UV exposure and the following heating effect. On the other hand, the carbene intermediates can also be quenched by water, adding negative effect to the immobilization function, so the generation of carbene by controlling the UV source intensities and the exposure time is worth exploring.

2. To evaluate the performance of the immuno-CFOS constructed by diazirine by (1) the parameters in the calibration curves comparing with previous methods; (2) the specificity test using polyclonal and monoclonal antibodies.

In the previous comparative studies between the CFOB and the traditional chemiluminescent ELISA assay, the CFOB immunosensors have shown outstanding advantages in the detection limit from 2 to 4 orders [8-9]. Amongst the CFOBs, the ones constructed by photoinduced immobilization through benzophenone had better

detection performances [4, 10]. The diazirine species are smaller in size, more stable in ambient light, and its photolytic intermediates are able to insert into a wider range of chemical bonds presenting in the protein molecules at a relatively shorter activating period. It is expected that, after condition optimization, the diazirine can immobilize immunomolecules on the fiber optic surface in a more efficient way and result in better detection ability. The specificity is another major feature of a biosensor and crucial in the detection activities. So, it was included in the last part of the performance evaluation.

6.2 Results and discussions

6.2.1 Protocol optimization

After determined the better diazirine functionalization route in Chapter 5, the selected route, Route B was optimized.

6.2.1.1 APTES modification temperature

The experimental details have been described in 3.3.3.1.1 and the florescence signal is recorded and presented in **Figure 6.1.**

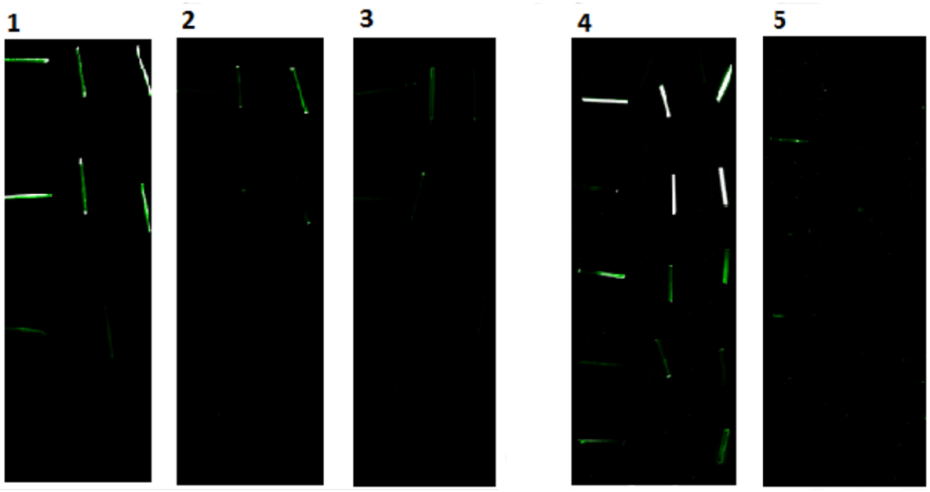

Figure 6.1 the florescence signal of the fibre optic pieces exposed at different incubation temperatures: 1, 90 ºC;2, 60 ºC; 3, 30 ºC; 4, 120 ºC; and 5, no silane as control.

As shown from the picture, the intensities of the fluorescent signal increased with the temperature. However, it was observed that from the temperature 120 ºC and above, yellow colour appeasred in the silane solution, in order to get rid of unnecessary interferences to the final results, 90 ºC was selected as the incubation temperature for silane functionalization in the following experiments.

6.2.1.2 The optimization of blocking conditions

The blocking step was performed after the immobilization of the capture antibodies, in which the blocking reagents (skim milk or BSA) bind to the unoccupied binding sites of the platform to prevent non-specific binding in the following steps [11]. From the signal/noise ratio results in **Figure 6.2.** The optimum condition was found to be 5% (w/v) skim milk in PBST solution and it was selected for the relevant experiments.

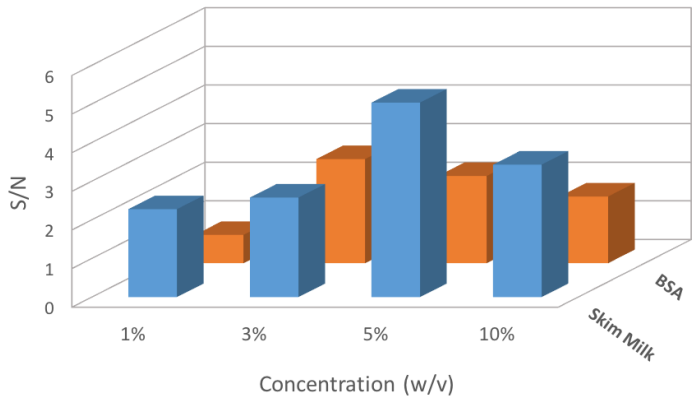

Figure 6.2 The optimization of blocking conditions. The skim milk and BSA were dissolved in PBST (0.1% v/v) solution in concentrations of 1%, 3%, 5% and 10% (w/v).

6.2.1.3 Irradiation light intensities and time interval of UV exposure

Two kinds of UV sources, that differ in the UV emitting materials, shapes and light intensities were used and compared in this study according to the recommendations of the product manual of SDA. One was the Max 303 Xenon light source (300W) capped with a single-band bandpass filter, giving a final UV output in the range of 340 - 370 nm with a power of 200 mW/cm^2 measured at 365 nm (referred as MAX 303). The

other source was Spectroline® ENF-280C (8W) hand-held UV lamp at 365 nm (referred as UV 365) with a power of 1090 µW/cm^2.

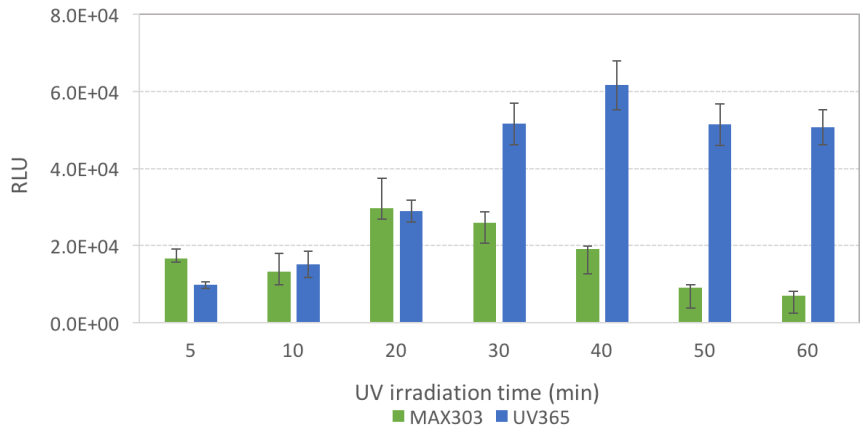

Figure 6.3 RLU immunoassay responses using two different UV light sources, illuminating from 5 to 60 minutes. MAX 303 stands for a Xenon UV lamp emitting light from 340 nm to 370 nm with a final power of 200 mW/cm^2 measured at 365 nm. UV 365 represents an ENF-280C (8 W) hand-held UV lamp emitting light at 365 nm with a power of 1090 µW/cm^2.

The evaluation of the efficiency of the equipment and irradiation time interval was based on the final RLU output of the biosensor. The highest signal was achieved by UV 365 at 40 minutes. A few more information was also released from the results. In general, both the intensity of light and duration of UV exposure were playing important roles in determining the final outcome. For the same light intensity, the outcome was in a time-dependent manner. The signal increased in the first 20 minutes (for MAX 303) or 40 minutes (for UV 365) and then started to drop. This may be explained by the fact that, the immobilized protein on the tip was partially destroyed by the heat developed from the UV light. Secondly, in the first 20 minutes, the signal from MAX 303 was higher than that from UV 354, probably because the higher intensity results in faster generation of carbene. However, faster and more is not always better, as the carbene was also exposed in an aqueous environment in which it can be quenched by water molecules [12-13] before contacting with target bonds in the protein, thus a balance should be adjusted between the rate of carbenes generation and carbene insertion reaction into protein moieties. In addition to generating carbenes, diazirines undergo isomerization

leading to the formation of the linear diazo intermediates, which have a longer lifetime and they also transform to carbenes upon further UV activation at a relatively lower rate [14]. From the results, it can be concluded that, a longer exposure time under a relatively lower intensity UV light is favoured.

6.2.1.4 Selection of silane spacer arm and diazirine types

In this examination, NH_2-tailed silanes with different spacer arm lengths were cooperated with both aliphatic and aromatic diazirines and the final output is presented in **Figure 6.4**, where the aliphatic diazirine (SDA) and silane with 4-atom space arm showed the highest RLU value.

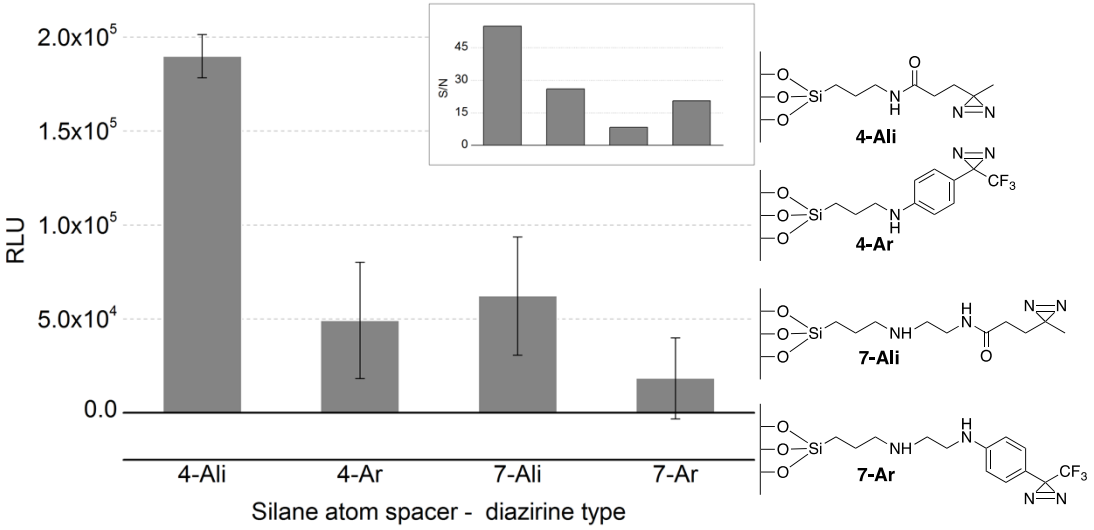

Figure 6.4 RLU responses from the immunoassay and S/N values reported for each silane and diazirine species combination illustrated on the right. The silane species employed were 4-atom and 7-atom spacer arm-length amine tailed silanes. A typical aliphatic and aromatic diazirine were adopted for comparison.

Aromatic diazirines (ArDia) bearing a trifluoro group on the diazirine carbon have been favoured due to a few advantages such as the higher carbene to diazo isomer ratio and higher singlet state carbenes generation ratio. Despite its advantages reported in the previous studies [6, 14-18], the aromatic diazirine didn't work as well as the aliphatic diazirines did in this system. The reasons can be various and complicated as diazirine mechanisms are still not thoroughly understood and studies have been putting forward new theories in addition to the old ones [19-20]. Here two directions may be considered as

the main factors that may hinder the ability of the aromatic diazirine in this system. One of them is the poor water solubility of the aromatic ring in the water solvent [12], being directly conjugated with π electrons from the phenyl ring with the contribution of electron drawing group -CF_3, the carbene is prevented from entering the water phase. The large standard deviation might be also owing to this phase barrier that the carbenes are only able to catch the proteins that diffuse to the interface. Moreover, the aromatic diazirines are reported with higher singlet carbene yield, which is more specific to nucleophilic bonds like O-H and N-H than C-H insertion and prone to water reaction [20-21], which further reduces the indiscriminative binding with proteins. On the other hand, NH_2 silane with 4-atom spacer arm is found to be more beneficial than 7-atom spacer arm silane. This can be explained by the flexibility of the longer chains that allows the primary amine group in the end and the secondary amine group in the middle to form hydrogen bonding with its surroundings thus the sites for further reaction are largely blocked.

6.2.2 Immunosensor performances

To evaluate the performance of the newly developed diazirine immobilization technique (AmDia), it was compared with the traditional chemiluminescent ELISA (CL-ELISA) and another FOBS using APTES and glutaraldehyde as a chemical crosslinker (AmGlu). The general performances of the three methods were described by the three calibration curves. Negative controls were set in parallel to provide cut-off values of the biosensors and non-specific binding investigation. Finally, the specificity was confirmed by testing against a range of samples.

6.2.2.1 Calibration

To further test the newly constructed system, the AmDia optical sensor was compared to other two techniques in their immunosensor behaviors. We started with the calibration curves, which describe the general performance of a detection system. The curves were constructed by plotting the RLU values against a set of *E. coli* cell dilutions ranging from $6.44*10^8$ to 6.44 CFU/ml, approximately (**Figure 6.5**). Unlike previous data obtained from the fibre optic immunosensor systems [9-10], a typical complete sigmoid curve didn't occur in any of the three conditions. In other words, the highest signal range didn't reach the saturation level. Our focus is, however, to obtain the

lowest detection limit and study their dynamic range, especially in the lower concentration domains.

The lower detection limit (LDL) was set by the Equations (1) and (2),

$$LDL = NEG + 3SD \quad (1)$$

$$SIG > NEG \quad (2)$$

which is the sum of the signal from the negative control (in the absence of *E. coli* cells) (NEG) plus 3 times of its standard deviation (SD). The signals which are higher than the LDL are then considered significant. The LDL for each technique was 734, 2050 and 3638 for CL-ELISA, AmGlu and AmDia, respectively, approximately corresponding to 6.44 * 10^5, 6.44 * 10^3 and 6.44 * 10^2 CFU/ml. In this aspect, the AmDia method is superior to the chemiluminescent ELISA and AmGlu techniques by orders of 3 and 1 in LDL, respectively.

The dynamic range is the concentration range where the detection system displays a linear relationship between the signal and the dilutions. It was calculated based on the data extracted from its calibration curve and fit into Equation (3).

$$y = y_{01} + D\log(x) \quad (3)$$

where y is the RLU output and x is the CFU of bacteria. The linear range cutoffs are determined by the r^2 values which show the reliability of the regression. The linear ranges were thus determined as 6.44 *10^8 to 6.44 *10^5 CFU/ml for all the three methods with r^2 values 0.98 for CL-ELISA, 0.97 for AmGlu and 0.98 for AmDia. Though not obvious from the plot, another linear range was noted in the lower CFU range of the AmDia group from 6.44 *10^2 to 6.44 *10^5 with an r^2 of 0.92. Such a phenomenon was not found in the other two groups. This may imply that the AmDia may be sensitive enough to detect the lower concentration environment, which is practical and useful for real sample applications.

The other aspect of the sensitivities of the biosensors are quantified as the slopes of the linear range as they show the power to discriminate the differences between two signals with changes in analyte concentrations, as represented by its form: $\frac{y_A - y_B}{x_A - x_B}$. The sensitivity of AmDia (D_1 = 44159; D_2 = 7254) was found to be higher than that of AmGlu (5838) and CL-ELISA (1008).

The lower LDL and higher sensitivity may be attributed to the effectiveness of the photo-induced reactions as the carbenes are able to react with a few different chemical bonds with fast insertion reactions. Additionally, during the irradiation, the protein solution temperature may have increased slightly due to UV, stimulating the motion of the proteins in the solution, and increasing the number of effective collisions. While in the AmGlu case, the system is incubated at 4 °C so that the molecular motion is impeded.

6.2.2.2 Negative control panel

In order to examine the influence of non-specific binding on the final signal response, a series of control experiments were carried out and the results are summarized in **Table 6.1**. The response values from Entry 2 (no capture antibody), 4 (no *E. coli* analyte). and 5 (no anti-*E. coli* HRP) are all relatively negligible. This indicates that the designed immunosensor didn't exhibit non-specific binding. The high value from Entry 2 pointed to the importance of the blocking step to ensure a low background noise. Entries 6 and 7 were designed to show the advantage of surface crosslinkers, the absence of which resulted in a lower overall response. In addition, glutaraldehyde rendered a relatively higher background signal, which might be due to the high reactivity of the aldehyde groups on the surface to interact with any protein molecules presented.

6.2.2.3 Specificity test

The specificity test was conducted by using both polyclonal and monoclonal as the capture antibodies covering a range of antigens. The results are presented in **Figure 6.6**.

The polyclonal antibodies responded to a series of *E. coli* strains regardless "O" or "K" antigenic serotypes and the crossreactions were observed with related *Enterobacteriaceae* like *Salmonella* and slightly with O-antigenic polysaccharide from *Vibrio cholera*. By applying the monoclonal antibody which is specific to the *E. coli* O157 antigen, the specificity was further enhanced as (1) the biosensor was able to differentiate different strains of *E. coli* based on their serotypes; (2) the cross-reactions with *salmonella* and O-antigenic polysaccharide from *Vibrio cholera* were eliminated. In addition, the biosensor with both polyclonal and monoclonal failed to detect all other antigen samples. The results show that the diazirine method can be used for both

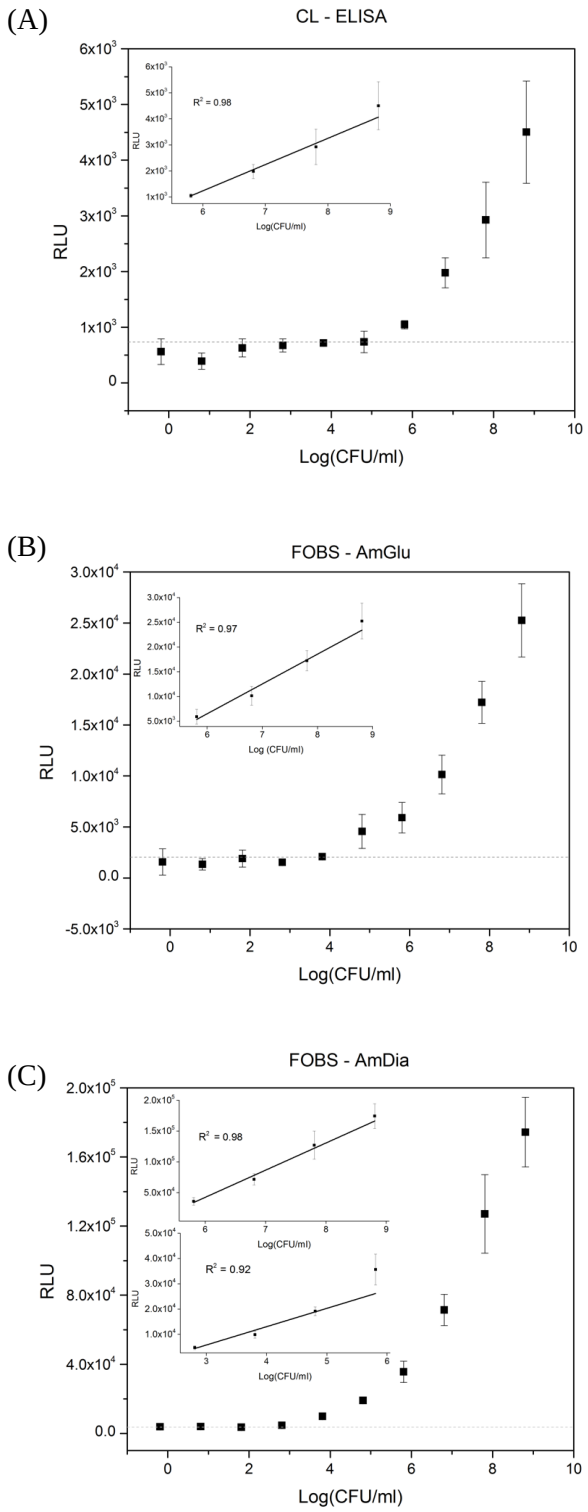

Figure 6.5 Calibration curves for A: chemiluminescent ELISA (CL-ELISA); B: optical fibre immunosensors using either glutaraldehyde as a crosslinker (FOBS-AmGlu); C: diazirine as crosslinker (FOBS-AmDia). The calibrations were obtained using target *E. coli* dilutions ranging from 6.44 CFU/ml to $6.44*10^8$ CFU/ml. In each calibration, the linear range are visualized on the top left corner with the r^2 values.

Table 6.1 Experiment control panel for attempted immunoassays and fibre optic immunosensor based on various immobilization construction chemistries to investigate the non-specific bindings. The "+" and "-" signs refer to the steps accomplished and avoided for each procedure.

Entry	Method[a]	Silica glass functionalization		ELISA Procedures				Normalized response[b]
		Silane	crosslinker	anti-*E. coli* IgG	Blocking	*E. coli* analyte	Anti-*E. coli*-HRP	
1	CL	*	*	+	+	+	+	1
	Glu	+	+	+	+	+	+	1
	Dia	+	+	+	+	+	+	1
2	CL	*	*	-	+	+	+	0.723
	Glu	+	+	-	+	+	+	0.028
	Dia	+	+	-	+	+	+	0.013
3	CL	*	*	+	-	+	+	2.810
	Glu	+	+	+	-	+	+	4.142
	Dia	+	+	+	-	+	+	0.810
4	CL	*	*	+	+	-	+	0.158
	Glu	+	+	+	+	-	+	0.039
	Dia	+	+	+	+	-	+	0.023
5	CL	*	*	+	+	+	-	~0
	Glu	+	+	+	+	+	-	0.002
	Dia	+	+	+	+	+	-	0.004
6	Glu	-	+	+	+	+	+	0.728
	Dia	-	+	+	+	+	+	0.084
7	FOBS	+	-	+	+	+	+	0.079

a. Type of an immunoassay or FOBS construction chemistry used: chemiluminescent ELISA (CL), amino silane and glutaraldehyde linker fibre optic biosensor (Glu), amino silane and diazirine linker fibre optic biosensor (Dia), fibre optic biosensor (FOBS).

b. The signal from a full immunoassay protocol was set as 1, the response of control experiments was calculated as a ratio between the results from Entry 2 -7 and Entry 1.

*. Not relevant to the chemiluminescent ELISA procedure.

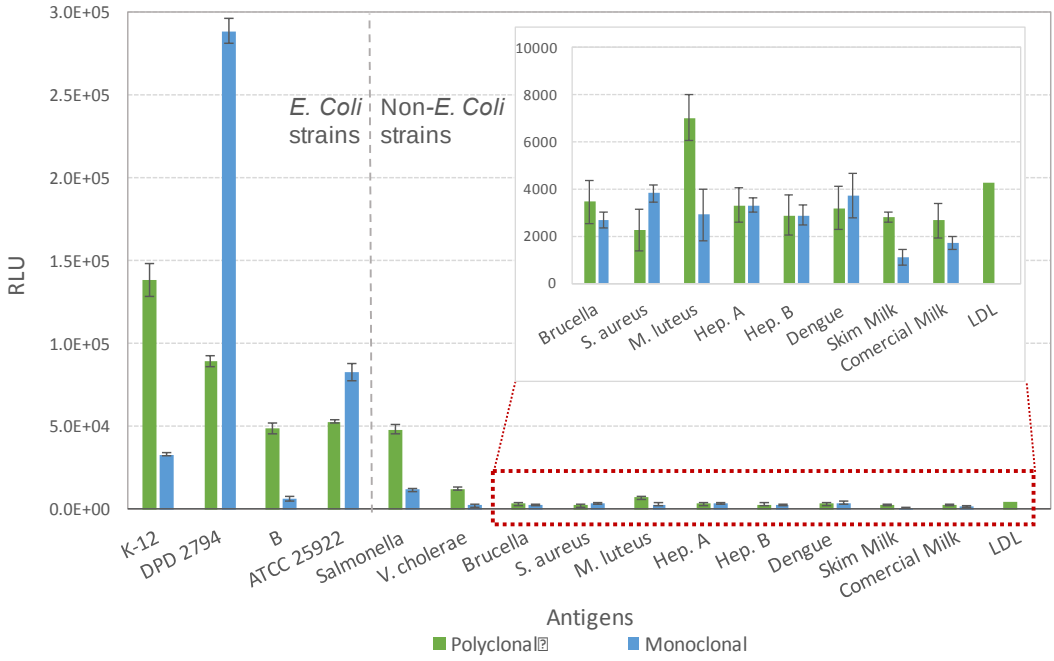

Figure 6.6 Specificity test covering several *E. coli* strains: K-12, DPD 2794, B and ATCC 25922; and antigens from other sources: *Salmonella* (*salmonella* bacteria culture), *V. cholerae* (LPS from *Vibrio cholerae*), *Brucella* (suspension of inactivated *Brucella*), *S. aureus* (suspension of inactivated *Staphylococcus aureus*), *M. luteus* (*Micrococcus luteus* bacteria culture), Hep. A (Hepatitis A virus VP3 antigen), Hep. B (Hepatitis B virus e antigen), dengue (dengue virus nonstructural protein 1), skim milk (1% w/v skim milk in PBST), commercial milk (1% w/v commercial milk in PBST), LDL (lower detection limit as determined by the calibration curve the of AmDia FOBS using polyclonal antibody).

polyclonal and monoclonal antigens. With polyclonal antibodies, the system demonstrates moderate specificity, a rough positive signal may be obtained, indicating the presence of a certain group of pathogens; with monoclonal antibodies, more detailed information regarding the specific strains or species may be available. The selection of the antibodies depends on the budget and requirement of the test.

6.2.3 Surface characterization by SEM

The SEM micrographs (**Figure 6.7**) provided us with the descriptive information about the morphology of the modified glass surface generated from each step. By comparing B with A, it can be seen that the silanization step had seemly given a relatively

homogenous coverage over the surface [4]. The EDX analysis further verified the functionalization of silane molecules, where the carbon and nitrogen peak appeared. Obvious changes can be recognized from C and D, reflecting the effect of the treatment to the surface coverage layers. The rod-shaped particles with length around 1.5 - 2.2 μm were visible in a relatively high population. This clearly indicates the bacteria attachment to the surface, which corresponded to a notable light output. (F) is the close look at the attached *E. coli* cells, showing a layer surrounding the surface of bacteria, which is suspected to be either the skim milk from the solution or the secretion from the inside of the bacteria.

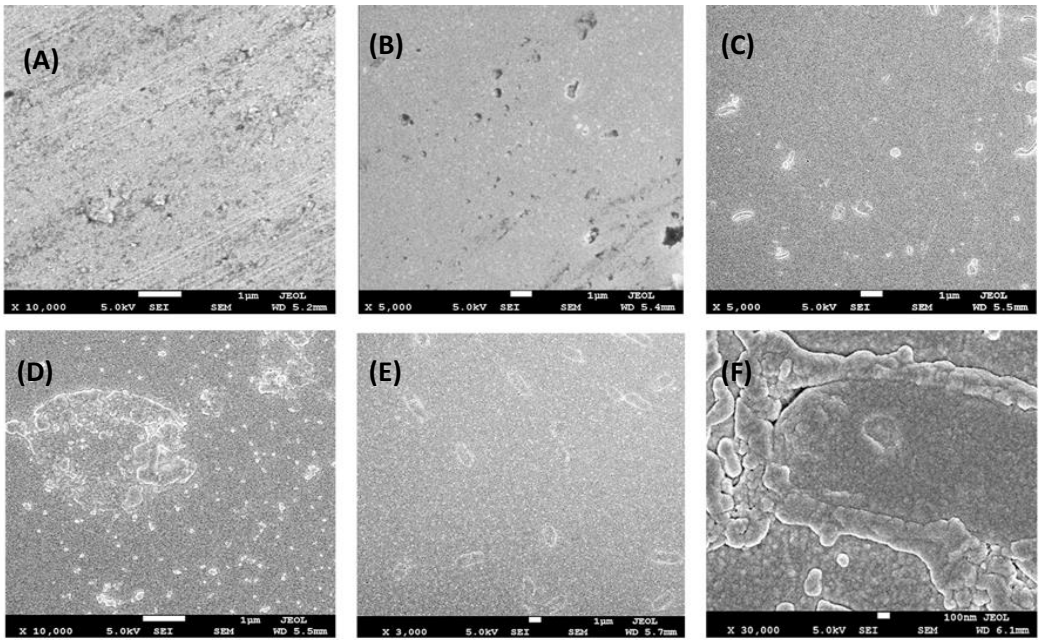

Figure 6.7 SEM images of optical fiber surfaces after each treatment in photoimmobilization procedures utilizing APTES as silane and SDA as diazirine source following Route B. (A) plain surface after piranha activation. (B) after silanization by APTES. (C) after reaction with SDA. (D) after antibody immobilization. (E). *E. coli* bacteria attached on the surface. (F) Zoom-in image of an immobilized bacteria.

6.3 Conclusions

6.3.1 Optimization of antibodies immobilization

The coverage of antibodies is one of the most critical factors that define the performance of a biosensor [3-4]. The aforementioned results shows that the biosensor performance has been greatly improved by optimizing the antibody immobilization process. During the UV inducing process, the best result was achieved by UV in a relatively lower intensity and a longer irradiation time (UV 365 for 40 minutes). This might be due to the property of carbenes that they can be easily quenched by water molecules, so a slow release of carbenes at lower UV intensities may be beneficial in aqueous conditions as it provides more opportunities for the protein molecules to participate in the carbene insertion reactions.

6.3.2 The advantages of the AmDia FOBS

From the aforementioned results, the AmDia sensor seems a superior FOBS over the other two detection methods. Firstly, the two FOBSs are in generaa more sensitive than the CL-ELISA method. Though a fibre cross-section (0.12 mm^2) has a much smaller binding surface area than a well in a 96-microplate (33.2 mm^2), the protein is attached through covalent binding unlike the physical absorption, thus the stability is increased. Besides, the chemiluminescent reaction happens in close proximity to the fibre surface, resulting in an enhancement of light collection. Between the two FOBS techniques, AmDia has shown a lower LDL and a higher sensitivity, which may indicate that there were more antibodies attached to the fibre tip. Last but not the least, during the preparation, the protocol of the AmDia method is much simpler and less time-consuming than that of the AmGlu.

References

[1] Rusmini, F.; Zhong, Z.; Feijen, J., *Biomacromolecules* **2007,** *8* (6), 1775-1789.

[2] Jung, Y.; Lee, J. M.; Kim, J.-w.; Yoon, J.; Cho, H.; Chung, B. H., *Analytical chemistry* **2009,** *81* (3), 936-942.

[3] Eltzov, E.; Marks, R. S., *IEEE instrumentation & measurement magazine* **2009,** *12* (5), 10-16.

[4] Liebes, Y.; Amir, L.; Marks, R. S.; Banai, M., *Talanta* **2009,** *80* (1), 338-345.

[5] Prestwich, G. D.; Dormán, G.; Elliott, J. T.; Marecak, D. M.; Chaudhary, A., *Photochemistry and Photobiology* **1997,** *65* (2), 222-234.

[6] Dubinsky, L.; Krom, B. P.; Meijler, M. M., *Bioorganic & medicinal chemistry* **2012,** *20* (2), 554-570.

[7] Husain, S. S.; Nirthanan, S.; Ruesch, D.; Solt, K.; Cheng, Q.; Li, G.-D.; Arevalo, E.; Olsen, R. W.; Raines, D. E.; Forman, S. A.; Cohen, J. B.; Miller, K. W., *Journal of Medicinal Chemistry* **2006,** *49* (16), 4818-4825.

[8] Algaar, F.; Eltzov, E.; Vdovenko, M. M.; Sakharov, I. Y.; Fajs, L.; Weidmann, M.; Mirazimi, A.; Marks, R. S., *Analytical chemistry* **2015,** *87* (16), 8394-8398.

[9] Liebes, Y.; Marks, R. S.; Banai, M., *Sensors and Actuators B: Chemical* **2009,** *140* (2), 568-576.

[10] Atias, D.; Liebes, Y.; Chalifa-Caspi, V.; Bremand, L.; Lobel, L.; Marks, R. S.; Dussart, P., *Sensors and Actuators B: Chemical* **2009,** *140* (1), 206-215.

[11] Xiao, Y.; Isaacs, S. N., *Journal of immunological methods* **2012,** *384* (1-2), 148-151.

[12] Sundarababu, G.; Gao, H.; Sigrist, H., *Photochemistry and photobiology* **1995,** *61* (6), 540-544.

[13] Gomes, A. F.; Gozzo, F. C., *Journal of mass spectrometry* **2010,** *45* (8), 892-899.

[14] Kumar, A. B.; Anderson, J. M.; Manetsch, R., *Organic & biomolecular chemistry* **2011,** *9* (18), 6284-6292.

[15] Ghiassian, S.; Ismaili, H.; Lubbock, B. D. W.; Dube, J. W.; Ragogna, P. J.; Workentin, M. S., *Langmuir* **2012,** *28* (33), 12326-12333.

[16] Hashimoto, M.; Hatanaka, Y., *European journal of organic chemistry* **2008,** *2008* (15), 2513-2523.

[17] Leshem, B.; Sarfati, G.; Novoa, A.; Breslav, I.; Marks, R. S., *Luminescence* **2004,** *19* (2), 69-77.

[18] Li, Z.; Hao, P.; Li, L.; Tan, C. Y. J.; Cheng, X.; Chen, G. Y. J.; Sze, S. K.; Shen, H.-M.; Yao, S. Q., *Angewandte Chemie International Edition* **2013,** *52* (33), 8551-8556.

[19] Wang, J.; Kubicki, J.; Peng, H.; Platz, M. S., *Journal of the American Chemical Society* **2008,** *130* (20), 6604-6609.

[20] Das, J., *Chemical Reviews* **2011,** *111* (8), 4405-4417.

[21] Ghiassian, S.; Biesinger, M. C.; Workentin, M. S., *Canadian Journal of Chemistry* **2014,** *93* (1), 98-105.

Chapter 7*

Development of A Chemiluminescent DNA Fibre Optic Genosensor to Hepatitis A Virus (HAV)

This chapter demonstrates the development of a chemiluminescent DNA fibre optic genosensor to Hepatitis A Virus (HAV). A set of ssDNA probes targeting HAV RNA sequence were designed and validated by nested qPCR technique. The capture probe was immobilized on the tip of fibre optic surface followed by the formation of a sandwich structure with the target sequence (cDNA and RNA) and a detection probe. A few steps of the protocol were optimized and lead to a satisfactory signal/noise ratio. Later the calibrations were established for both cDNA and RNA target. Specificity test showed the probes were highly specific to HAV RNA sequences.

*This section published substantially as Ye, K., M. Manzano, R. Muzzi, K.Y.-H. Gin, N. Saeidi, S.G. Goh, A.I.Y. Tok, and R.S. Marks, *Talanta*, **2017**. 174: p. 401-408. [1]

7.1 Rationale and introduction

The objectives of this chapter include:

1. To design the ssDNA probes and primers and to validate the ssDNA probes by the traditional PCR-based method.
2. To explore the optimum immobilization and working conditions for the geno-CFOS.
3. To explore the genosensor performance by evaluating the calibration curves and specificity.

Previous optical fibre genosensor approach on the *Brettanomyces bruxellensis* has shown a satisfactory signal-noise ratio after the condition optimization of the concertation of the probes and hybridization conditions [2]. It provides the proof-of-the-concept of a DNA genosensor. However, there are still many challenges in the proposed work, one being that it requires the ssDNA probe to detect the RNA sequence instead of the DNA. On the other hand, the ssDNA probe has to be designed and optimized to fit the detection requirement. The next one is the integration of the ssDNA probes onto the CFOB platform, mainly the capture probe immobilization. The previous study used a capture probe with the length of 53 bases, while in this study, the designed capture probe was in the length of 24 bases. Studies show that the optimum concentration of the single stranded DNA probes with different lengths could be significantly different [3]. So, the optimum incubation condition of capture probe should be re-explored. And a hybridization buffer called church buffer [4] was not included in the previous test, which is worth exploring. At last, the previous study didn't give the calibration for the detection, which is one of the directions of the effort in this work to better evaluate the genosensor.

7.2 Results and discussions

The ssDNA probes were designed and validated first and the construction of the genosensor follows the procedures shown in **Figure 3.5**, with condition optimization applied in each step.

7.2.1 Probe design and validation by qPCR and dot blot

PCR and qPCR as conventional methods were conducted to confirm the cDNA products from the reverse transcription from HAV RNA samples and served as the further investigational lab tools for putative HAV contaminated sample as indicated by the in-field fibre biosensor system. Herein, the nested-PCR technique was conducted for this purpose as it not only provided the quantitative measurement of the sample but also offered higher specificity by the combination of the 'outer' and 'inner' PCR primers.

Set 1: outer primers: (forward, 5'-ACTTGATACCTCACCGCCGTTTGC-3') and (reverse 5'-AGTCCTCCGGCGTTGAATGG-3'); inner primers: (forward 5'-CGGGGTCAACTCCATTA-3') and (reverse 5'-CGCCGCTGTTACCCTATCC-3').
Set 2: outer primers: (forward, 5'- GGACTTGATACCTCACCGCC-3') and (reverse 5'-CAAACACCACATAAGGCCCCA-3'). Inter primers: (forward 5'-GGGGTCAACTCCATGATTAGCA-3') and (reverse 5'-GGTTTCACCCGTAGCCTACC-3').

The efficiency of the primers was evaluated by the gel-electrophoresis analysis of the PCR product. The results of Set 1 primers are shown in **Figure 7.1**. In the first run of PCR using outer primers, clear bands were shown in the region of 450 bp which was consistent with the anticipant results. The primers showed high specificity to both cDNA templates from the two resources. However, when we further amplified the amplification products using the inner primers within the first PCR product, two sequences showed at 400 and 200 bp. This indicates that the inner primers were not strictly specific to the target sequence in the amplicons samples. The 200 bp band, being the expected one, showed much higher intensity than the interference band, which may due to the minor overlap. **Figure 7.2 (A) (B**) shows the PCR products from the primer Set 2, where each of the PCR product presented a single band at 500 bp and 200 bp, which were the desired lengths for the primers. Later qPCR experiment using Set 2 resulted in the standard curve in **Figure 7.2 (C)**, demonstrated a significant linear relationship ($r^2 = 0.99$), indicating the reliability of the quantitative HAV detection.

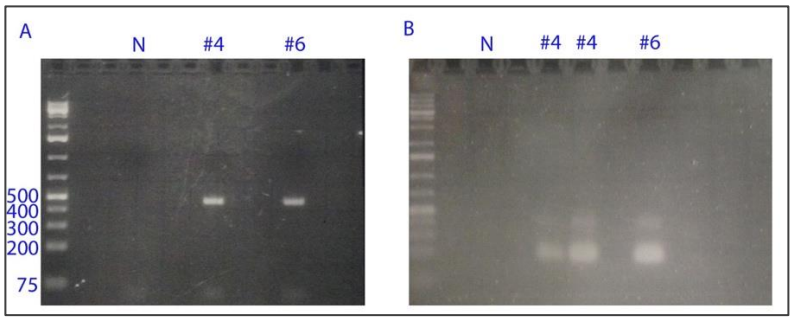

Figure 7.1 DNA agarose gel from the conventional end-point PCR using Set 1 primers. (A) The PCR products from the outer primers using cDNA samples and templates and (B) Tthe products from the inner primers using PCR products from (A) as templates. Water instead of cDNA was used as the negative control (N).

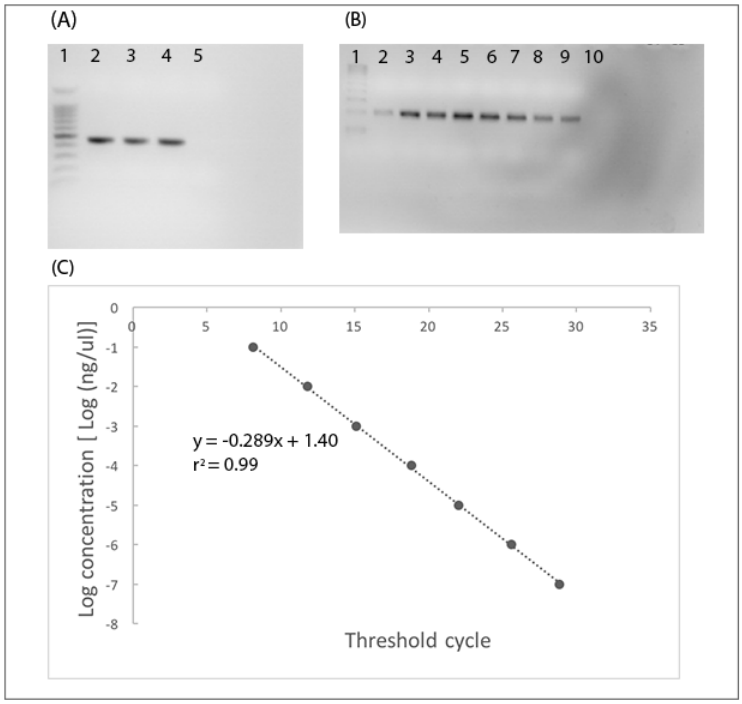

Figure 7.2 PCR and qPCR results from Set 2 primers. (A) Results of external PCR; (B) Results of the internal PCR. In both pictures: Lane 1~ 10: DNA Ladder 100 bp; HAV5 1.0 ng/µL; 0.1 ng/µL; 0.01 ng/µL; 0.001 ng/µL; 1.0 * 10^{-4} ng/µL; 1.0 * 10^{-5} ng/µL; 1.0 * 10^{-6} ng/µL; 1.0 * 10^{-7} ng/µL; blank. (C) Standard curve from qPCR using 10-fold serial dilutions.

The dot blot test was used to test the ssDNA capture probes. The sensitivity was tested by dilutions of the positive control and the specificity was tested by the cDNA and

RNA of HAV and the cDNA of norovirus. The designed capture probe was immobilized by spotting 1 µl solution onto a positively charged nylon membrane followed by UV shining for 10 minutes at UV 254 nm. The synthesized complementary sequence to the capture probe was used as the positive control. The result is present in **Figure 7.3**.

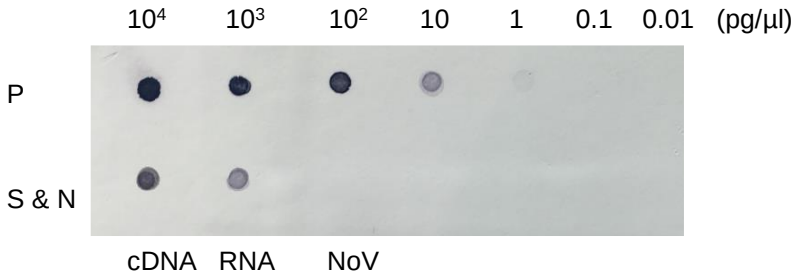

Figure 7.3 Optimized dot blot results showing: P (positive controls) the sensitivity of the capture probe to its complementary sequence as the positive control. The concentrations of the complementary sequence are labeled on the top; S & N (samples and negative control), the responses to the reverse transcribed cDNA and RNA of HAV as samples and the cDNA of Norovirus as negative control.

The results of the dot-blotting assay are reported in **Figure 7.3**. In the first row, blue dots corresponding to the sequence complementary to the first probe were visualized as positive controls, in which sequential dilutions were appreciated until 1 pg/µl. In the lower row, the visible dots indicate that the target sequences were present in the HAV RNA and the cDNA samples. No dot was observable from the negative control, which had encouraged further testing of the probes.

7.2.2 Fibre optic genosensor optimization

The full protocol includes fibre surface immobilization of functional groups for the crosslinking with ssDNA probes, followed by the nucleic acid sequence hybridization in one step with target sequences and the detection probes. In the optimization work, the capture probe concentration and immobilization buffer, the blocking condition, the avidin-HRP concentration and the hybridization buffer were optimized to improve signal/noise ratio.

7.2.2.1 Capture probe incubation concentration and buffer

The amount of immobilized ssDNA probe is one of the critical factors that affect the hybridization efficiency [3, 5-6]. In this study, silanization chemistry was employed to functionalize the surface of the fibre tip and then the probe's working concentration was optimized to achieve the best capture probe coverage. As illustrated in **Figure 7.4** and **Figure 7.5**, the best working concentration of the capture probe was found to be 12 ng/µl in borax buffer after 15 hours incubation at 4 ºC, which gave the highest RLU values among the conditions tested.

The optimized concentration was around half (calculated as a molar concentration) of that in the previous study [2], which was 50 ng/µl for a 53 base DNA probe. This is probably due to the different behaviors brought by the differences in ssDNA probes' lengths [3], and when using 24 base strand, a relatively lower probe concentration is favoured. The effect of the addition of BSA was also explored in the test, no enhancement was observed for the immobilization in the range of probe concentrations tested.

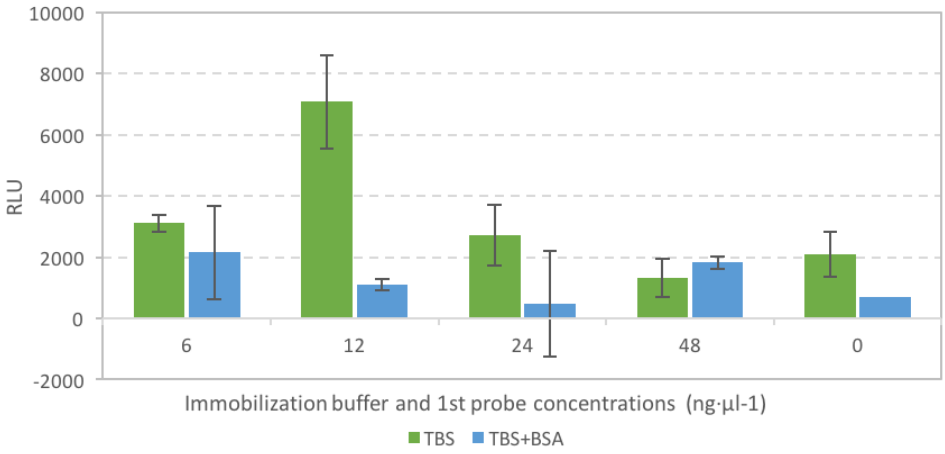

Figure 7.4 Optimization of the capture probe concentration during overnight incubation at 4 °C. The concentrations for testing are 6 ng/µl, 12 ng/µl, 24 ng/µl and 48 ng/µl. The effect of BSA in the incubation mixture was also included in this test.

Regarding the incubation buffer, a good candidate should maintain the stability of the ssDNA sequence and facilitate the immobilization. On the other hand, it should be inert to the –CHO tails layer on the fibre surface. The results using various buffers are shown

in **Figure 7.5,** showing that the light responses differed notably in different buffers. Initially, TBS was used in the concentration test as a tris-based buffer, one of the most popular buffers used for many experiments involving DNA molecules [7-8]. However, the main drawback is its competing reaction with ssDNA chains due to its presence of amine groups, which considerably decreases the immobilization efficiency. The inclusion of $NaBCNH_3$ was intended to improve the binding and avoid non-specific binding by the reduction of imine bond under a relatively acidic condition. However, it is possible that due to the harmful effect to the DNA molecule in the relatively low pH environment, the immobilization efficiency was not satisfying. The improved performance by the borax buffer may be due to the stabilization effect by the formation of a ssDNA-borate complex [9], which leads to both the highest RLU value and lowest SD.

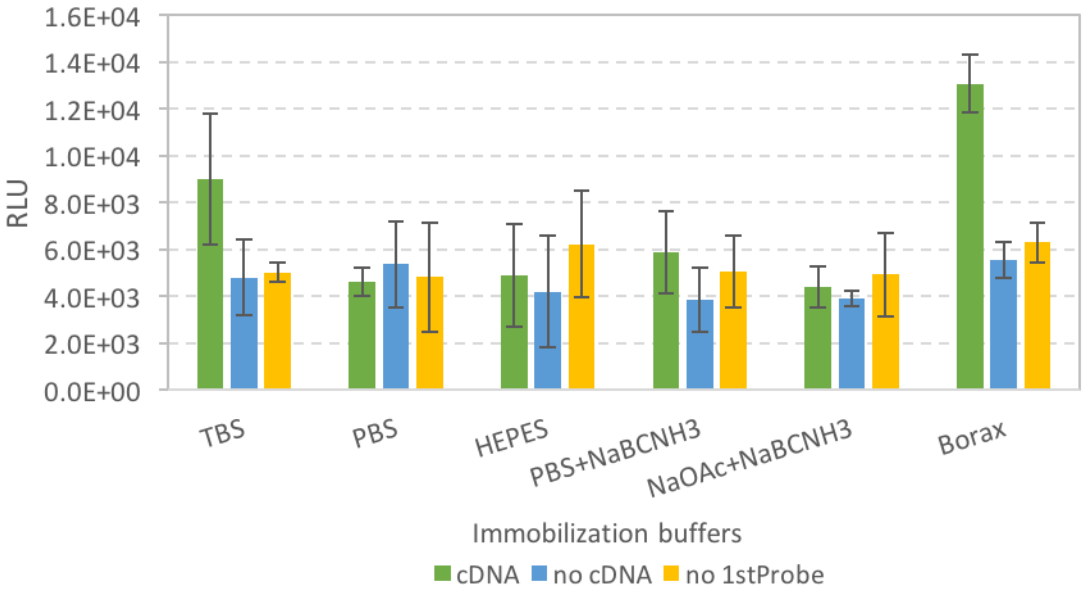

Figure 7.5 Optimization of the immobilization buffer during overnight incubation at 4 °C: TBS solution (25 mM Tris, 150 mM NaCl, 2 mM KCl, pH7.4); PBS (10 mM phosphate buffer, 2.7 mM potassium chloride and 137 mM sodium chloride, pH 7.4), HEPES (20 mM, pH 7.4), PBS + $NaBCNH_3$ (0.3 M), NaOAc (30 mM, pH 5.2) + $NaBCNH_3$ (0.3M), Borax (100 mM boric acid, 25 mM sodium tetraborate, 75 mM NaCl, pH 8.1).

7.2.2.2 Blocking condition

Blocking is another crucial step in avoiding non-specific binding by exhausting the free -CHO groups on the fibre surface and washing away the unbound ssDNA chains [10]. BSA has been considered to be one of the most common blocking agents used for the latter purpose [11-12]. As indicated in **Figure 7.6**, it was found that 3% (w/v) BSA in TBS was the best blocking condition for this system compared to a lower (1%) or higher (5%) BSA concentrations as well as skim milk or glycine solutions.

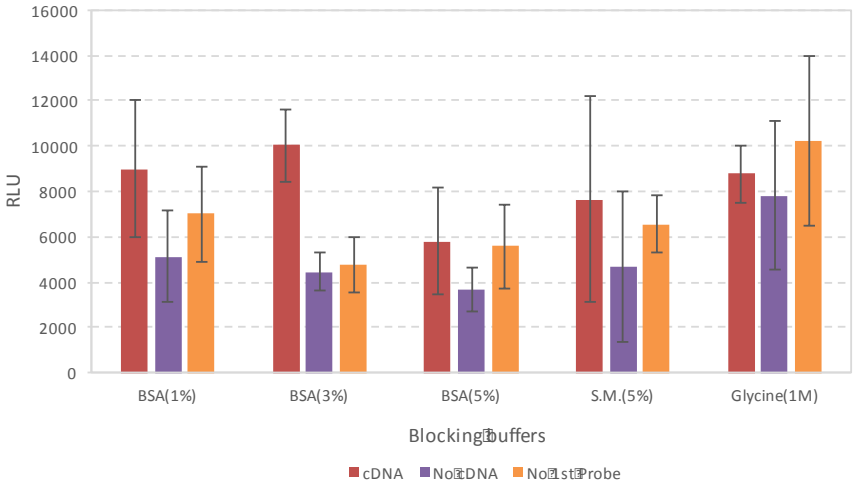

Figure 7.6 Selection of the blocking conditions after the immobilization of the 1st probe. The blocking agents were dissolved in TBST (0.1% v/v) buffer and the incubation was at 40 °C for 1.5 hours. The concentrations are described in w/v.

7.2.2.3 AV-HRP concentration

HRP serves as the catalyst in the reaction to generate chemiluminescence and it was introduced in the two-probe system by the highly stable biotin-avidin interaction (K_d = 10^{-15}M [13]), the results in **Figure 7.7** shows that an appropriate stoichiometric control gave a good signal to noise ratio with 5/500 being the best concentration.

7.2.2.4 Hybridization buffer

A few hybridization buffers (Church (0.5 M Na2HPO4, 0.5 M NaH2PO4, 1% (w/v) SDS and 10 mM EDTA, pH 7.5), Church + 1% (w/v) BSA, TBS pH 7.4, PBS pH 7.4, 0.1% (v/v) PBST pH 7.4, TBS pH 7.4 + 1% (w/v) SDS + 10 mM EDTA, Borax as in

immobilization step + 1% (w/v) SDS + 10 mM EDTA), were examined in this step and the information was collected in **Figure 7.8.**

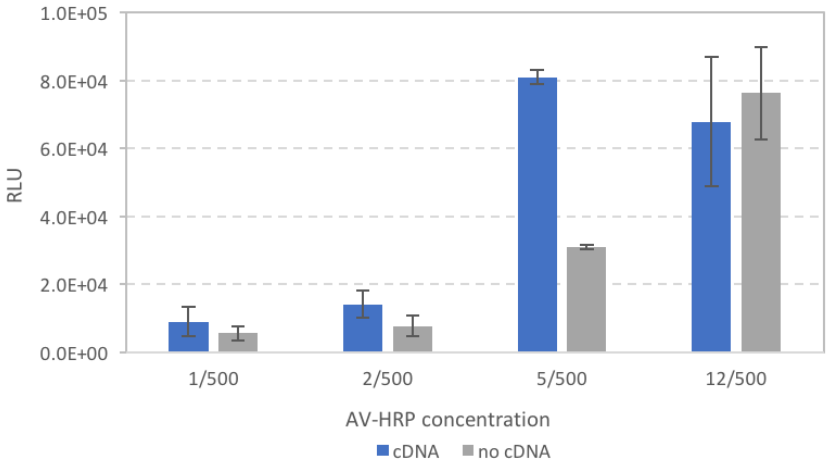

Figure 7.7 Effect of the avidin-HRP concentration on the light response. The labeled concentrations represent the ratio of the volume of the avidin-HRP to the volume of the incubation buffer. The light response from the group without cDNA targets was used as the reference.

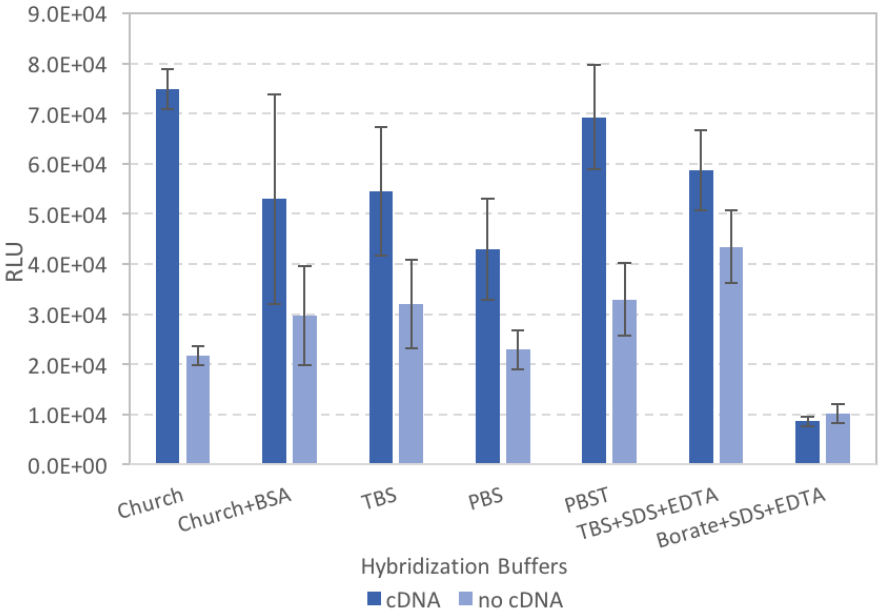

Figure 7.8 Optimization of the hybridization buffer: Church (0.5 M Na_2HPO_4, 0.5 M NaH_2PO_4, 1% (w/v) SDS and 10 mM EDTA, pH 7.5), Church + 1% (w/v) BSA, TBS pH 7.4, PBS pH 7.4, 0.1% (v/v) PBST pH 7.4, TBS pH 7.4 + 1% (w/v) SDS + 10 mM EDTA, Borax as in immobilization step + 1% (w/v) SDS + 10 mM EDTA.

The borate-based buffer was inefficient in the hybridization step as indicated by the lowest response and signal/noise ratio, which may have been caused by the formation of a DNA-borate complex. The Church buffer [4] turned out to be the best buffer condition for the hybridization. The addition of BSA in the Church buffer was observed to increase the viscosity of the hybridization mixture solution, both hindering the process and increasing the SD. The other TBS and PBST-based buffers gave satisfactory positive results, but the significant non-specific bindings presented a major drawback.

7.2.3 Genosensor performance

The performance of this genosensor was evaluated by the calibration and specificity test. From the calibration for both cDNA and RNA detection, a few parameters including a lower detection limit (LDL) and linear range parameters were obtained. Finally, the specificity test was conducted by involving the DNA or RNA sequences from a variety of pathogens

7.2.3.1 Calibration

The calibration curve generally describes the performance of a detection system. The results are presented in **Figure 7.9**, which were obtained by collecting the light responses (RLU) of several dilutions of cDNA or RNA samples, from where, the lower detection limit (LDL) and linear range can be determined.

7.2.3.1.1 Lower Detection Limit (LDL)

The LDL was set by Equation (1):

$$LDL = NEG + 3SD \quad (1)$$

$$SIG > NEG \quad (2)$$

which is the sum of the signal from the negative control (in the absence of *E. coli* cells) (NEG) plus 3 times of its standard deviation (SD). The signals which are higher than the LDL are then considered significant. The LDL reading calculated from the equations were 17,954 for cDNA and 23,367 for RNA, which corresponded to the nucleic acid concentrations of 5 pg/µl and 50 pg/µl, respectively. The LDL performance was much better than that in the dot blotting technique, as the PMT is more sensitive to

the photons than the raw observation of the coloured dots. On the other hand, it seemed much lower than that in some well-studied real-time PCR methods, the best of which is able to detect the concentration as slow as $1.1*10^{-4}$ pg/µl [14]. However, because the NanoPhotometer® concentration reading of the sample stock is the sum of a mixture of nucleic acids in different lengths, the actual nucleic acid concentration could be much lower than the reported value. In addition, as the genosensor is a relatively new technique, there is a lot of room for the improvement of the LDL of genosensor, such as optimization of the probe design, better probe immobilization methods, improved HRP linkage techniques and enhancement of light signals.

7.2.3.1.2 Linear range

The linear range, also known as the dynamic range, is the concentration range where the detection system displays a linear relationship between the signals and the dilutions. It was calculated based on the data extracted from its calibration curve and fit into Equation (3).

$$y = y_0 + D \log\left(concentration\ in \frac{pg}{\mu l}\right) \quad (3)$$

The linear fit was shown in the top right corner of each diagram in **Figure 7.9**. It was found to be 5 pg/µl to 10 ng/µl for cDNA and 50 pg/µl to 10 ng/µl for RNA with r^2 values of 0.93 and 0.87, respectively. The sensitivity is described by the slope D, as it reflects the impact of the change of the concentration to the change of the light response, which was 43948 for cDNA and 23819 for RNA.

7.2.3.2 Specificity test

The specificity test was conducted by covering a wide range of other pathogens' DNA or RNA, the results being summarized in **Figure 7.10**. Both the genosensor and dot blotting method presented a good specificity as the responses to all other noise samples were below the LDL or not visible on the membrane. The rest of the pathogens' samples mentioned in **3.3.4.1** all presented negative results in the dot blot and/or genosensor test. This is mainly attributed to the specificity of the designed probes, being further improved by the second probe in genosensor, carries less risk of potential cross-reactivity comparing to the immune system.

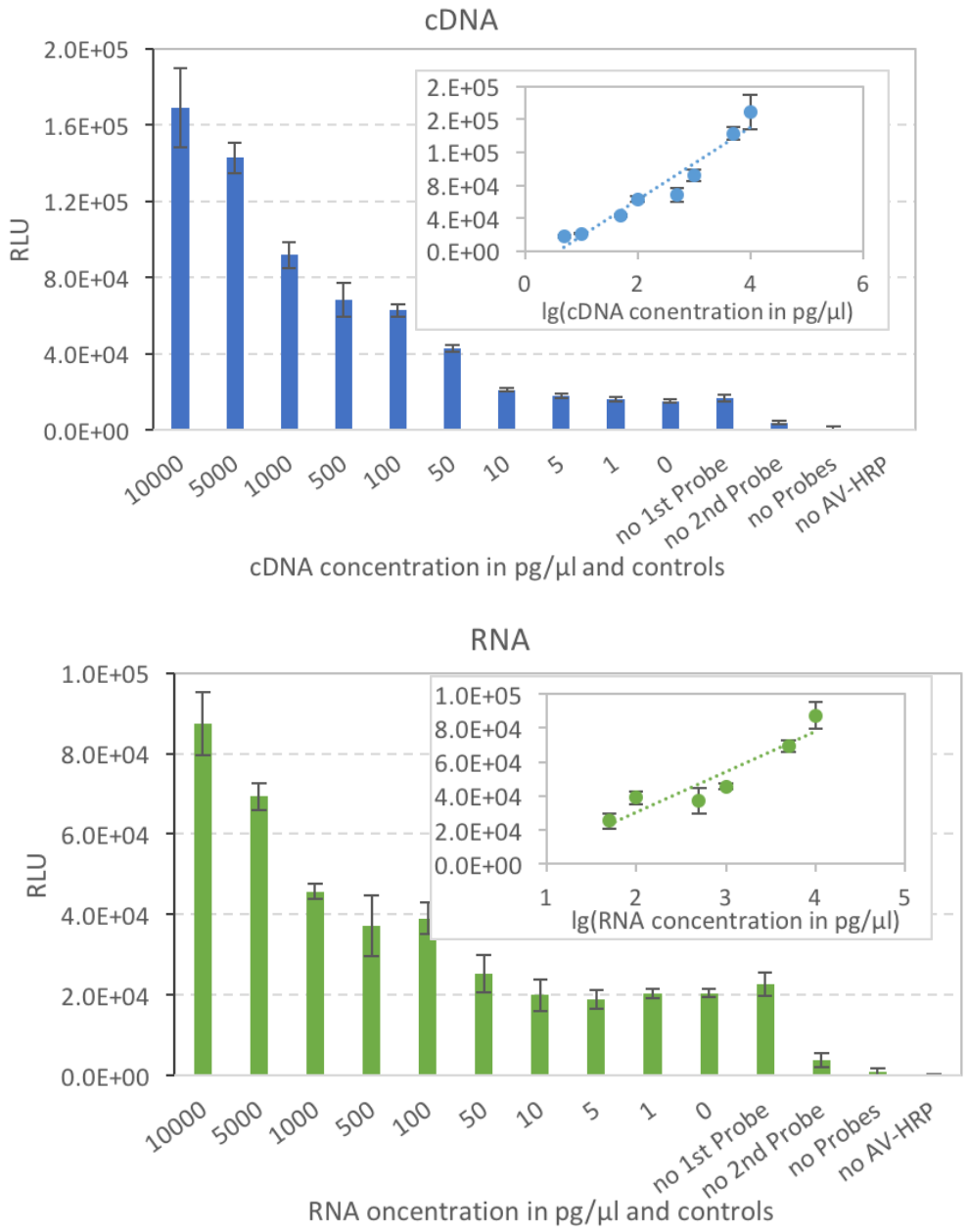

Figure 7.9 Light responses to nucleic acid dilutions and controls. The linear range can be visualized on the top right corner, by plotting the RLU values against the lg values of nucleic acid concentrations in pg/µl. The linear range was found to be 5 pg/µl to 10 ng/µl for cDNA (r^2 = 0.93) and 50 pg/µl to 10 ng/µl for RNA (r^2 = 0.87). The sensitivity of the biosensor was determined by the slope of the linear range as it describes the power to discriminate the difference between the two signals with the change of the analyte concentrations, as represented by its form $\frac{y_A - y_B}{x_A - x_B}$. It was found to be 43948 for cDNA and 23819 for RNA.

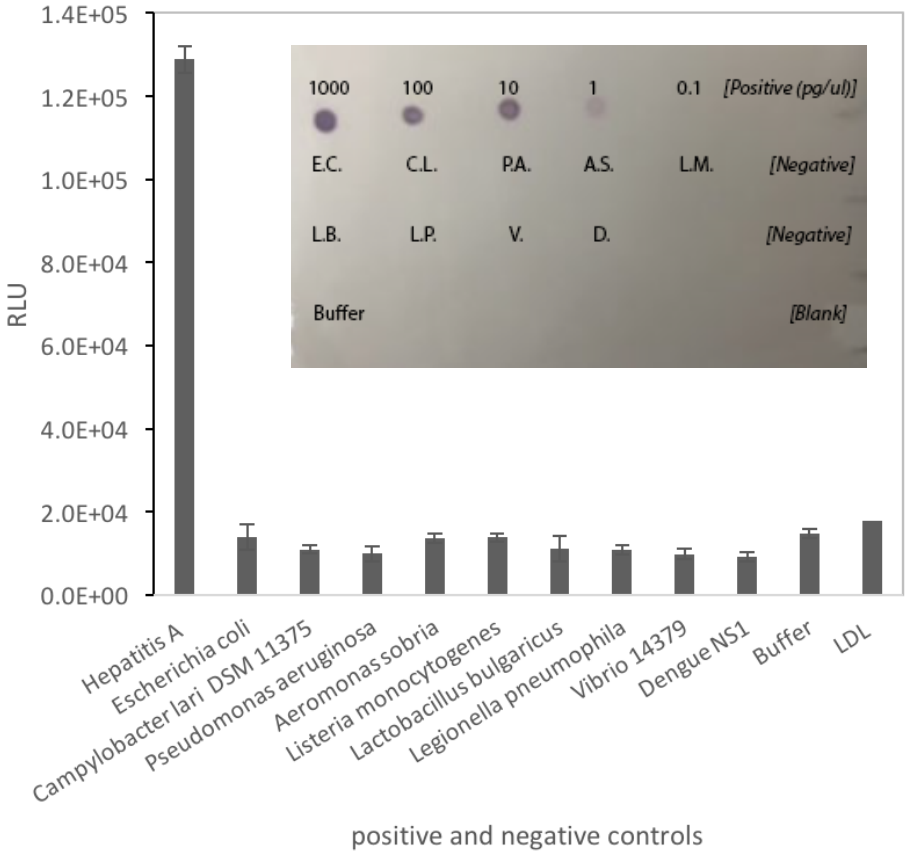

Figure 7.10 Specificity test covering a series of other pathogens' cDNA or proteins. The column chart shows the results from fibre optic genosensor, where the dashed line represents the LDL (lower detection limit). The picture on the top right corner shows the results from the dot blotting experiment. The aberrations are corresponding to the names of the pathogens shown in the x-axis labels of the chart.

7.3 Conclusions

Traditional PCR and qPCR methods were firstly developed to validate the HAV probe method and to serve as a further investigational tool for putative HAV contaminated samples. To get rid of the inhibitive effect of polyphenol compounds to DNA polymerases and to achieve a faster field-detection of HAV virus contamination, a two-probe sandwich-type system on a fibre optic platform was proposed. We have shown a relatively large signal/noise ratio after the assay was optimized. The genosensor system worked for both cDNA and RNA at a detection limit of 5 pg/µl and 50 pg/µl respectively. The linear ranges were found to be 5 pg/µl to 10 ng/µl for cDNA (r^2 = 0.93) and 50 pg/µl to 10 ng/µl for RNA (r^2 = 0.87). An excellent specificity was also

confirmed by screening with a broad range of other pathogens' samples. The whole device is miniaturized in a portable confined black box (350/250/200 mm). This preliminary research shows the potential for applying the two-probe genosensor concept as an in-field early warning system for the presence of HAV virus. development with the focus on the lower detection limit could be approached from optimizing the probe design, probe immobilization methods, HRP linkage techniques and an enhancement of the chemiluminescent signal.

References

[1] Ye, K.; Manzano, M.; Muzzi, R.; Gin, K. Y.-H.; Saeidi, N.; Goh, S. G.; Tok, A. I. Y.; Marks, R. S., *Talanta* **2017,** *174*, 401-408.

[2] Cecchini, F.; Manzano, M.; Mandabi, Y.; Perelman, E.; Marks, R. S., *Journal of Biotechnology* **2012,** *157* (1), 25-30.

[3] Steel, A. B.; Levicky, R. L.; Herne, T. M.; Tarlov, M. J., *Biophysical Journal* **2000,** *79* (2), 975-981.

[4] Church, G. M.; Gilbert, W., *Proceedings of the National Academy of Sciences* **1984,** *81* (7), 1991-1995.

[5] Keighley, S. D.; Li, P.; Estrela, P.; Migliorato, P., *Biosensors and Bioelectronics* **2008,** *23* (8), 1291-1297.

[6] Steel, A. B.; Herne, T. M.; Tarlov, M. J., *Analytical Chemistry* **1998,** *70* (22), 4670-4677.

[7] Kejnovský, E.; Kypr, J., *Gen Physiol Biophys* **1993,** *12* (4), 317-324.

[8] Saeki, K.; Kunito, T.; Sakai, M., *Microbes and Environments* **2011,** *26* (1), 88-91.

[9] Stellwagen, N. C.; Gelfi, C.; Righetti, P. G., *Biopolymers* **2000,** *54* (2), 137-142.

[10] Raoof, M.; Jans, K.; Bryce, G.; Ebrahim, S.; Lagae, L.; Witvrouw, A., *Microelectronic Engineering* **2013,** *111*, 421-424.

[11] Chan, V.; Graves, D. J.; Fortina, P.; McKenzie, S. E., *Langmuir* **1997,** *13* (2), 320-329.

[12] Xu, C.; Taylor, P.; Fletcher, P. D. I.; Paunov, V. N., *Journal of Materials Chemistry* **2005,** *15* (3), 394-402.

[13] Green, N. M., *Advances in protein chemistry* **1975,** *29*, 85-133.

[14] Kim, M.; Lee, S.; Kim, H.; Lee, J.; Joo, I.; Kwak, H.; Kim, H., *Journal of microbiology and biotechnology* **2016**.

Chapter 8

Summary, Implications and Future Suggestions

Chapter 8 draws the threads of the thesis: (1) summarizes the overall results of the construction, optimization, verification and the performance of the fibre optic immuno- and genosensors; (2) states the extent to which the hypotheses were proven; (3) suggests the future work based on the findings. The performances of the immuno- and geno-CFOS were summarized in a table showing the LDL, dynamic range, sensitivity, rapidity skill of operator and portability. For the development of the photoinducible silane diazirine crosslinker in the immunosensor construction, the optimum conditions were obtained and the resulted immunosensor showed superior performances compared to the traditional method. For the genosensor construction, the designed ssDNA probes were successfully integrated onto the fibre optic platform in an optimized condition. The final sensor was able to perform the sensing ability to HAV cDNA and RNA. The proposed hypotheses were verified by the results. At last, a few future work on the work to expand the use of the diazirine as crosslinker and the improvement of the sensor performances, were suggested.

8.1 Summary

This work was dedicated to developing and improving the immuno- and geno-CFOS for the rapid, sensitive and specific detections of *E. coli* and HAV, respectively. The transducing element was a silica fibre optic with a diameter of 400 µm, with the near-end surface being chemically and biologically modified for probe immobilization, target recognition and chemiluminescent signal generation. The light signal was transferred through the fibre optic and collected by a PMT at the far-end. The detection and transduction elements and the PMT were fitted in a black box with dimensions of 350/250/200 mm, which provides convenience for the portable, simple while accurate and sensitive detection. The relatively affordable and dispatchable biosensor can be used in the early warning monitoring for the putative presence of target pathogens either in an individual sample screening or in continuous monitoring of the environment to indicate the need for further investigation.

An immune interaction-based CFOB was constructed through a diazirine crosslinker for *E. coli* (as a fecal indicator bacteria) detection. The silane-diazirine crosslinker method was developed, optimized and applied to the capture antibody immobilization, which was then evaluated by the comparison with the traditional 96-well ELISA method and an immunosensor constructed by a glutaraldehyde method. The specificity was tested with a range of negative controls.

A genosensor was constructed based on the formation a sandwich type hybridization structure. A set of ssDNA probes were designed, integrated and optimized to adapt to the application in the genosensor environment. The specificity was examined by screening a broad range of pathogens' RNA/DNA/cDNA sequences.

The performances of the optimized fibre optic biosensors are summarized in **Table 8.1** and the conclusions based on the objectives achievement scale are summarized in 8.1.1 and 8.1.2.

Table 8.1 Summary table of the performances of optimized fibre optic biosensors

Parameters	Immunosensor for *E. coli*	Genosensor for HAV
LDL	6.44 * 10 ^{2} CFU/ml	5 pg/µl (cDNA) and 50 pg/µl (RNA)
Dynamic range	6.44 * 10^2 - 6.44 * 10^5 CFU/ml, (R^2 = 0.92); 6.44 * 10^5 - 6.44 * 10^8 CFU/ml, (R^2 = 0.98).	cDNA: 5 to 10000 pg/µl, (R^2 = 0.93) RNA: 50 to 10000 pg/µl, (R^2 = 0.87)
Specificity	The polyclonal antibody cross-reacted with other species with similar serotypes; the monoclonal antibody can not only distinguish different species but also different strains in the same species.	Very specific over a broad range of negative controls.
Rapidity	2 minutes on average for a single measurement	6 minutes on average for a single measurement
Skill of operator	No special skill needed	
Portability	Portable black box that can operate at the site of interest	

8.1.1 Immunosensor for *E. coli* constructed by silane diazirine

The silane-diazirine can be synthesized by a coupling reaction between APTES and NHS-diazirine as confirmed by the 1H and 13C NMR unique peaks including the NH hydrogen peak (7.77 ppm, m, 1H) and carbonyl carbon peak (170.96 ppm) of the newly formed amide bond and the diazirine carbon peak (26.26 ppm) (**Table 4.1, Figure 4.2, Figure 4.3, Figure 4.4 and Figure 4.5**). However, due to the challenge of a proper purification and storage method of the final product, it still recommends the two-step diazirine functionalization route as it offers more stability and higher efficiency.

The immobilization ability of silane diazirine was proved by the observation that the S/N value was as high as 4.31 under UV shining at 340 - 370 nm compared to the signal in the dark at 1.08, in the immobilization model using only HRP-IgG (**Figure 4.6**). It further confirmed that the immunoactivities of the antibodies were maintained after UV induced immobilization in a full ELISA detection format in Chapter 5 (**Figure 5.1** lower). The two-step diazirine functionalization route was found to bring much better signal (**Figure 5.1,** RLU values: 151029 vs. 36720 in HRP-IgG model; 2367 vs. 975 in the full ELISA model) at the price of longer modification process (additional 4 hours).

The optimization work has revealed a few favoured parameters in this application: a longer irradiation (40 minutes) at a lower intensity (1090 μW/cm^2) (**Figure 6.3**); an aliphatic diazirine (succinimidyl 4,4'-azipentanoate) was favoured over an aromatic diazirine (3-[4-(Bromomethyl)phenyl]-3-(trifluoromethyl)-3H-diazirine) on a shorter spacer arm length (4-atom rather than 7-atom) (**Figure 6.4**);

The diazirine immunosensor was found to be superior compared to the traditional methods through plotting the calibration curves: (1) Lower detection limit: AmDia sensor had an LDL of 8.64 * 10^{-2} CFU/ml, which is 2 orders lower than ELISA and 1 order lower than AmGlu; AmDia has a dynamic range of 10^{-2} to 10^{-5} CFU/ml, which was not observed in other two competitors (**Figure 6.5**). Regarding the specificity, it depends on the choice of antibodies, polyclonal antibodies were able to detect a few numbers of species with identical or similar serotypes while monoclonal antibody was possible to distinguish different strains in the same species (**Figure 6.6**).

8.1.2 Genosensor for *HAV* detection

A set of ssDNA probes target on HAV RNA sequence were designed and validated by the nested qPCR technique (**Figure 7.1 and Figure 7.2)** and further confirmed by a dot blotting technique (**Figure 7.3)**. When integrating the ssDNA probes into the genosensor platform, the optimum conditions of the construction genosensor were found to be: the 24-base ssDNA capture probe was immobilized in borax buffer in the concentration of 12 ng/μl followed by a blocking by 3 % BSA in TBS solution; the best hybridization buffer is church buffer (0.5 M Na2HPO4, 0.5 M NaH_2PO_4, 1% (w/v) SDS and 10 mM EDTA, pH 7.5) and the optimum AV-HRP concentration is 5/500 (**Figure 7.4, 7.5, 7.6, 7.7 and 7.8**). The genosensor system works for both cDNA and RNA at a detection limit of 5 pg/μl and 50 pg/μl respectively. The linear ranges were found to be 5 pg/μl to 10 ng/μl for cDNA (r2 = 0.93) and 50 pg/μl to 10 ng/μl for RNA (r^2 = 0.87) (**Figure 7.9)**. An excellent specificity was also confirmed by screening with a broad range of other pathogens' samples (**Figure 7.10)**.

8.2 Verified/nullified hypotheses

Hypothesis #1 An aliphatic silane diazirine can be used as a bifunctional crosslinker to immobilize antibody in the aqueous buffer solution onto the fibre optic surface by UV

activation and maintain its immunoactivity. The hypothesis is based on the facts that, upon UV activation at 340 - 370 nm, which is not harmful to the protein structures at different levels, the diazirine molecule transforms to a carbene intermediate which inserts into various chemical bonds on the side chains of the antibodies as illustrated in **Figure 1.2**. The silane moiety on the other end is able to connect to the hydroxyl groups on the silica-based fibre surface.

This hypothesis was supported by results. The distinguish difference of the S/N value between the UV (340 – 370 nm) shining group and dark group (4.31 vs. 1.08) in the IgG-HRP immobilization model (Chapter 4) has showed the immobilization ability. The success in full ELISA model in Chapter 5 has further confirmed that the immunoactivities were maintained. In addition, the SEM characterization in Chapter 6 showed the *E. coli* cells captured on the surface, which supported the ability of immunoactivity (cell capture ability) from another side.

Hypothesis #2 The combination of the better stability and proximity of covalent binding and the higher immobilization efficiency of the diazirine crosslinker will bring higher sensitivity of an immuno-CFOS compared to the traditional 96-well ELISA method and the immuno-CFOS constructed by glutaraldehyde silane method. The hypothesis is based on the facts that, the covalent binding method used for capture antibody immobilization on optical fibre is more stable and bring closer proximity of the light signal generation than the physical absorption used in the 96-well ELISA method. On the other hand, the carbene intermediates react with a broader range of functional groups in a considerably shorter time than the chemical silane tails do, which will lead to more efficient antibody binding.

This hypothesis was verified by the results from Chapter 6. In the comparison to previous methods, the diazirine immunosensor was found to be superior in the aspects of (1) Lower detection limit: AmDia sensor had an LDL of $8.64 * 10^{-2}$ CFU/ml, which was 2 orders lower than ELISA and 1 order lower than AmGlu; (2) dynamic range: AmDia had a dynamic range of 10^{-2} to 10^{-5} CFU/ml, which was not observed in other two competitors. However, the specificity depended on the selection of the antibodies and was not improved by the immobilization method.

Hypothesis #3 The sandwich structure formed by the NH_2-modified 24 base ssDNA capture probe, target sequence and the HRP linked 24 base ssDNA detection probe on the end face of the fibre optic (shown in **Figure 1.1**) will enable the geno-CFOS to perform the sensing ability to HAV cDNA and RNA in high specificity and sensitivity due to the following suppositions: (1) the unique region of the HAV target sequence; (2) the enhanced selectivity by the combination of two probes targeting at different target regions, which makes the complementarity degree to 48 base-pairs, leading to a stronger and more specific hybridization.

This hypothesis was supported by the results. The two ssDNA probes (the capture probe: NH_2C_6-5'-TCTTAACAACTCACCAATATCCGC-3') and the detection probe: 5'-CCAATTTAGACTCCTACAGCTCCA-3'-Biotin) were integrated into the CFOB platform after a series of condition optimization, which can be seen from the considerably higher RLU signal of the sample groups than those of a series of control groups (no 1st probe, no 2nd Probe, no target, no HAV).

The genosensor system worked for both cDNA and RNA at a detection limit of 5 pg/µl and 50 pg/µl respectively. The linear ranges were found to be 5 pg/µl to 10 ng/µl for cDNA ($r^2 = 0.93$) and 50 pg/µl to 10 ng/µl for RNA ($r^2 = 0.87$). An excellent specificity was also confirmed as the RLU signal from a broad range of other pathogens' samples were all below the LDL including: DNA or RNA strands or proteins extracted from bacterial and viral samples, *Escherichia coli, Campylobacter lari DSM 11375, Pseudomonas aeruginosa, Aeromonas sobria, Listeria monocytogenes, Lactobacillus bulgaricus, Legionella pneumophila, Vibrio 14379, Lactococcus lactis, Morganella morganii, Proteus vulgaris, Bacillus subtilis, Staphylococcus aureus Pseudomonas putida*, Norovirus G1, Norovirus G2, Dengue virus and South Bay virus.

8.3 Implications and future work

Based on the current results and conclusions from the construction of the immuno- and geno-CFOS for *E. coli* and HAV detection in water, a few directions for further studies can be considered to explore and expand the scope of the current work as well as to provide a better understanding of the diazirine chemistry in biomolecule immobilization and the genosensor working mechanisms.

8.3.1 Further optimization of the immunosensor

The work has shown the ability to detect *E. coli* of the immunosensor constructed by diazirine. After optimization, it has already performed better LDL and dynamic range. To better adapt the method into real applications, there is still room to lower down the detection limit to 10^2 CFU /100 ml [1], which can be achieved from the following aspects: (1) Amplification of the intensities of the chemiluminescence to increase the signal resolution. It can be done by indirect detection method that uses a first detection antibody followed by a second HRP-attached antibody to increase the number of HRP and thus amplify the signal [2]. Besides, chemical enhancement of chemiluminescence can also be considered through metal nanoparticles [3-5] or luminol enhancers [6] (**Figure 8.1**). (2) Oriented antibody immobilization by using Fc region receptors, such as protein A or G [7]; Oxidized carbohydrate on the Fc region and covalently binding with amine-coated surfaces [8]; and using the exposed thiol bonds in the Fc region by reduction and attachment to C=C bond covered surface by UV activation [9-10] (**Figure 8.2)**.

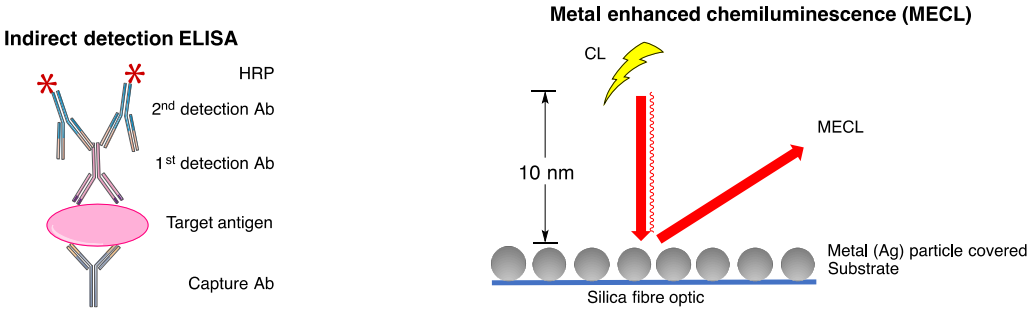

Figure 8.1 Chemiluminescence (CL) enhancement by: left, indirect detection ELISA; and right, metal nanoparticles enhanced chemiluminescence (MECL).

8.3.2 Environmental *E. coli* samples and other bacteria pathogens detection

The current work was based on the laboratory *E. coli* strains detection. The application of the immunosensor on environmental *E. coli* samples is the immediate following work to expand its use in the real world. It is suggested to select the appropriate antibodies first by ELISA before integrating with the immunosensor platform.

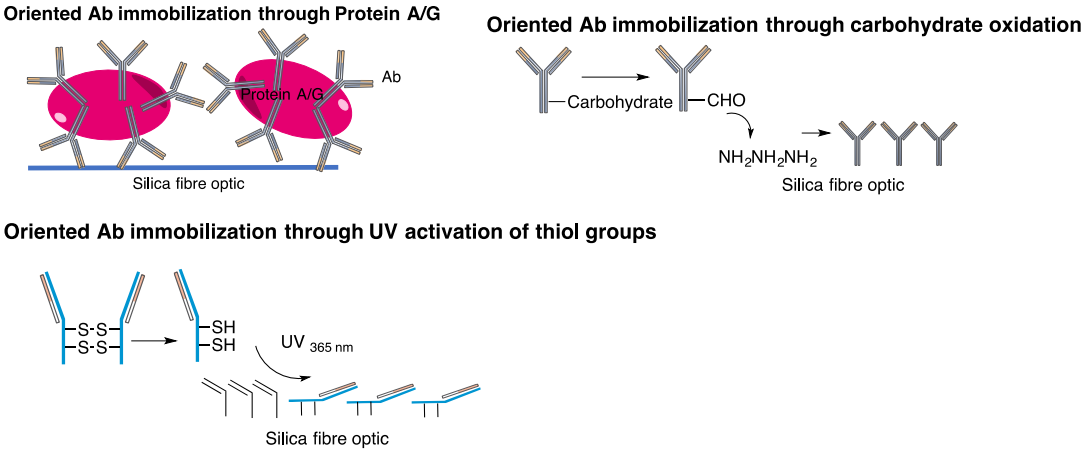

Figure 8.2 Orientated antibody immobilization strategies: proteins A/G facilitate immobilization; the reaction of -NH2 functionalized surface and the –CHO bonds through oxidation of carbohydrates; and UV induced immobilization between C=C bonds and thiol bonds from IgG cleavage.

8.3.3 Expand the use of diazirine crosslinker

This work has demonstrated the crosslinking ability of diazirine to the antibody molecules through the highly reactive carbene intermediates by UV activation. Same mechanism is also applicable to other protein-based molecules immobilization like some antigens and enzymes on the fibre optic end face. Other than silane, diazirine can also be incorporated with other moieties including pyrrole to adapt to other platforms like electrode in the electrochemical-based biosensor applications.

8.3.4 Functional diazirines synthesis

It has shown in this study that the two-step diazirine functionalization route is better in this application. However, it was mainly due to the highly moisture sensitive property of the silane moiety. Whenever it is suitable to use other kind of molecules, it worth trying the synthesis route using a variety of diazirines as it provides much more conveniences to the protocol.

The aromatic and aliphatic diazirines have shown distinguishable differences in immobilization efficiency due to the influence of the functional groups connecting to the diazirine group. The introduction of appropriate functional groups to diazirine moieties is suggested to increase the carbene insertion efficiency, which can be done

by stabilizing the carbene intermediate, increasing the carbene/diazo ratio and the singlet/triplet carbene ratio and adjusting the hydrophobic/hydrophilic properties according to the specific working environments. This will not only benefit the immobilizing application of diazirine but also the protein labeling functions. The related details have already been discussed in Chapter 2.

8.3.5 Further optimization of the genosensor

The genosensor concept using a set of ssDNA probes targeting at HAV RNA has been proven to be highly specific and sensitive. However, there are still room for the optimization of LDL. It is suggested to put effort in the following directions: (1) chemiluminescence enhancement as described in 8.2.1; (2) a dendritic format of probes can be considered: for the capture probe, with a dendritic structure, it provides more capture sites for target sequences [11-12]. For the detection probe, the dendritic structure can be used to introduce more HRP enzymes [13] . Both of the modifications will improve the signal. However, the dendrimer introduces an additional level of complexity to the probe synthesis, which might negate the improvement in sensitivity [14].

References

[1] Sanders, E. C.; Yuan, Y.; Pitchford, A., *Water* **2013,** *5* (1), 243-261.

[2] Atias, D.; Liebes, Y.; Chalifa-Caspi, V.; Bremand, L.; Lobel, L.; Marks, R. S.; Dussart, P., *Sensors and Actuators B: Chemical* **2009,** *140* (1), 206-215.

[3] Chen, W.; Hong, L.; Liu, A.-L.; Liu, J.-Q.; Lin, X.-H.; Xia, X.-H., *Talanta* **2012,** *99*, 643-648.

[4] Li, X.; Sun, L.; Ge, A.; Guo, Y., *Chemical Communications* **2011,** *47* (3), 947-949.

[5] Golberg, K.; Elbaz, A.; McNeil, R.; Kushmaro, A.; Geddes, C. D.; Marks, R. S., *Journal of Nanoparticle Research* **2014,** *16* (12), 2770.

[6] Maeztu, R.; González-Gaitano, G.; Tardajos, G., *The Journal of Physical Chemistry B* **2010,** *114* (32), 10541-10549.

[7] Rusmini, F.; Zhong, Z.; Feijen, J., *Biomacromolecules* **2007,** *8* (6), 1775-1789.

[8] Tsarfati-BarAd, I.; Gheber, L. A., Recent and Future Developments of Microarrays: Miniaturization and Lab-on-Chip Approaches. In *Microarrays in Diagnostics and Biomarker Development: Current and Future Applications*, Jordan, B., Ed. Springer Berlin Heidelberg: Berlin, Heidelberg, 2012; pp 153-168.

[9] Sharma, H.; Mutharasan, R., *Analytical Chemistry* **2013,** *85* (4), 2472-2477.

[10] Weinrich, D.; Lin, P. C.; Jonkheijm, P.; Nguyen, U. T.; Schröder, H.; Niemeyer, C. M.; Alexandrov, K.; Goody, R.; Waldmann, H., *Angewandte Chemie International Edition* **2010,** *49* (7), 1252-1257.

[11] Wang, J.; Jiang, M.; Nilsen, T. W.; Getts, R. C., *Journal of the American Chemical Society* **1998,** *120* (32), 8281-8282.

[12] Nakamura, F.; Ito, E.; Sakao, Y.; Ueno, N.; Gatuna, I. N.; Ohuchi, F. S.; Hara, M., *Nano Letters* **2003,** *3* (8), 1083-1086.

[13] Sassolas, A.; Leca-Bouvier, B. D.; Blum, L. J., *Chemical reviews* **2008,** *108* (1), 109-139.

[14] Rosi, N. L.; Mirkin, C. A., *Chemical Reviews* **2005,** *105* (4), 1547-1562.